Assessment of Fault Level in Power Systems with High Penetration of Non-Synchronous Generation

A Thesis submitted to The University of Manchester for the degree of

Doctor of Philosophy

in the Faculty of Science and Engineering

2020

Rafat Radwan Aljarrah

School of Electrical and Electronic Engineering

Table of Contents

Table of Contents 2

List of Figures 7

List of Tables 10

List of Abbreviations 11

Nomenclature 12

Abstract 16

Declaration 18

Copyright Statement 19

Acknowledgements 20

1 Introduction 21

1.1 Overview and Motivation 21

1.2 Project Objectives 25

1.3 Thesis Outline 26

1.4 Publications from this Thesis 29

2 Background and Literature Review 30

2.1 Fault Level (Definition) 30

2.2 Importance of the Fault Level 32

2.2.1 Power System Protection 32

2.2.2 Voltage Support 33

2.2.3 Stability of Power Electronics-Based Sources 36

2.3 Characteristics of Fault Current in Classical Power Systems 38

2.3.1 Fault Current Contribution from Synchronous Generator 38
2.3.2 Modelling of SG in Fault Calculations 39
2.4 Steady-State Fault Calculation Methods 43
2.4.1 The Equivalent Voltage Source Method 43
2.4.2 The Superposition (Complete) Method 45
2.5 Background and Review about Non-Synchronous Generation 47
2.5.1 Fully-Rated Converters Technology 47
2.5.2 Control of Non-synchronous Generation 48
2.5.3 Fault Ride Trough and Grid Code Requirement 49
2.5.4 Short Circuit Current Behaviour of FRC-based NSG 52
2.5.5 Modelling of FRC-based NSG in Steady-State Fault Calculations 55
2.6 Calculation of Fault level in systems with high penetration of NSGs (review) 57
3 Analyzing the Impact of Increased Penetration of NSGs on the Fault Level 61
3.1 Control of the NSGs Considering the Fault Ride Through 61
3.2 Fault Response of NSGs Considering Different FRT Control Strategies 63
3.2.1 Fault Response without Reactive Current Injection during the Fault (FRT_{NQ}) 64
3.2.2 Fault Response with an Immediate Reactive Current Injection (FRT_{IQ}) 66
3.2.3 Fault response with a delayed reactive current injection (FRT_{DQ}) 69
3.3 Characteristics of SC Current under Different Penetration Levels of NSGs 73
3.3.1 The Adjusted Single Machine System 73
3.3.2 Case Study Using IEEE 9-Bus Test System 79
3.4 Conclusion 84

4 Evaluating the Accuracy of Steady-State Fault Calculation Methods with High Penetration of NSGs 86

4.1 Introduction 86

4.2 Modelling of NSG Utilising FRC in Steady-State Fault Calculations 86

4.2.1 According to IEC60909 Standards 86

4.2.2 According to the Complete Method 89

4.3 Results and Discussion 91

4.3.1 Assessment of SSFC Methods Performance Using the Single Machine-Infinite Bus Test System 91

4.3.2 Assessment of SSFC Methods Performance Using the IEEE 9-Bus Test System 96

4.4 Conclusion 99

5 Proposed Modification of the Latest Version of IEC60909 Standards to Consider the Fault Contribution of NSGs 100

5.1 Introduction 100

5.2 Fault Calculation According to IEC60909 Standards 101

5.2.1 Calculating the Fault Current without Considering the NSGs 102

5.2.2 Calculating the Fault Current of the NSGs 103

5.2.3 Calculating the Total Fault Current I''_{K_Total} 103

5.3 The Proposed Modification Method 104

5.3.1 Calculating the Fault Current without Considering the NSGs 104

5.3.2 Calculating the Fault Current of the NSGs 104

5.3.3 Calculating the New Total Fault Current $I''_{K\_Total\_New}$ 106

5.4 Results and Discussions 106

5.4.1 Single-Machine Infinite Bus Test System 107

5.4.2 IEEE 14-Bus Test System 110

5.5 Conclusion 114

6 Novel MVA-based Fault Level Calculation Method in Future Grid Scenario with High Penetration of NSGs 116

6.1 Introduction 116

6.2 Fault Level Contribution from SG and its MVA Representation 118

6.3 Augmenting FLC Method Including the Impact of PE-Based Generation 120

6.3.1 Penetration Level Metric 120

6.4 Main Steps of the Proposed Methodology 121

6.5 Non-Numerical Case Study 125

6.6 Special Case (uniform PE penetration scenario) 127

6.7 Flow chart of the proposed FLC Method 129

6.8 Results and Discussion 130

6.8.1 Two-Area System 130

6.8.2 IEEE 9-Bus Test System 133

6.8.3 The IEEE 39-Bus Test System 136

7 Possible Solutions to Substitute the Low Fault Level in Future Power Systems with High Penetration of NSGs 141

7.1 Maximizing the *k*-Factor 141

7.2 Maximizing the Overrating Capability of the NSGs 142

7.3 Installation of Synchronous Condensers 143

7.4 Simulation Results 144

7.4.1 Impact of the Increased Penetration on the Fault Level 144

7.4.2 Impact of the Low Fault Level on the System Strength 147
7.4.3 Maximizing the *k*-Factor 150
7.4.4 Maximizing the Overrating Capability of the NSG 152
7.4.5 Installation of Synchronous Condensers 154
7.5 Conclusion 157
8 Thesis Summary 160
8.1 Conclusions 160
8.2 Contributions and Key Findings 166
8.3 Future Work 169
References 171
Appendices 180

List of Figures

Fig.1: National change in Fault Level 2019-2030 [2].....22

Fig.2: Regional change rates in fault level across UK [2] 22

Fig.3: The single line diagram of a capacitor bank switching event 34

Fig.4: Waveforms of the SC currents of the synchronous generator.....38

Fig.5: The circuit model of sub-transient fault period 40

Fig.6: The circuit model of transient fault current.....41

Fig.7: The circuit model of steady-state fault current.....42

Fig.8: SC current according to IEC60909 (far-from-generator fault).....45

Fig.9: A Fully-rated converter technology in PV system 47

Fig.10: A Fully-rated converter technology in Type-4 wind.....47

Fig.11: Control of NSG (grid side converter).....49

Fig.12: The FRT profile of a Power Generating Module according to ENTSO-E.....50

Fig.13: The FRT requirements for Denmark, Germany and Great Britain 50

Fig.14: The requirement for reactive current injection from RES during 51

Fig.15: The SC current from a 50 MVA generation unit in response to a three-phase bolted fault at the generator terminal:a) SG, and b) FRC-based NSG (type-4 wind).....52

Fig.16: Control of NSG (grid side converter).....62

Fig.17: The single machine-infinite Bus test system.....63

Fig.18: The SC current from the NSG during (FRT_{NQ} control) at different output power 65

Fig.19: The SC current from the NSG during (FRT_{NQ} control) at different PCC voltage levels66

Fig.20: The SC current from the NSG during (FRT_{IQ} control) at different output power,.....67

Fig.21: The SC current from the NSG during (FRT_{IQ} control) at different values of *k*-factor .68

Fig.22: The SC current from the NSG during ($\mathrm{FRT_{IQ}}$ control) at different values of transient overrating factor α.....69

Fig.23: The SC current from the NSG in case of a) FRT_{IQ} b) FRT_{DQ20} c) FRT_{DQ50} 72

Fig.24: The adjusted single machine-infinite Bus test system.....73

Fig.25: The SC current at different penetration levels (FRT_{IQ} control).....75

Fig.26: The SC current at different penetration levels (FRT_{DQ20} control 75

Fig.27: The SC current at different penetration levels (FRT_{DQ50} control).....75

Fig.28: The adjusted IEEE 9-Bus test system.....79

Fig.29: The SC current of Bus-6 at different penetration levels (FRT_{DQ20} control).....80

Fig.30: The SC current of Bus-6 at different penetration levels (FRT_{DQ50} control).....80

Fig.31: Voltage behind impedance used for FRC modelling in the static converter-fed drive method.....87

Fig.32: The current source model with infinite impedance 89

Fig.33: Results for (Ik") at different voltage dip levels seen by the NSG 92

Fig.34: Results for (Ib) at different voltage dip levels seen by the NSG 94

Fig.35: Results for I_p at different voltage dip levels seen by the converter 95

Fig.36: Fault currents on Bus 8 with 22% penetration of NSG in the grid.....97

Fig.37: Fault currents on Bus 8 with 55% penetration of NSG in the grid.....97

Fig.38: A 10 MW PV system connected to a 132 kV external grid 107

Fig.39. Injected currents in response to a different voltage dip levels for the case (k=2) 108

Fig.40. Injected currents in response to a different voltage dip levels for the case (k=10) 108

Fig.41: The modified IEEE 14-Bus test system.....110

Fig.42: The resulted values of the fault currents from different methods for the case (k=2) .112

Fig.43: The resulted values of the fault currents from different methods for the case (k=10)113

Fig.44. SG fault contribution (a) single line diagram, (b) equivalent circuit, and.....118

Fig.45. Fault level contribution from the compound generation unit 120

Fig.46: The representation of the fault level at non-uniform penetration Scenario.....126

Fig.47: The flow chart of the proposed FLC 129

Fig.48: The two-area test system with a PE-based generation on Bus 2. 130

Fig.49: The fault level on 2-area test system with different levels of P_2(*Scenario 1)*.....131

Fig.50: The fault level on 2-area test system with different levels of P_T (*Scenario 2)*.....132

Fig.51: The adjusted IEEE 9-Bus test system with a PE-based generator on Bus 2 133

Fig.52. Fault level in the modified IEEE 9-Bus test system with different.....134

Fig.53. Results from the adjusted 9-Bus test system with different 135

Fig.54: The adjusted IEEE 39-Bus system with PE-based generators (*Scenario 1*) 136

Fig.55: The fault level on Bus 9 at different penetration levels of NSGs.....137

Fig.56: The fault level on Bus 16 at different penetration levels of NSGs.....137

Fig.57: The adjusted IEEE 39-Bus test system.....144

Fig.58: The fault level in the adjusted IEEE 39-Bus test system.....145

Fig.59: Voltage dip propagation due to a fault at Bus 16 147

Fig.60: Voltage change due to a 100 MVAr capacitor bank switching at Bus 21.....149

Fig.61: The enhanced fault level using higher vlues of *k*-factor.....151

Fig.62: The enhanced fault level using higher overrating capability.....153

Fig.63: The enhanced fault level using Synchronous condensers 155

List of Tables

Table 1: Typical values of the fault level for different system voltages.....31

Table 2: The impact of low fault level on different protective device.....32

Table 3: Strength of the ac/dc connection.....36

Table 4: Reactance values during the SC event.....42

Table 5: The parameters for the FRT profile as defined by ENTSO-E.....50

Table 6: The requirement for the speed of reactive current injection according.....71

Table 7: Currents with different penetration levels at FRT_{IQ}.....77

Table 8: Fault currents at the PCC with different penetration levels at FRT_{DQ20}.....78

Table 9: Fault currents at the PCC with different penetration levels at FRT_{DQ50}.....78

Table 10: Fault currents at Bus 6 with different penetration levels for FRT_{DQ20}.....81

Table 11: Fault currents at Bus 6 with different penetration levels for FRT_{DQ50}.....81

Table 12: Different SSFC Methods.....91

Table 13: The recommended SSFC methods besed on the location of the fault.....96

Table 14: The injected Current from PV System at Different Voltage Dip Levels.....109

Table 15: Fault currents on the adjusted IEEE 14-Bus test system (k=2).....112

Table 16: Fault currents on the adjusted IEEE 14-Bus test system (k=10).....114

Table 17: Bus 9 Fault level on the adjusted IEEE 39-Bus test system.....138

Table 18: Bus 16 Fault level on the adjusted IEEE 39-Bus test system.....138

Table 19: The fault level of adjusted IEEE 39-Bus test system.....146

Table 20: During-fault voltage due to a bolted fault at Bus 16.....149

Table 21:Impact of increasing the k-factor on the fault level.....152

Table 22: The impact of increasing the overrating capability on the fault level.....154

Table 23:Impact of installation of synchronous condensers on the fault level.....156

List of Abbreviations

CB	Circuit Breaker
DGs	Distributed Generators
EMT	Electromagnetic Transients
ENTSO-E	European Network of Transmission System Operators for Electricity
FGs	Future Grids
FL	Fault Level
FLC	Fault Level Calculation
FRC	Fully Rated Converter
FRT	Fault Ride Through
HVDC	High Voltage Direct Current
IEC	International Electrotechnical Commission
IEEE	Institute of Electrical and Electronics Engineers
LCC	Line-Commutated Converter
LVRT	Low Voltage Ride Through
MVA	Mega Volt Amp
NSGs	Non-Synchronous Generations
PCC	Point of Common Coupling
PEs	Power Electronics
PLL	Phase-Locked Loop
PV	Photovoltaic
RESs	Renewable Energy Sources
RMS	Root Mean Square
SC	Short Circuit
SCR	Short Circuit Ratio
SG	Synchronous Generator
SSFC	Steady-State Fault Calculation
TSOs	Transmission System Operators

Nomenclature

Chapter 2

MVA_C	The rating of a capacitor bank in MVAr
$V_{i,j}$	The voltage at Bus-*i* due to a fault at Bus-*j*
$V_{j,i}$	The voltage at Bus-*j* due to a fault at Bus-*i*
$\mathbf{Z}_{SC(i,j)}$	The (*ij*) element of the short circuit impedance matrix
$\mathbf{Z}_{SC(j,j)}$	The (*jj*) elements of the short circuit impedance matrix
$[\mathbf{Z}_{SC}]$	The short circuit impedance matrix
P_{C}	The power rating of the NSG in MW
X''	Sub-transient reactance in p.u.
X′	Transient reactance in p.u.
X	Synchronous reactance in p.u.
X_{l}	leakage reactance of the synchronous machine in p.u.
X_{a}	The armature reaction reactance of the synchronous machine in p.u.
X_d	damper windings reactance of the synchronous machine in p.u.
X_{f}	The field windings reactance of the synchronous machine in p.u.
I''_{k}	The initial symmetrical short-circuit current
I_{p}	The peak instantaneous short-circuit current
I_{k}	Steady-state short-circuit current
i_{DC}	DC component of short-circuit current
A	The initial value of the dc component
P-Q	Active-Reactive Power
k	A proportional gain which determines the relation between the reactive current injection and the voltage during the fault

Chapters 3 & 4

$V_{\text{Threshold}}$	The threshold voltage at which the FRT control is activated in p.u.
V_{Measured}	The measured voltage during the fault in p.u.
I_{Active}	Injected active current during the fault in p.u.
I_{Rective}	Injected reactive current during the fault in p.u.
I_{Max}	the maximum combined current (active and reactive) the converter can supply during the fault in p.u.
FRT_{NQ}	FRT capability without reactive current injection during the fault
FRT_{IQ}	FRT capability with an immediate (0 ms delay) reactive current injection during the fault
FRT_{DQ20}	FRT capability with a 20 ms delayed reactive current injection during the fault
FRT_{DQ50}	FRT capability with a 50 ms delayed reactive current injection during the fault
V_{PCC}	The voltage at the point of common coupling in p.u.
α	A factor representing the overrating capability of the NSG
I_{Rating}	The rating current of the converter in p.u.

Chapter 5

Z_k	the equivalent impedance at the faulty point in Ω
$I_{\text{Max}j}$	the maximum fault current contribution of the NSG connected to the j-th Bus in p.u.
Z_{ij}	the transfer impedance between the faulty Buses *i*, and *j*, where the NSG is connected in Ω
N	number of the connected NSGs.
$I''_{\text{k\_RESs}}$	the total fault current contribution of all connected NSGs in kA
Z_k	the equivalent impedance at the faulty point in Ω
$I''_{\text{k\_Grid}}$	the initial symmetrical current of the grid to the faulty point in kA
V_{n}	Nominal pre-fault phase voltage in kV
c	Voltage correction factor

$V_{\text{L-L}}$	Nominal pre-fault line to line voltage in kV
$I''_{\text{k\_Total}}$	The total fault current from all connected sources in kV

Chapter 6

MVA_{SC}	Total fault level at the faulty point in MVA
I_{SC}	Symmetrical three-phase fault current in kA
V_{N}	Pre-fault Nominal line–line voltage at the faulty point in kV
G	Set of the connected synchronous generators
g	Synchronous generator $\in G$
I_g^{SC}	Synchronous generator g short circuit current in kA
V_g	Generator Internal line–line voltage in kV
Z_g^{eq}	Equivalent impedance from the internal voltage up to the faulty point in ohm
MVA_g^{SC}	Synchronous generator fault level contribution in MVA
X''_g	Sub-transient reactance of the synchronous generator in ohm
Z_s	Series impedance from the generator terminal up to the faulty point in ohm
$MVA_{g,t}^{\text{SC}}$	Fault level contribution from the synchronous generator at its terminal in MVA
MVA_{g,Z_s}^{SC}	MVA associated with the impedance Z_s
$MVA_g^{\text{SC},*}$	Fault level contribution from the compound generation unit (including the PE-based generator) in MVA
$MVA_{g,\text{t}}^{\text{SC},*}$	Fault level at the terminal of the compound generation unit (including the PE-based generator) in MVA
RES	Set of the connected renewable energy sources
PE	Power Electronic-based generator $\in RES$
MVA_{PE}	PE-based generator rating in MVA
MVA_{T}	Total generation capacity of the compound generation unit (including the PE source) in MVA
$MVA_{PE,\text{t}}^{\text{SC}}$	Fault level contribution from the PE-based generator at its terminal in MVA

$x_g^{"}$	The per-unit value of X'' in p.u.
MVA_g	Synchronous generator rating in MV
α_{PEi}	The overrating factor of the *i*-th PE-based generator
$MVA_{\text{grid}}^{\text{SC}}$	The unchanged grid part fault level contribution in MVA
$MVA_{g,\text{t}}^{\text{SC,Agg}}$	Fault level contribution from the aggregated synchronous generator at its terminal in MVA
$MVA_{g,Z_s}^{\text{SC,Agg}}$	Fault level associated with the aggregated impedance Z_s^{Agg} in MVA

Abstract

The main goal of this thesis is to develop efficient methods for monitoring the fault level in the power system with increased penetration of non-synchronous generations (NSGs). This includes analyzing the dynamics of the fault current, evaluating the steady-state fault calculation methods and proposing new fault level calculation (FLC) methods to accurately quantify the variable fault level in future power systems.

In classical power systems, where a large number of synchronous generators (SGs) are connected, the entire power system has a high fault level (i.e. high short circuit current). This high fault level contributes to a secure and reliable operation of the power system. Particularly, a secure power system protection as protective devices can easily distinguish between a normal (small currents) and faulty (high currents) system state. This is usually aided by the steady-state fault level calculation (FLC) approaches and standards which can accurately provide an estimation of fault currents. This accuracy is a result of the well-understood fault current response of SG, which is traditionally modelled as a voltage behind a reactance in steady-state fault calculations.

However, power systems start changing their dynamic properties due to the increased penetration of renewable energy sources, e.g. wind-farms, photovoltaic (PV), or battery storage systems, as well as decommissioning large SGs to reduce CO2 emission. These types of sources are also referred to as NSGs. They use the Power Electronics based interface, i.e. inverters, to be connected to the existing synchronously operated ac network. Therefore, they have low and a very different fault current contribution, compared to those fed from SGs. Consequently, the dynamic of the short circuit current will potentially change and the accuracy of the fault calculation methods will be under question as this new technology

requires different modelling. Furthermore, the fault level becomes significantly low, directly affecting power system protection and the system strength. As a result of the changes above, a need to monitor both the system fault level and the fault calculation methods becomes critical, especially in future scenarios with high penetration of NSGs.

This thesis proposes a modification of the up-to-date IEC60909 fault calculation standards to include the fault contribution of NSGs more accurately, in addition to a novel FLC method which formulates for the changing fault level as a function of the penetration level of NSGs in the system. This enables the assessment of the system fault level for large numbers of the future grid (FG) scenarios more accurately without a need for a detailed system modelling and/or time-domain simulations. The thesis also proposes innovative solutions to substitute the low fault level as well as to mitigate the negative implications of the low fault level due to the increased penetration of NSGs. The thesis also proposes representative solutions to substitute the low fault level as well as to mitigate the negative implications of the low fault level due to the increased penetration of NSGs.

Declaration

No portion of the work referred to in the thesis has been submitted in support of an application for another degree or qualification of this or any other university or other institute of learning.

Copyright Statement

I. The author of this thesis (including any appendices and/or schedules to this thesis) owns certain copyright or related rights in it (the "Copyright") and s/he has given The University of Manchester certain rights to use such Copyright, including for administrative purposes.

II. Copies of this thesis, either in full or in extracts and whether in hard or electronic copy, may be made only in accordance with the Copyright, Designs and Patents Act 1988 (as amended) and regulations issued under it or, where appropriate, in accordance with licensing agreements which the University has from time to time. This page must form part of any such copies made.

III. The ownership of certain Copyright, patents, designs, trademarks and other intellectual property (the "Intellectual Property") and any reproductions of copyright works in the thesis, for example graphs and tables ("Reproductions"), which may be described in this thesis, may not be owned by the author and may be owned by third parties. Such Intellectual Property and Reproductions cannot and must not be made available for use without the prior written permission of the owner(s) of the relevant Intellectual Property and/or Reproductions.

IV. Further information on the conditions under which disclosure, publication and commercialization of this thesis, the Copyright and any Intellectual Property and/or Reproductions described in it may take place is available in the University IP Policy(see http://documents.manchester.ac.uk/DocuInfo.aspx?DocID=24420), in any relevant Thesis restriction declarations deposited in the University Library, The University Library's regulations (see http://www.library.manchester.ac.uk/about/regulations/) and in The University's policy on Presentation of Theses.

Acknowledgements

I would like to thank my lovely family including my dear dad, my dear mum and my beloved brothers and sisters for all the continuous love, patience, support and encouragement.

I would like also to take this opportunity to thank my supervisor Prof. Vladimir Terzija for his continued support and guidance. I am grateful to him for giving me this opportunity to be a member in his great team and for having patience and confidence in me throughout my PhD journey.

Special thanks to my dear friend Dr. Hesamoddin Marzooghi for his continuous support and feedback on my work under the supervision of Prof. Vladimir Terzija.

I would also like to acknowledge my sponsor Princess Sumaya University for technology (PSUT) through a dean's council under resolution no. ((6) 17-2015/2016).

I would like also to acknowledge support from EPSRC (EP/L016141/1) through the Power Networks Centre for Doctoral Training and the European Union's Horizon 2020 research and innovation programme under grant agreement no. 691800 (MIGRATE project). Also, I acknowledge the motivation coming from Scottish Power through MIGRATE project.

Finally, I would also take this opportunity to thank all my friends and colleagues without any exception, especially those who supported me and helped me during my journey towards the PhD and during my time in Manchester.

1 Introduction

1.1 Overview and Motivation

Sustainability and low carbon emissions are the main driving reasons behind the revolution towards renewable energy sources (RESs). In recent years, RESs have been introduced to the electrical network heavily, as they have started to replace the traditional fossil fuel power generation units. It is not unknown that most RESs utilise power electronics (PEs) technologies to be interfaced with the power grid such as wind and photovoltaic (PV). Thus, they are considered non-synchronous generation (NSG) sources. This gives them different characteristics and brings some operational challenges. As a result, there has been worldwide recognition of the problems associated with the high penetration of NSGs. More specifically, those are entirely connected through PE converters. Such sources do not contribute to the system inertia and fault level as much as the synchronous generators (SGs) do. Consequently, some research projects have been already launched to investigate the challenges associated with increased penetration of NSGs. For example, MIGRATE project which aims to help the pan-European transmission system to handle massive integration of renewable energy. It tries to provide a better understanding of the modified dynamic behaviour of the power system and tackling the negative impacts resulting from the proliferation of PEs [1].

Fault level is one of the key aspects of any power system that should be always known for design and operational purposes. It is expected that the changing characteristics of the RESs will alter the dynamic of the short circuit (SC) currents. In addition, there is a strong potential to operate power systems with reduced fault level, more specifically, after the proliferation of large-scale RES into the transmission system instead of using the traditional SG units.

National Grid, in the United Kingdom, starts to pay attention to the challenge of reduced fault level and the negative implications on the different aspects of the power system due to the increased penetration of NSGs [2, 3]. In [2], it has been reported that the fault level will witness a steady decline in future Scenario with the increased penetration of NSGs and decommissioning of SGs., Fig.1 shows the average decline in the national fault level during the period from 2019 and 2030. This decline is region-dependent as can be shown in Fig.2, which shows the largest decline in the fault level that is expected to occur in the North- East and East midlands.

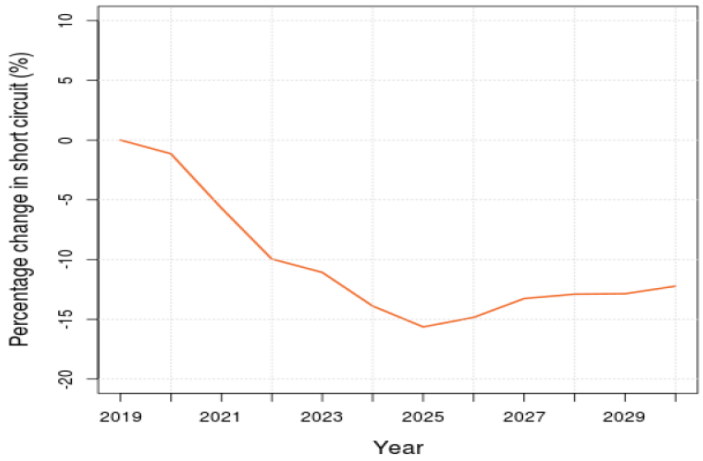

Fig.1: National change in Fault Level 2019-2030 [2]

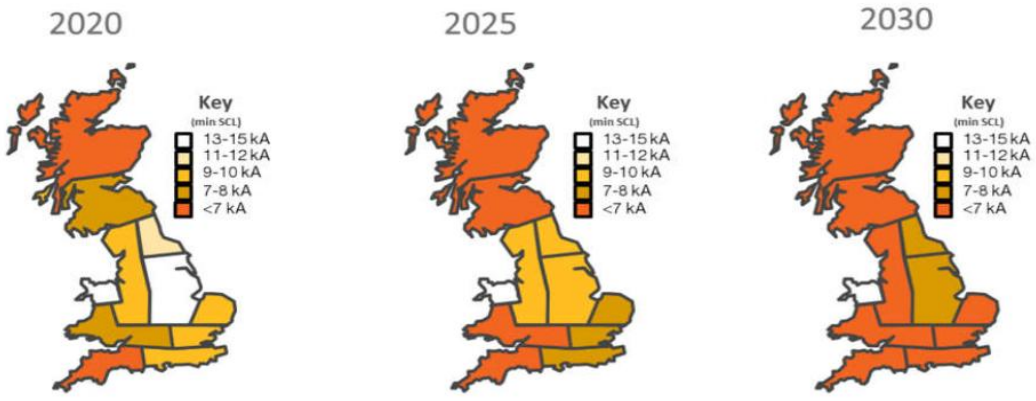

Fig.2: Regional change rates in fault level across UK [2]

In fact, this changing trend in the fault level (i.e. fault level decline) will affect several aspects of the power system including, but not restricted to, protection settings and coordination, system strength and power system stability [1-5]. Therefore, there is a need for monitoring the variable fault level and quantifying the fault level decline on the transmission system at different penetration of NSGs.

Traditionally, such a task could have been easily accomplished by using the steady-state calculation methods and standards (e.g. IEC60909 and IEEE standards) which can provide decent approximations for the fault level [6, 7]. This is due to the full understanding of the fault current contribution from SG and the way of their modelling as they form the main source feeding the faults in classical power systems.

However, in the future scenario where the most of demand is expected to be met by the NSGs (i.e. RESs), the fault calculation methods might be either misleading or they might provide poor estimation for fault currents. This because of the very different characteristics of the fault currents fed from NSGs compared to SGs. The fault contribution of the NSGs depend on several factors (e.g. control, grid code) and cannot be simply modelled as SG in the fault calculation methods [8-10]. This brings a new challenge to the surface and raises a concern about the ways and methods of calculating the fault currents in future power systems with high penetration of NSGs.

Therefore, this thesis aims to propose new tools for fault level calculations in power systems with high penetration of NSGs. This enables tracking the variable fault level in different scenario more accurately in future scenario. To do so, the work focuses on understanding the fault currents fed from NSGs and the correlation between the changing trend of fault level and the penetration level of NSGs. Then, the thesis has discussed the challenges in modelling

of NSGs focusing on the IEC60909 standards and has proposed a modification to include the fault current contribution from NSGs more accurately.

A formulation for the correlation between the changing fault level and the penetration level of NSGs has been proposed and validated against the dynamic simulations and the steady-state calculation methods available in literature. Such formulation has provided an effective way to quantify the expected reduction fault level as a function of the penetration level of NSGs.

Finally, some possible solutions have been also proposed in order to tackle the problem of low fault level in future scenario. These cover the enhanced fault ride through (FRT) capability of the converter, oversizing the converter interfacing the NSGs and installation of synchronous condensers to substitute the low fault levels.

1.2 Project Objectives

The thesis undertakes a comprehensive review on the related literature that covers several aspects: Fault current contribution from NSGs, the impact of the increased penetration of NSGs on the system fault level, the steady-state methods and standards for fault calculation with the presence of NSGs. On the basis of the review, the thesis identifies some primary objectives as follows:

- To investigate the fault current contribution fed from the NSGs considering most of the factors might influence this fault contribution with a focus on control of NSGs and the grid code requirements.
- To analyse the impact of the increased penetration of NSGs on the short circuit response and the fault level.
- To assess the ways of modelling of the NSGs and the accuracy of existing steady-state calculation methods with high penetration of NSGs scenario.
- To modify the up-to-date IEC60909 standards in order to consider the fault contribution from the NSGs more accurately.
- To propose a novel formulation for fault level calculation (FLC) method to quantify the variable fault levels as a function of the penetration level of NSGs in the system.
- To address the negative impact of the fault level reduction, due to the increased penetration of NSGs, and to propose some solutions to improve the fault level profile in future power systems.

1.3 Thesis Outline

The rest of the thesis is divided into eight chapters that are structured as follows:

Chapter 2- Background and Literature Review

This chapter presents a comprehensive background as well as an up-to-date literature review about the theme of fault level in power systems. This covers several aspects and challenges related to the fault level in future power systems with high penetration of RESs. At first, it presents a background and literature on the definition of the fault level showing its importance for different applications. Then, it discusses the requirements for fault level in line with the negative implications which might be manifested in future systems due to the increased penetration of RESs. After that, it provides an overview of the fault current contribution fed from SGs and their modelling for fault calculation purposes. In addition, it presents the concept of NSGs by providing deep-look literature on the fault contribution from these sources considering various factors. Finally, the existing steady-state fault calculation methods and the commercial standards (e.g. IEC60909) are introduced and the ways of modelling and calculating the fault level with a high share of NSGs are also reviewed.

Chapter 3- Analyzing the impact of increased penetration of NSGs on the Fault Level

This chapter analyses the impact of the increased penetration of NSGs on the fault level. It discusses the control of NSGs considering the FRT and grid code requirement. Then, the SC current characteristics of NSGs are investigated under different FRT control strategies. This includes a comprehensive study of the factors, which might affect the fault contribution of NSGs such as the FRT control parameters, the operation conditions and the overrating capability of the generator. Finally, a sensitivity analysis of the SC current characteristics to the penetration level of NSGs is conducted using different test systems.

Chapter 4- Evaluating the accuracy of Steady-state Fault calculation methods with high penetration of NSGs

This chapter studies the performance of steady-state fault calculation (SSFC) methods in power systems with a high penetration of NSGs, i.e. generation connected to the grid over fully rated converter (FRC) technologies. At first, the ways of modelling and representing NSGs in SSFC methods are presented and studied. Then, the accuracy of the existing SSFC methods is evaluated with the increased penetration of NSGs. The results are compared and validated against dynamic simulation results. Finally, it identifies issues and challenges of these SSFC methods when applied for networks with a high penetration of NSGs.

Chapter 5- Proposed Modification of the latest version of IEC60909 standards to consider the fault contribution of NSGs

Chapter 5 presents a proposed modification for the fault calculation method according to the latest version of IEC60909 standard to consider the fault contribution from the NSGs more accurately. At first, the way of calculating the fault currents including NSGs according to the latest version of IEC60909 standards will be presented. Then, the proposed modification considering the reactive current injection according to the FRT and grid code will be explained. Finally, the results of both the current IEC60909 as well as the proposed methods will be validated against the actual fault currents obtained from the RMS simulations.

Chapter 6- Novel MVA-based Fault Level Calculation Method in Future Grid Scenario with High Penetration of NSGs

This chapter proposes a novel fault level calculation (FLC) method to quantify the fault level in future grid (FG) scenario including various penetrations of NSGs, i.e. renewable

energy sources (RESs). The MVA representation of the fault level in classical power system is presented. Then, the proposed methodology for augmenting the FLC method to consider the fault level fed from NSGs is explained and discussed in more detail. Finally, it presents a mathematical formulation of the proposed FLC method including the impact of NSGs on the basis of their penetration level. Finally, the efficacy of the proposed FLC method is demonstrated for large numbers of NSGs' penetration after compared with time-domain simulations and the IEC60909 standards performed in several test systems.

Chapter 7- Possible Solutions to improve the fault level profile in Future Power Systems

This proposes some solutions to substitute the low fault level resulted from the increased penetration level of NSGs. This includes the enhanced FRT capability of the NSGs and installation of Synchronous condensers (Synchronous condensers) in low fault level systems. In addition, it discusses the negative implications of the low fault level on the system strength showing the efficiency of the suggested solutions in mitigating this negative impact due to the increased penetration of NSGs.

Chapter 8- Conclusion and Future Work

This chapter concludes the thesis. It presents the key points and the outcomes drawn from the overall research. It also summarizes the main findings and the contributions of the thesis. In addition, it provides an overview of the potential research and ideas resulted from this thesis for future work.

1.4 Publications from this Thesis

- ***Submitted Journal Papers***

1. **R. Aljarrah**, H. Marzooghi, J. Yu and V. Terzija, "Monitoring of Fault Level in Future Grid Scenario with High Penetration of Power Electronics-Based Renewable Generation". *Submitted to IET Generation, Transmission & Distribution.*

2. **R. Aljarrah**, H. Marzooghi, J. Yu and V. Terzija, "Sensitivity Analysis of Transient Short Circuit Current Response to the Penetration Level of Non-synchronous Generation". *Submitted to International Journal of Electrical Power & Energy Systems.*

- ***Published Conference Papers***

1. **R. Aljarrah**, H. Marzooghi, J. Yu and V. Terzija, "Issues and Challenges of Steady-State Fault Calculation Methods in Power Systems with a High Penetration of Non-Synchronous Generation," *2019 IEEE Milan PowerTech*, Milan, Italy, 2019, pp. 1-6.

2. **R. Aljarrah**, H. Marzooghi, J. Yu and V. Terzija, "Modifying IEC60909 Standard to Consider Fault Contribution from Renewable Energy Resources Utilizing Fully-Rated Converters," *2019 9th International Conference on Power and Energy Systems*, Perth, Australia, 2019,pp. 1-6.

2 Background and Literature Review

This chapter presents a comprehensive background as well as an up-to-date literature review about the theme of fault level in future power systems. This covers several aspects related to the fault level in the classical power systems. At first, it presents a background and literature on the definition and the importance of the fault level. Then, it discusses the requirements for fault level in line with the negative implications that might be manifested in future systems due to the decline in the fault level. Then, it provides an overview of the fault current contribution fed from SGs and their modelling for fault calculation purposes. In addition, it presents the concept of NSGs and provides deep-look literature related to the fault contribution from these sources considering various factors might affect such fault contribution. Then, the existing steady-state fault calculation methods and the commercial standards (e.g. IEC60909 standard) are introduced and the ways of modelling and calculating the fault level with a high share of NSGs are reviewed.

2.1 Fault Level (Definition)

The fault level is a term used to describe either the short-circuit current or the short-circuit power MVA. In this thesis, this term will be used to refer to the short circuit power MVA associated with the maximum current that could flow at a certain point when a fault (i.e. short circuit) occurs at that point in a power system. It provides a measure of the strength or weakness of a system describing the ability to provide both current and voltage at the faulty point. System strength is referred to as the system impedance seen at that point [11]. Thus, a higher fault level (the lower impedance) implies that the power system is stronger at that point and vice versa [11, 12]. In a three-phase transmission system, this is given as follows:

$$MVA_{SC} = \sqrt{3} V_N I_{SC} \quad (1.1)$$

Where I_{SC}, is the maximum symmetrical short circuit current in kA.

The above equation defines the fault level value for the symmetrical condition (symmetrical three-phase bolted fault) based on the maximum SC currents associated with such faults. Note that fault level values depend on several factors mainly on the point at which the fault occurs considering various system voltage levels. In conventional power systems, SGs are considered as the main source providing the SC currents. In such systems, the highest value of the fault current is observed immediately at the instant of the fault initiation, and then the SC current shows a decaying characteristic before reaching its steady-state value [6]. The fault level MVA usually defines the value for the symmetrical condition. It has different values depending on the point at which the fault occurs considering the various system voltages. Table 1, shows some typical values of the fault level according to [13]. It is an important design parameter for the protection coordination and the interrupting capability of the circuit breakers. Using the MVA representation instead of the fault current (kA) might have its advantages. The fault level (MVA) is a better indicator of the stress on circuit breakers (CBs) than the SC current; as the CBs have to withstand the recovery voltage across breaker following the arc interruption [13].

Table 1: Typical values of the fault level for different system voltages

Nominal Voltage (KV)	Fault Level (MVA)
132	5000-25000
33	500-2500
11	10-250

2.2 Importance of the Fault Level

2.2.1 **Power System Protection**

The fault level is an important component in power system protection. It plays a key role in the design and operation of protective devices. While a higher fault level requires electrical components with the higher capability to withstand the fault currents (i.e. higher cost) [14, 15], high fault level contributes to secure and reliable operation of power system protection.

Table 2: The impact of low fault level on different protective device

Protection Scheme	Operating Principle	Impact of Low Fault Level
Differential Protection	Compares the current infeed and output from the equipment; if the difference between the two is greater than bias current; the relay is set to trip.	If the difference between the currents is very small, it may not be detected by the relay. The bias may need to be set comparatively high at times of low short circuit level to avoid mal-operation.
Distance Protection	Calculates the impedance at the relay point and compares it with the reach impedance; if the measured impedance is lower than the reach impedance, the relay is set to trip.	Not affected if the ratio of voltage to current decreases following the short circuit. This ratio however will be affected by the significantly different volumes of synchronous generation at peak and minimum demand and may drive additional settings.
Over Current Protection	The operating time of the relay is inversely proportional to the magnitude of the short circuit current.	This type of protection is the most likely to be affected by low short circuit levels, however these schemes are mainly used for back-up protection and therefore the consequences may not be severe, provided that main protection schemes are not compromised.

In other words, an adequate fault level is required to detect the faults and to allow protective devices distinguishing between normal and faulty conditions. According to recent literature,

it is potentially expected that the decline in fault level would negatively affect the operation of protective devices (e.g. Overcurrent, distance and differential relays) [3, 16-18]. According to national grid in UK [16], it has been reported that the expected decline in the minimum required fault level might lead to maloperation of transmission system protection in Great Britain as shown in Table 2.

2.2.2 **Voltage Support**

Fault level is required to support the grid voltage in normal and abnormal conditions. A low fault level represents ("weak area") with high sensitivity of voltage to changes in power change (both active and reactive). On the other hand, High fault levels represents ("stiff area") with a low sensitivity of a voltage to changes in power change[19]. In other words, low fault level conditions might lead to a significant voltage change in response to change in the power, which might lead to a voltage collapse.

2.2.2.1 Voltage Step Limit (During Switching Events)

Capacitor banks are used for voltage support purposes on large load at both transmission and distribution levels (usually near to large load center) as shown in Fig.3. The voltage step change depends on the strength of the system at the connection point characterised by the fault level. The higher the fault level, the less the voltage changes due to capacitor banks switching. Therefore, a minimum fault level is required to ensure that the voltage step after a switching event is still within the voltage limits (e.g. +/- 5% of the nominal voltage).

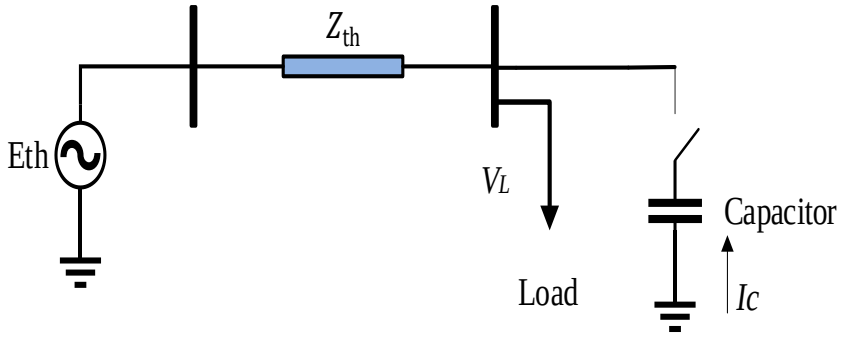

Fig.3: The single line diagram of a capacitor bank switching event

There is a strong correlation between the fault level and the voltage deviation result from such events. The higher the fault levels the smaller the voltage step. The relation between the fault level and the voltage change due to capacitor bank switching is expressed in (1.2).

$$\Delta V\% = \frac{MVA_C}{MVA_{SC}} \times 100 \tag{1.2}$$

Where, MVA_{SC}, MVA_C are the fault level and the rating of the capacitor bank respectively. It can be shown from (1.2) that the voltage step is inversely proportional to the fault level (MVA). Hence, the higher the fault level, the lower the change in the voltage. In other words, a minimum fault level should be available to guarantee the voltage limit when switching a capacitor bank. For example, if a voltage limit is chosen to be 0.1 p.u. (i.e.+/- 10% of the nominal voltage), a minimum fault level that equals to 10 times of the switched capacitor bank rating (i.e. $MVA_{SC} > MVA_C$) is required to avoid violating the voltage limits.

2.2.2.2 Dynamic Voltage Support

During the faults, it is required from the NSGs to dynamically support the terminal and non-terminal voltages in the system by injecting reactive current. This dynamic voltage support helps to limit the voltage dip propagation, achieving a smooth voltage recovery after clearing the faults, and avoiding voltage collapse [20-22].

The level of dynamic voltage support depends on the fault level itself. The voltage dip propagation during the faults depends also on the amount on the strength of the system (i.e. fault level). This requires a certain fault level should be fed during the faults in order to limit the severity of the voltage dip and the affected area as well. Therefore, a shortfall in the fault levels will potentially form a serious challenge for the dynamic voltage support during the fault. Furthermore, the voltage recovery after the fault might potentially be affected. According to [23, 24], the voltage at Bus-i due to a fault at Bus-j ($V_{i,j}$), and the voltage at Bus-j due to a fault at Bus-i ($V_{j,i}$), are correlated to the fault level by the following relations in (1.3).

$$\begin{aligned} \mathbf{V}_{i,j} &= 1 - \mathbf{Z}_{(i,j)} \times I_{SC(j)} \\ \mathbf{V}_{j,i} &= 1 - \mathbf{Z}_{(j,i)} \times I_{SC(i)} \end{aligned} \tag{1.3}$$

Where, $\mathbf{Z}_{(i,j)}$, and $\mathbf{Z}_{(j,j)}$ are the (*ij*) and (*jj*) elements of the *Z-Bus* matrix respectively. Knowing that $[\mathbf{Z}]$ is a symmetrical matrix, then the elements $\mathbf{Z}_{(i,j)}$ and $\mathbf{Z}_{(j,i)}$ are equal. This means that the voltage at a certain Bus during the fault on another Bus depends on the fault level at the faulty Bus itself. In other words, the stronger Bus (e.g. Bus-*i*) which has the has higher fault level (i.e. $I_{SC(i)} > I_{SC(j)}$) will have a higher voltage during the fault (i.e. $\mathbf{V}_{i,j} > \mathbf{V}_{j,i}$) and vice versa.

Hence, the voltage dip propagation from the faulty point to the other Buses in the system not only depends on the transfer impedance between the two Buses (i.e. $\mathbf{Z}_{(i,j)}$), but also on the fault level at each Bus. The higher the fault level the less severe voltage dip will be observed due to a fault on another Bus in the system.

2.2.3 **Stability of Power Electronics-Based Sources**

Most of RESs utilise converters to be interfaced with the grid. This includes those are directly connected sources as well as those connected through HVDC links (e.g. offshore wind). Such sources require a minimum level of system strength to operate properly. It is common to use the short circuit ratio (SCR) to characterize the system strength at the point of connecting the converter to the grid. The SCR is defined in (1.4) as follows:

$$SCR = \frac{MVA_{SC}}{P_C} \tag{1.4}$$

Where,

MVA_{SC} : The fault level (MVA) at the point of common coupling without the contribution from the converter-connected source.

P_C : The rated power of the converter-connected source (MW).

According to [25], the system strength of the ac/dc connection is categorized on the basis of the values of the SCR as shown in Table 3. Operating these sources in low SCR conditions (SCR<3) might lead to failure or instability.

Table 3: Strength of the ac/dc connection

SCR value	**Strength**
SCR >3	HIGH
3>SCR>2	LOW
SCR<2	VERY LOW

2.2.3.1 LCC HVDC Links

Fault level is an important design parameter for HVDC links, more specifically, those which utilise line-commutated converter (LCC). In this technology, the commutation between the switches depends on the line voltage. In weak connection, conditions (i.e. low SCR), the line voltage will be more vulnerable to disturbances. Consequently, operating the HVDC in weak grids (i.e. low SCR) might potentially lead to several issues such as the commutation failure of the valves, overvoltage from load rejections, frequency resonances and voltage instability [26, 27]. These can be avoided by having a sufficient fault level (SCR).

2.2.3.2 Non-Synchronous Generation

NSGs utilise phase-locked loop (PLL) controllers to be synchronized with the grid. PLL tracks the phase and frequency of the grid voltage which is a crucial task for controlling the power transfer between the converter and the grid. However, PLL might not be able to operate properly during the low fault level conditions (weak ac/dc connection) [2, 3, 28, 29]. This is mainly due to the distortion might occur to the voltage in case of disturbances. According to [28], it is difficult to operate the PLL at low SCR and a high gain is required in such conditions for dynamic coefficient adequacy.

Furthermore, these NSGs might not be able to ride through the faults in the case of weak connections. Low SCR means that a severe voltage dip might be observed at the point of common coupling (PCC) in case of severe faults as discussed earlier. Accordingly, converter blocking or instability issues might be faced. As a result, a minimum fault level should be available to guarantee a stable operation of NSGs and the FRT during the fault [29].

2.3 Characteristics of Fault Current in Classical Power Systems

2.3.1 Fault Current Contribution from Synchronous Generator

Traditionally, SG is considered the main source of feeding the SC currents. The characteristic of maintaining the field excitation of the SG allows producing a voltage which gives the generator the capability to keep providing SC current to the faulty point. The SC current produced by the SGs has time-dependent characteristics as shown in Fig.4. It can be observed that the highest value immediately at the instant of the fault initiation, with decaying characteristics before reaching the steady-state value. As can be shown in Fig.4, the SC current shows its maximum contribution initially at the first few cycles (i.e. it might reach up to 10 times the rated current). This can be a result of the air gap flux of the synchronous generator that has its highest value at the instant at which the SC occurs. Thus, the availability of this high flux leads to producing the highest SC current. Note that the initial instantaneous peak current usually includes a dc component.

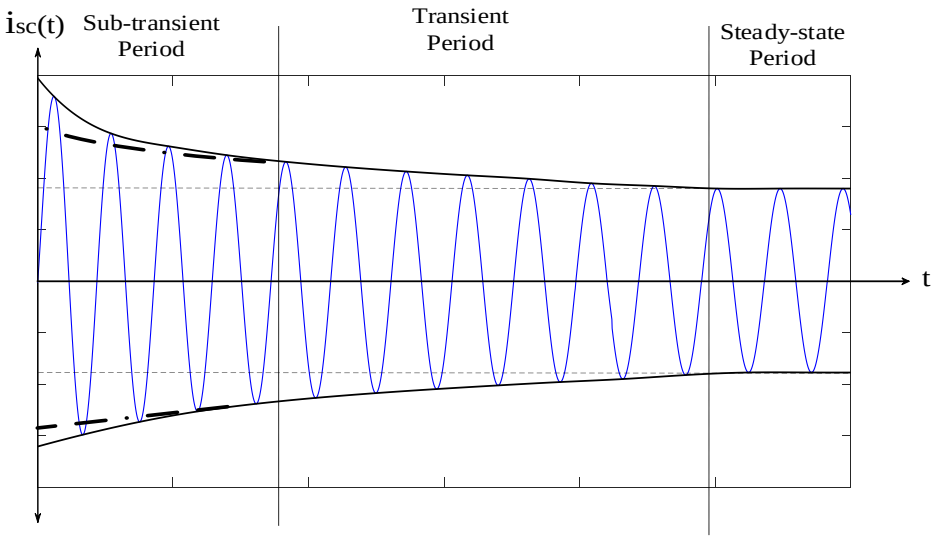

Fig.4: Waveforms of the SC currents of the synchronous generator

This dc has a maximum value if the SC occurs when the voltage at zero. However, the air gap flux starts decreasing with the time, followed by a reduction in the stator current. Accordingly, the generated internal voltage by the air gap flux will be also reduced. As a result, the SC current will show a more gradual reduction by the time. It is worth mentioning that the decaying rate of the SC current and the value of the steady-state current depend on the machine time constants, as well as the regulation of the field current [11, 13, 30].

The fault current from SG behaviour can be divided into three current contributions (i.e. Sub-transient, transient and steady-state component) as previously shown in Fig.4. Therefore, it is a common practice to represent the decaying nature of the SC current by using a varying reactance of three different values to account for these three current contributions. Each period has its importance and used for different purposes. For instance, the sub-transient current is crucial for fault detection while the transient current determines the breaking capability of the circuit breakers. The following section presents more detail concerning modelling the SG for fault calculation purposes.

2.3.2 **Modelling of SG in Fault Calculations**

In order to model the fault response of the SG, a voltage behind impedance (reactance) is usually used. Such a way of modelling has been proven in the literature for its accuracy as it can provide decent approximations for the fault current in steady-state calculation methods with almost negligible errors [11, 13, 30]. As stated earlier, the fault current from SG shows a time-decaying behaviour which is divided into three current contributions (i.e. Sub-transient, transient and steady-state component). To account for these three periods, a varying reactance of three different values is used. In other words, three different circuits are used to model the SC current of SG [30].

- **Sub-Transient Period**

In the sub-transient period, see Fig.5, the Sub-transient reactance, $X^{"}$, includes a leakage reactance of the machine , X_{l}, in searies with a parallel combination of three reactances: armature reaction reactance, X_{a} ,the field windings reactance X_{f} and damper windings reactance X_d. The damper windings are used to provide additional paths for circulating damping currents in a form of solid copper bars run through the rotor [31]. Note that the reactances (X_{d} and X_{f}) appear in the sub-transient equivalent circuit as a result of the induced current at the initial stage of the fault. The equivalent reactance of the sub-transient circuit is expressed in (1.5).

$$X^{"} = X_{\mathrm{l}} + \frac{1}{\frac{1}{(X_{\mathrm{a}})} + \frac{1}{(X_{\mathrm{d}})} + \frac{1}{(X_{\mathrm{f}})}} \tag{1.5}$$

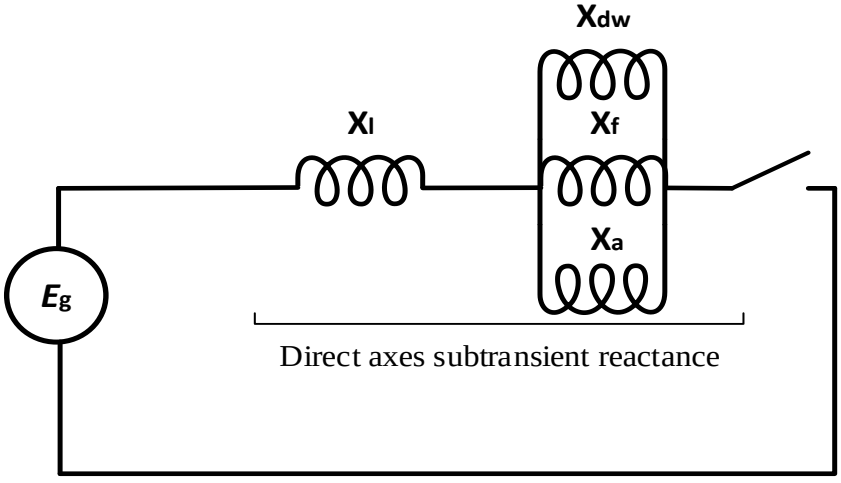

Fig.5: The circuit model of sub-transient fault period

- **Transient Period**

As the damper winding currents die after few cycles, the damper winding reactance is eliminated and replaced by an open circuit as shown in Fig.6. Therefore, the equivalent circuit of the SG during the transient period is limited to the leakage reactance (X_l) in sereas with a parallel combination of two reactances (X_a and X_f) as expressed in (1.6).

$$X' = X_l + \frac{1}{\frac{1}{(X_a)} + \frac{1}{(X_f)}} \tag{1.6}$$

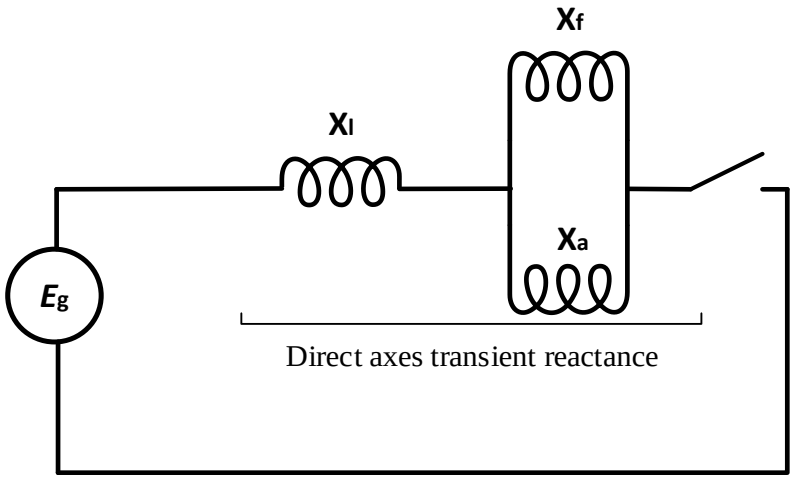

Fig.6: The circuit model of transient fault current

- **Steady-state period**

In this period, the current will show its final value and stop decaying. Hence, the equivalent circuit will be limited to include the leakage reactance (X_l) in series with the armature reaction reactance (X_a) only as shown in Fig.7. The equivalent reactance of the circuit is formulated in (1.7). This means that the currents in the field windings also have already died.

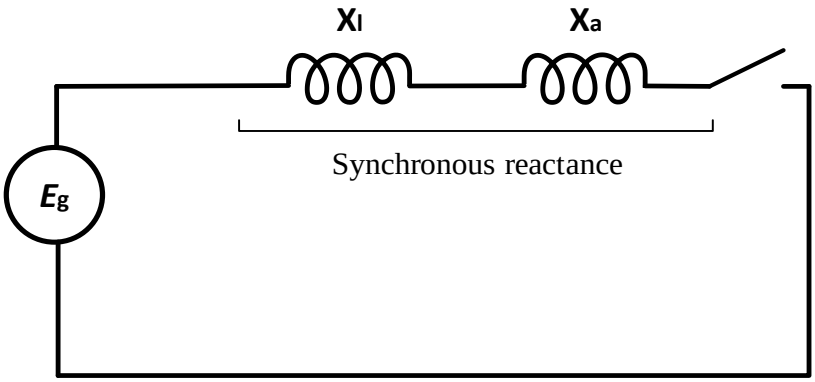

Fig.7: The circuit model of steady-state fault current

Note that this steady-state reactance is also called synchronous reactance or direct axes synchronous reactance in case of salient pole SG.

$$X = X_{\mathrm{l}} + X_{\mathrm{a}} \tag{1.7}$$

Each reactance has a certain value to represent the corresponding period. The typical values of these reactances can be approximated as shown in Table 4 [32, 33].

Table 4: Reactance values during the SC event

Reactance	Symbol	Range per-unit	Period
Sub-transient	X″	0.09 – 0.17	0 – 6 cycles
Transient	X′	0.13 – 0.20	6 cycles to 5 sec.
Synchronous	X	1.7 – 3.3	after 5 sec.

2.4 Steady-State Fault Calculation Methods

Fault current calculations are required for planning and operation studies in power systems. Simplicity, a need for less detailed network modelling, and speed are the main reasons behind using the SSFC methods for fault current estimations instead of the detailed and time-consuming dynamic simulations [34]. There are two main SSFC methods for fault current estimation including: 1) the equivalent voltage source method, and 2) the complete (superposition) [11, 34, 35].

2.4.1 The Equivalent Voltage Source Method

This method applies a voltage source at the faulty point after neglecting other voltage sources in the system. It represents the system during the fault condition by the equivalent impedance seen by the faulty point connected to a voltage source. The equivalent impedance includes other system elements, which are represented by their corresponding impedances in the equivalent circuit for fault currents estimation. In the equivalent voltage source method, pre-fault conditions and load currents are ignored, but correction factors are used instead to represent their impacts in the fault estimation. Most of fault calculation standards such as the IEEE [7] and the IEC60909 [35] standards are on the basis of this methodology. In the IEC60909 standard, the nominal values of the system parameters are considered with correction factors for the pre-fault voltages and impedances. These methods, however, may provide conservative estimations for fault currents. In IEC60909 standards, where the equivalent voltage source method is considered, the nominal values of the system parameters with correction factors for the voltages and impedances. Although this might give an extreme estimation for SC currents, IEC60909 standards have been accepted in many countries. These standards are mainly used for planning purposes when the operational conditions are not

known. They are applicable in both low voltage, and high voltage three-phase AC systems operating at 50 Hz or 60 Hz. The main assumptions that used to calculate the SC currents on the basis of IEC60909 standards are:

- The three-phase SC occurs on all phases at the same time.
- The number of the faulted phases is maintained constant during the whole fault period.
- The pre-fault conditions and the load currents are not considered.
- The considered voltages are the nominal values.
- Correction factors are applied to the nominal voltages to guarantee the conservative results for both minimum and maximum SC currents.

In fact, any calculation method aims to represent the current as a function of time at the faulty point during the SC event, from the initiation to the end as shown in Fig.8. However, IEC60909 standards for SC calculation [6, 35], define some parameters to characterize the SC current waveform, as shown in Fig.8. These parameters can be concluded in the following points:

- Initial symmetrical short-circuit current $(I_k^{''})$: The RMS value of the AC symmetrical component of a prospective (available) SC current, which is applicable at the instant of a SC if the impedance remains at zero-time value.
- Peak instantaneous SC current (I_p): The Maximum possible instantaneous value of the prospective (available) SC current.
- Steady-state SC current (I_k): The RMS value of the SC current that remains after the decay of the transient phenomena.

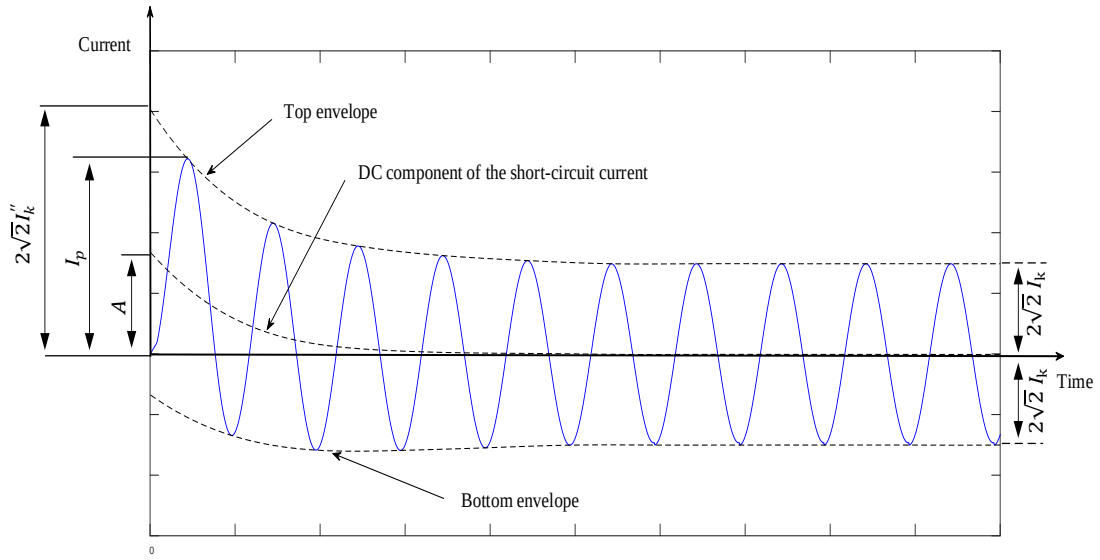

Fig.8: SC current according to IEC60909 (far-from-generator fault)

- DC component of SC current (i_{DC})
- The Initial value of the dc component (A)

In such a method, the initial symmetrical fault current is calculated firstly, and then the other fault components are calculated on the basis of this value. The calculation procedure for the initial symmetrical fault current will be discussed in chapter 5.

2.4.2 **The Superposition (Complete) Method**

This method is known for its improved accuracy compared to the equivalent voltage source method. It considers the pre-fault load flow information to determine the accurate voltage at the faulty point without using correction factors. In the complete method, the calculated pre-fault negative operating voltage is applied at the faulty point, while the other voltage sources are neglected. Further, it considers the effects of the excitation for all generators, tap positions of transformers, and the status of circuit breakers. By adding both pre-fault and fault

results from their corresponding circuits, this method determines the system conditions after the fault assuming that the system impedances are linear.

So far, the above methods have provided reasonable estimations of system fault currents in the conventional power systems. However, their performance and accuracy in power systems including high penetration of NSG may not be satisfactory. This will be investigated and discussed in more detail in the following chapters.

2.5 Background and Review about Non-Synchronous Generation

2.5.1 Fully-Rated Converters Technology

FRC technology is becoming popular in modern power systems [31, 36]. This new technology is currently used in connecting different RESs (such as type-4 wind, PV, and fuel cell), as well as to transmit the electrical power through HVDC links. Moreover, FRC-based wind turbines (i.e. type-4 wind turbines) are expected to be dominating the future market due to their advantageous properties such as full power and speed controllability, decoupled control of active power and voltage regulation and a better grid support capability [36-38]. Regardless of the type of the electrical generator (conventional SG, a permanent magnet or as an asynchronous generator) the entire power is transferred to the grid side through AC-DC-AC converter in case of wind. Fig.9 and Fig.10 show a typical configuration of the FRC technology in Type-4 wind and PV system respectively.

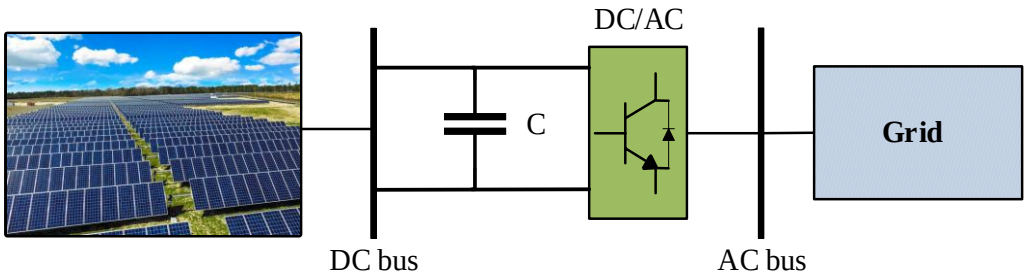

Fig.9: A Fully-rated converter technology in PV system

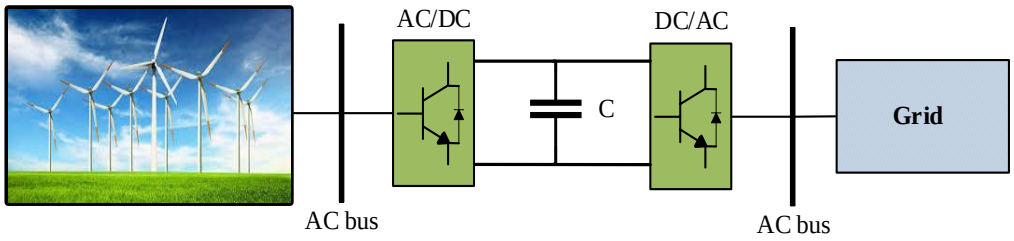

Fig.10: A Fully-rated converter technology in Type-4 wind

However, a DC-AC converter is used in the case of PV systems. Due to the fact that all the power at the generator side is transferred through the power converter, the generator characteristics and dynamics are completely isolated from the grid. Consequently, the grid side converter and its controller play a key role in determining these dynamics including the response during the faulty conditions.

2.5.2 **Control of Non-synchronous Generation**

The control of the NSG is usually simplified to consider only the grid side converter. This is because the dynamic of the generator side is isolated from the grid. It is used to control the active power (by controlling the DC voltage) and the reactive power (or the ac voltage) delivered to the grid. The structure of the classical controller consists of cascaded controllers: outer P-Q controller and an inner current controller [39-47]. The P-Q controller compares the measured active and reactive power values with the corresponding set points before it applies a control action by employing PI controllers.

The output of the P-Q controller form references of the active and reactive currents, which will be fed to the inner current controller. Then, these reference currents will be compared with the measured values and then controlled using faster controllers. Those regulated currents determine the commanded output voltages, which are fed to the converter through the pulse width modulator. It is worth pointing out that this is usually done in the synchronous d-q frame with the assistance of a PLL which provides the reference angle. Fig.11, shows the structure of the grid side converter [47].

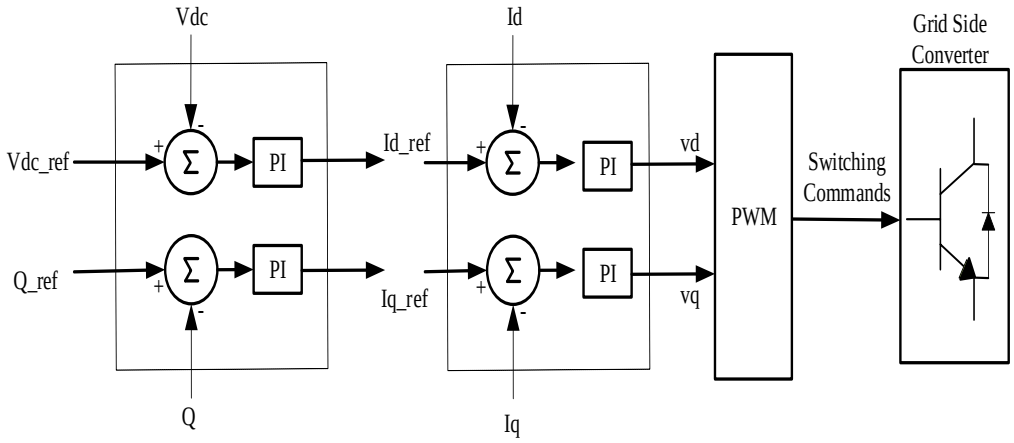

Fig.11: Control of NSG during normal conditions (grid side converter)

2.5.3 **Fault Ride Trough and Grid Code Requirement**

Grid codes are specifications and rules, which define the technical requirements for connecting generation units to the grid. These requirements are defined by the Transmission System Operators (TSOs) to ensure reliable and stable grid performance [48, 49]. FRT capability, also referred to as Low Voltage Ride Through (LVRT), is one of the key aspects of grid codes defining the rules for connecting RESs to the grid [48, 50-54]. It defines the required performance of the connected RESs during the faulty conditions. FRT requirements are mainly used to maintain the continuity of the supply and to avoid any potential generation loss during and after severe faults [55, 56]. Traditionally, the contribution of RESs to systems fault currents was negligible. However, with the increased penetration of such resources, most power system operators and grid codes require RESs to ride through the fault. Hence, RESs are required to remain connected during system faults. The FRT requirements of RESs vary among the countries depending on several factors such as the penetration level of RESs, the size of the generation unit and the robustness of the grid [48, 55]. In Europe, the European network of transmission system operators for electricity (ENTSO-E) requires from each TSO to provide a voltage-against- time profile defining the FRT requirement of the generators connected at the transmission level.

Table 5: The parameters for the FRT profile as defined by ENTSO-E

Voltage Parameters (p.u.)		**Time Parameters (s)**	
$\mathbf{U_{ret}}$	0.05-0.15	t_{clear}	0.14-0.25
$\mathbf{U_{clear}}$	U_{ret}-0.15	t_{rec1}	t_{clear}
$\mathbf{U_{ret1}}$	U_{clear}	t_{rec2}	t_{rec1}
$\mathbf{U_{ret2}}$	0.85	t_{rec3}	1.5-3.0

While Fig.12 shows this FRT profile, Table 5 provides a guidance for the values of these parameters as defined by ENTSO-E [57]. Fig.13 also shows the FRT profiles defined by

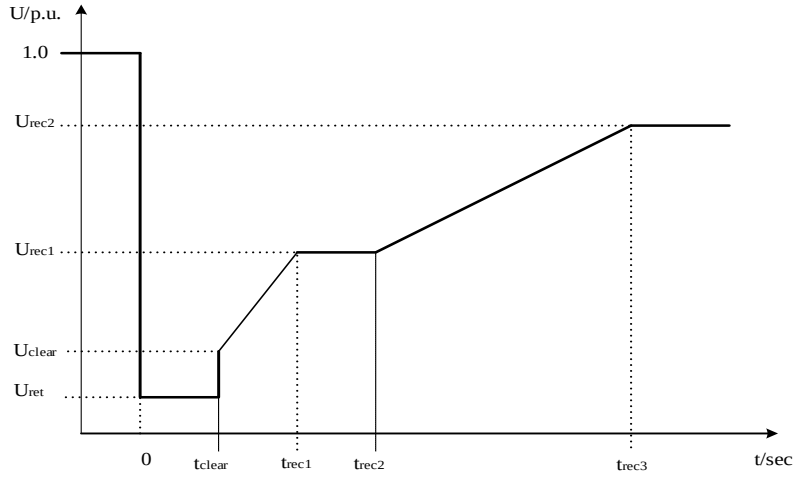

Fig.12: The FRT profile of a Power Generating Module according to ENTSO-E

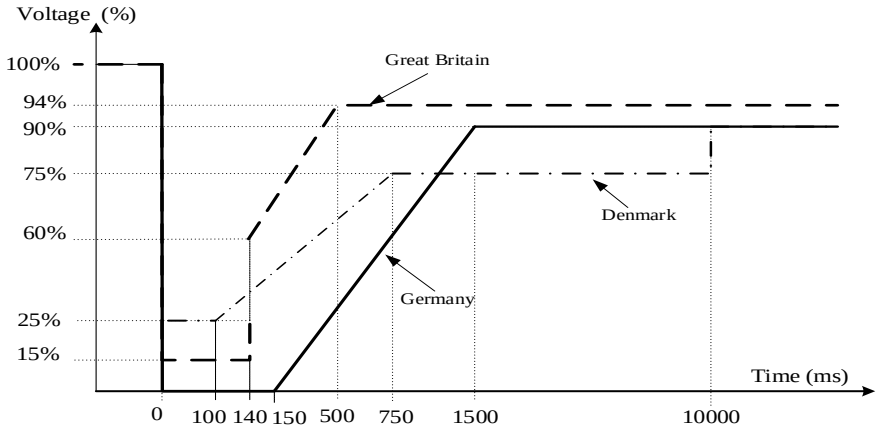

Fig.13: The FRT requirements for Denmark, Germany and Great Britain

different national grid codes such as Denmark, Germany and Great Britain[58]. In most of the grid codes, RESs are not only required to remain connected to the grid during system faults, but also to provide dynamic voltage support. In other words, they should be able to inject reactive current during the voltage dip period [48-53, 55, 57-61]. This additional reactive current injection helps to support the voltage dip during the fault, recovering the voltage after the fault and providing enough fault current required for protection systems [59]. Note that grid codes define a positive sequence current injection (i.e. balanced currents) even in the case of unbalanced faults [62]. However, some recent work starts to consider the negative sequence control and the injection of unbalanced currents during unbalanced faults [63-66]. The value of the injected reactive current depends on the FRT control that varies according to the used grid code. While some grid codes entail the NSGs to inject the maximum reactive current during the fault like Great Britain [67] and Denmark [68, 69], others define a proportional gain (e.g. German grid code) [60, 62]. Fig.14 shows the requirement for reactive current injection during the voltage dip according to the German grid code [62].

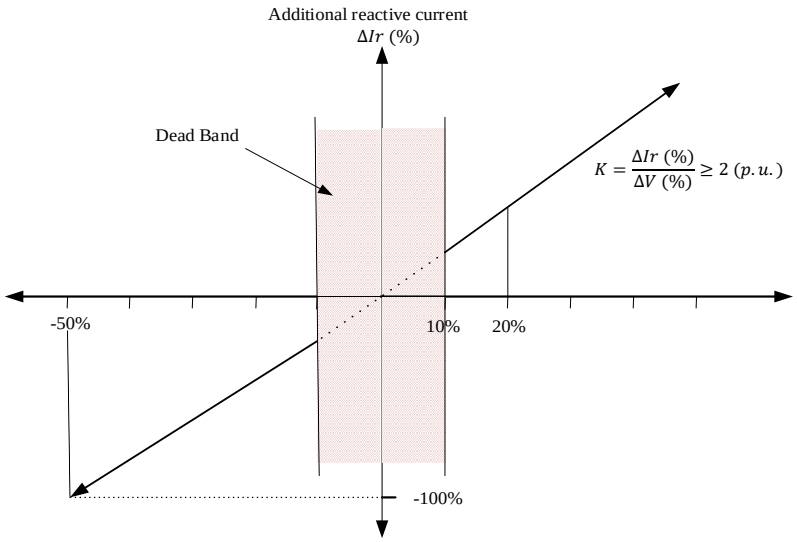

Fig.14: The requirement for reactive current injection from RES during the low voltage conditions according to German grid code

This gain is referred to as k-factor and it can have any value between 2 to 10 (i.e. 2<K<10) with *k*=2 as a default value. In the present, the control of the converter and the reactive current injection strategy will be only restricted to the positive sequence control. However, the control of the converter will be adjusted to allow for applying different grid code requirements if needed.

2.5.4 **Short Circuit Current Behaviour of FRC-based NSG**

As discussed above, most grid codes require RESs to remain connected during the faults and to dynamically support the voltage by injecting reactive current. Consequently, the fault current contribution from the RESs cannot be ignored anymore, especially in power systems with high penetration of RESs. Generally speaking, NSGs may provide low fault currents (e.g. small values above the rating of the generator) compared to SG, which might provide high fault currents as shown in Fig.15. Observe the difference between the fault currents in both the value and the dynamic characteristics with time.

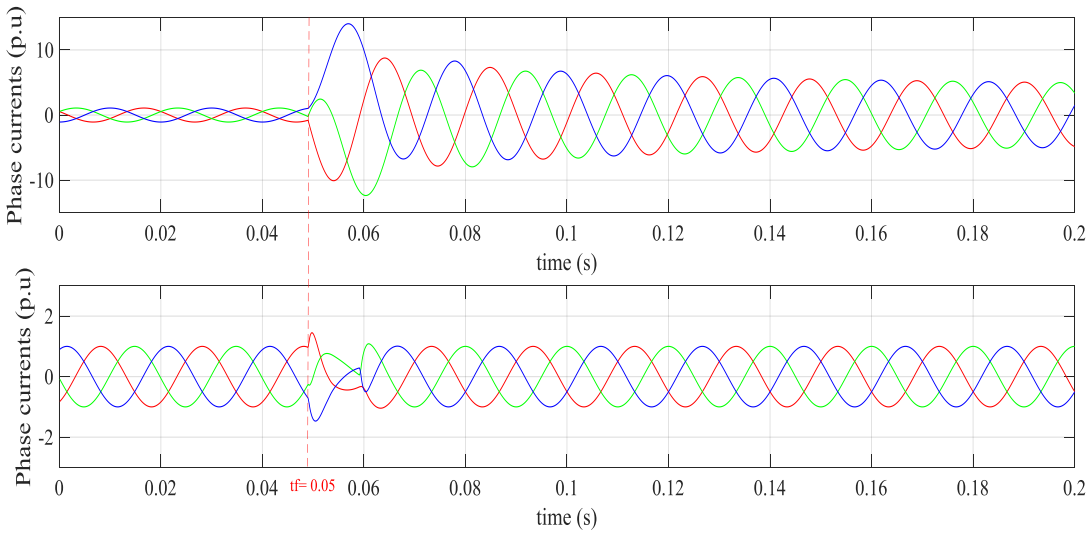

Fig.15: The SC current from a 50 MVA generation unit in response to a three-phase bolted fault at the generator terminal:a) SG, and b) FRC-based NSG (type-4 wind)

In general, the fault current of NSG is limited to protect power electronic switches that have limited overrating capability. Beside the reactive current injection during the voltage dips, several factors affect the fault contribution from the NSGs (e.g. FRC rating, control and the pre-fault operation conditions).

Note that this will be studied in more detail later, considering most of these factors might influence the fault response of the NSG during the faults. Recently, a considerable amount of literature has been published on the fault contribution of NSGs. These studies can be categorized into two main classes: Those focused on investigating different characteristics of SC currents supplied from NSGs considering different FRT control strategies [8-10, 59, 70-85]. Those studied modelling and representation of the NSGs in steady-state fault calculations [9, 35, 86-90].

Generally, the fault contribution includes a very fast transient followed by a steady-state current. In recent literature, there is no clear insight regarding neither the lasting time nor the value of this immediate fault contribution from NSG utilising FRC. However, some research has pointed to this transient fault current which might usually be observed immediately at the instant of the fault. As far as the steady-state fault contribution is concerned, the FRT control and the overrating capability of the converter define the upper limit of the steady-state fault current supplied from the NSGs. It is also limited to around the rating of the Power Electronic converter connecting the NSG to the AC grid. For instance, according to [11], the RMS transient fault contribution of NSG is limited to 0.28 p.u. of the rated current in response to a bolted fault at the PCC. For this approximation, it has been assumed that, prior to the fault, the converter is operated at the rated values with no additional reactive current injection during the FRT control.

In [72], FRC-based NSG might contribute to a transient current of value between 1.1 p.u. and 1.5 p.u. depending on the pre-fault operating condition and the retained voltage during the fault. It also claimed that the initial transient fault current might be observed within 1 to 2 cycles from the fault inception. However, the steady-state fault contribution depends on the FRT control and the injected reactive current, which also will be limited according to the overrating capability of the converter.

Another study in [73] states that the maximum RMS value of the transient fault current might range between 2 to 3 p.u. in the first 2 cycles. While the steady-state fault current ranges between the pre-fault load current magnitude as a lower limit, and an upper limit of (1.5 p.u.).

Researchers in [78], investigated the fault current contribution of a 3 MW photovoltaic system connected to a medium voltage power system. The results have illustrated that the inverter has a small peak current during the transient period. In addition, this transient current contribution has only a duration of some milliseconds (ms). In terms of the steady-state fault current, it is mentioned that PV inverters could be able to supply a positive sequence current even for unsymmetrical faults. This current might exceed 1.0 p.u. depending on the overload current limitation of the generation system.

In [74], the converter of the NSG contributes to a limited steady-state fault current according to the converter current limiting module which switches to a pre-defined fault current reference of (2 p.u.).

A 1 MW inverter has been tested in an experimental study in [70], the inverter had the capability to remain connected during the fault (i.e. FRT capability), and it contributed to a steady-state fault current of approximately 1.2 times the rating of the converter. This current could last until 7 cycles from the time of the fault initiation.

According to some technical information about the PV inverters provided in [82], the SC current can be characterised by three components: first, a very fast transient (e.g. lasts for less than 40 μs) which might have a high instantaneous peak value, e.g. might reach up to (5 p.u.). Second, an initial symmetrical RMS current which might reach up to (1.4 p.u.) and lasts for less than (30 ms) Third, a steady-state symmetrical RMS current of 1.0 p.u. and lasts till clearing the fault.

Researchers in [76], stated that the fault current contribution is limited to small values due to the fast control action used to protect the power electronics. They have studied the fault response of type-4 wind generator when a three-phase fault has been initiated at the point of connecting the wind power plant to the transmission system. The results of the study showed a momentary peak transient, which equals to (2.4 p.u.), has been observed initially in the first half cycle. After that, a steady-state current has followed the initial transient and lasts to till clearing the fault. It is reported that the steady-state current has a slightly higher value than the pre-fault loading current. However, it has been mentioned that this current will not exceed 110% of the generator rating as a maximum.

2.5.5 **Modelling of FRC-based NSG in Steady-State Fault Calculations**

Much of the current literature on the fault currents of NSGs pays particular attention to the way of modelling and representation of the NSGs in steady-state fault calculations. This has taken exceptional importance in power systems with high penetration of NSGs. Particularly, some literature has pointed to the necessity need to look for alternative modellings for NSGs as the traditional model (i.e. a voltage behind an impedance) will not be valid anymore for NSGs [9, 35, 76, 86-91]. Overall, most of the studies have suggested modelling the NSG as a

current source due to the limited fault current contribution. This current usually represents the injected reactive current according to the FRT control.

In [11], a positive sequence current source is proposed for modelling the fault current supplied from NSG (i.e. type-4 wind generator) to the grid. This current, which does not have any dc component, might reach up to (3.0 p.u.) according to the FRT control.

Another study in[90], has also used a current source model to represent the response of the PV generation under fault conditions. It has stated that the value of the current source is controlled by the amplitude of the positive sequence voltage at the PCC.

One more study has suggested a constant 3-phase balanced current source to model the NSG [91]. This current might be pure reactive or has both active and reactive components depending on the prior setting of the controller.

On the other hand, some literature has proposed a model for SG representation (i.e. voltage behind impedance). However, the variable impedance will be assumed to limit the fault contribution of the NSG. The impedance will be adjusted iteratively to obtain the appropriate pre-defined fault contribution [76].

Although such studies provided valuable insight into the fault current contribution of NSGs, they were mostly restricted to analyzing the faults at the PCC using time-domain simulations. Moreover, the impact of the penetration level of NSGs on the fault level has not been considered into account especially at the transmission system fault level.

2.6 Calculation of Fault level in systems with high penetration of NSGs (review)

Recently, few methods have been proposed for FLC with NSGs [92-100]. The application of IEC60909 standard for fault calculation considering the NSGs, was first investigated by researchers in [92]. The work has proposed extending the provisions of the IEC60909 by a current source representation of the NSGs with a pre-defined fixed fault current contribution. The fault contribution of NSGs sources (type-4 DGs) is algebraically added to the fault current contribution from the other sources. However, the adopted method has been tested using a distribution feeder only. In addition, the authors have highlighted the need to revise both IEC60909 and IEEE standards for short-circuit current calculations to consider the NSGs more accurately.

In the updated version of IEC60909 [35] has also utilised the current source representation for NSGs which was proposed in [92]. After that, some researchers have adopted the recommendation of the new version of IEC60909 standard in modelling and calculating the fault current of NSGs. For example, recent studies in [93, 94] have assumed a fixed contribution from the NSGs according to the overrating capability of the converter. The current, purely inductive, has been modelled as a current source and added to the fault current from the SGs using the principle of superposition.

Conversely, other studies have argued that an iterative-based method to manipulate the impedance in the classical SG model (i.e. a voltage behind an impedance) to account for the fault contribution from NSGs. In [95], IEC60909-based iterative method is proposed to consider the dynamic voltage support and the fault current from RESs.

According to [96], an adaptive fault calculation algorithm has been suggested to consider the fault contribution of the NSGs. The algorithm is on the basis of power flow as it uses iterative technique such as the Newton–Raphson method. It deals with the Bus connecting the NSG as a PQ Bus during fault in case the fault current contribution is less than the maximum threshold current the inverter can carry. On the other hand, it assumes a constant current source mode in case of the inverter current exceeds the maximum threshold current. Although researchers have claimed that the proposed algorithm was convenient for fault calculation with NSG for all fault types, their validation has been restricted to a simple system.

The study in [98] has suggested an equivalent circuit to represent the transient and the steady-state fault contribution of VSC-based RESs. However, the suggested method requires measured short-circuit current waveforms to extract a full current expression and equivalent circuit. Moreover, a relative error of (10%) might be expected when using that method on a system scale studies.

An algorithm has been proposed to calculate the fault current on distribution feeders with high penetration of PV systems in [99]. At first, the algorithm calculates the nodal voltages and the branch current during the fault. Then, the injected current from the PVs has been calculated on the basis of the terminal voltage using an iterative method. However, a value of (2 p.u.) has been assumed as an upper limit for the injected current from the inverter. Although the researchers have provided an accurate estimate, they have only presented results from a distribution feeder. In addition, neither detailed equations nor mathematical explanations for the proposed fault level calculation method have been presented in the work.

In [100], a universal fault current calculation model has proposed to allow better considering of the fault contribution from the NSGs. The work has theoretically analysed the fault current

characteristics of NSG considering the (FRT) ability. Although researchers have shown the validity of the proposed analytical model in fault calculation through simulation and experimental test, the results have only been validated using a simple test system for a fault at the PCC of the NSG.

Overall, these studies have provided valuable insight into the theme of fault calculation with NSGs. However, they were either restricted to analyzing the faults at the point of common coupling (PCC) using time-domain simulations, or they only considered the distribution system without providing adequate validation for the proposed methods on a system scale studies with high penetration of NSGs. These necessitate a need to augment the existing modelling methodologies of NSGs and the steady-state fault calculation methods to better represent the dynamic behaviour of NSG utilising FRC for such analysis.

To best of author's knowledge, no studies have so far attempted to formulate the correlation between the fault levels in power systems and the penetration level of NSGs. Hence, this thesis intends to calculate the fault level in transmission systems with high penetration of large scale NSGs resulting in decommissioning of SGs. While these calculations can be directly done using the dynamic simulations (RMS, EMT), it would be inconvenient to use such simulations in large networks with high penetration of NSGs. This is due to the high computational effort and detailed modeling requirement in dynamic simulations which use differential equations and small simulation steps to capture the dynamics of the fault currents. This necessitates a need for developing alternative methods to consider the fault contribution from NSGs in large networks in simple and reliable way. Hence, this thesis proposes a novel FLC method, which is based on generic modeling, to provide an efficient and quick fault calculations in power systems with high penetration of NSGs with less computational efforts.

Such FLC formulation might also provide efficient guidance regarding margins for the maximum allowable penetration level of PE-based generation for system operators. In addition, this thesis will propose a modification for the way of considering the fault contribution of NSGs in the up-to-date IEC 60909 standard.

3 Analyzing the Impact of Increased Penetration of NSGs on the Fault Level

This chapter analyses the impact of the increased penetration of NSGs on the fault level. It discusses the control of NSGs considering the FRT and grid code requirement. Then, the SC current characteristics of NSGs are investigated under different FRT control strategies. This includes a comprehensive study of the factors might affect the fault contribution of NSGs such as the FRT control parameters, the operation conditions and the overrating capability of the generator. Finally, a sensitivity analysis of the SC current characteristics to the penetration level of NSGs is conducted using different test systems.

3.1 Control of the NSGs Considering the Fault Ride Through

In order to meet the grid code requirement, the control of the grid side converter will switch to FRT control during the faults. To do so, the voltage at the entry point with the grid is continuously measured and then fed to an additional block (i.e. FRT block) which determine the reactive power requirement and switch from the normal condition to the faulty condition on the basis of the voltage level. Fig.16 shows the control structure of the grid side converter during the FRT. Once a voltage dip is lower than a threshold value (i.e. dead-band), the FRT control re-calculate the new reference currents on the basis of the additional reactive current injection requirement considering the maximum overrating capability of the converter. These currents feed new values to the inner current controller to adjust the PWM commands accordingly. It is worth mentioning that the new reference currents are calculated in such a way to prioritize the reactive current injection for voltage support purposes. Commonly, the active current component will be limited to allow for more injection of reactive current.

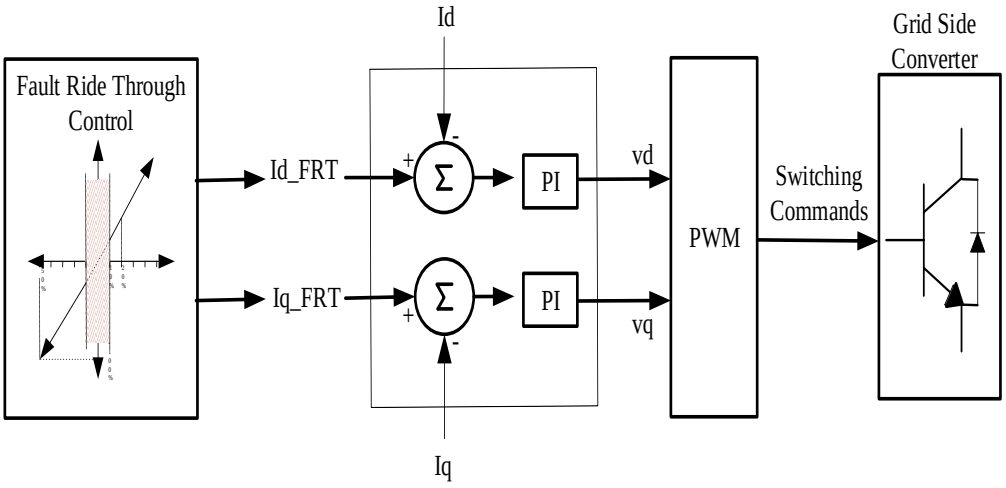

Fig.16: Control of NSG during the faulty conditions (grid side converter)

To do so, the controller of the grid side converter is adjusted in such a way to consider the above-mentioned proportional gain (i.e. *k*-factor) to correlate the reactive current injection according to the voltage dip level seen by the converter interface during the fault, as expressed in (3.1). A *k*-factor of 2 implies that the injected reactive current is twice proportional to the voltage dip seen by the converter. Then, the active current, I_{Active} , is determined on the basis of the injected reactive current, I_{Reactive}, in such a way to allow for more reactive current injection without exceeding the maximum combined current, I_{Max}, as expressed in (3.2). It is worth pointing out that this maximum combined current depends on the overrating capability of the converter interface. It has typical value around the rating of the NSG which might range between (1.1 -1.4 p.u.).

$$I_{\text{Recative}} = k \times \left| V_{\text{Threshold}} - V_{Measured} \right| \tag{3.1}$$

$$I_{\text{Acative}} = \sqrt{I_{\text{Max}}^2 - I_{\text{Reactive}}^2} \tag{3.2}$$

Where, $V_{\text{Threshold}}$, V_{Measured} are the voltage at which the FRT control will be activated and the measured voltage during the fault in p.u., respectively. Note that if the total reactive current

exceeds the maximum limit (i.e. the maximum overrating capability of the FRC), then (3.1) and (3.2) become as follows:

$$I_{\text{Recative}} = I_{\text{Max}} \tag{3.3}$$

$$I_{\text{Acative}} = 0 \tag{3.4}$$

Note that a threshold voltage of (0.9 p.u.) is usually defined to activate the reactive current injection under the FRT control mode.

3.2 Fault Response of NSGs Considering Different FRT Control Strategies

We firstly investigate the SC current characteristics of NSGs under different FRT controls. For this purpose, a 50 MW wind farm on the basis of FRC technology (i.e. type-4) including 10 wind turbines (i.e.5 MW per each turbine) is modelled for this assessment here and connected to the grid, as shown in Fig.17. It is worth mentioning that the dynamic of the FRC is determined on the basis of positive sequence control with the FRT capability and injecting reactive current requirement according to various grid codes. The control structure of the grid side converter is already explained in more detail in the previous section. The fault response of the wind farm to different faults is monitored assuming different FRT control strategies as follows:

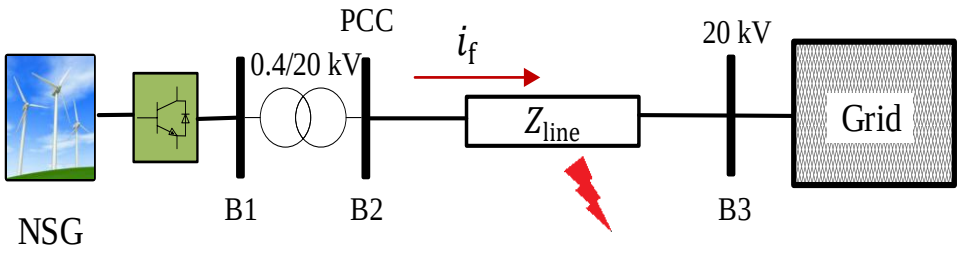

Fig.17: The single machine-infinite Bus test system

- $\boldsymbol{FRT_{NQ}}$**:** FRT capability without reactive current injection during the fault.
- $\boldsymbol{FRT_{IQ}}$**:** FRT capability with an immediate reactive current injection during the fault (0 ms delay).
- $\boldsymbol{FRT_{DQ}}$**:** FRT capability with a delayed reactive current injection during the fault (20 ms and 50 ms delay).

For the last control strategy, FRT_{DQ}, where the reactive current injection is delayed, the controller of the converter is designed to inject the reactive current after a specific time of detecting the fault. These values are 20 ms and 50 ms, which represent delays of 1 and 2.5 cycles respectively.

3.2.1 Fault Response without Reactive Current Injection during the Fault ($\boldsymbol{FRT_{NQ}}$)

The SC current contribution from the NSG is monitored in response to different faulty conditions under the $\mathbf{FRT_{NQ}}$ Control. This assumes that the NSG has the capability to ride through the fault and to stay connected but without additional reactive current injection. It is worth mentioning that the faults have been initiated at the voltage zero-crossing to observe the value of the maximum instantaneous peak in all cases. Further, the impact of the different output power from the wind farm as well as the different voltage dip levels seen at the PCC (i.e. due to different fault impedances) have been investigated in this section. The results imply that the NSG's fault contribution is decomposed into two components: 1) an initial transient component (observed in the first cycle after the fault inception), and 2) a steady-state component which last to the end of the fault period. The following discussion illustrates the impact of the output power as well as the impact of the voltage dip level considering the FRT_{NQ} control as shown in Fig.18 and Fig.19.

3.2.1.1 Impact of the Output Power

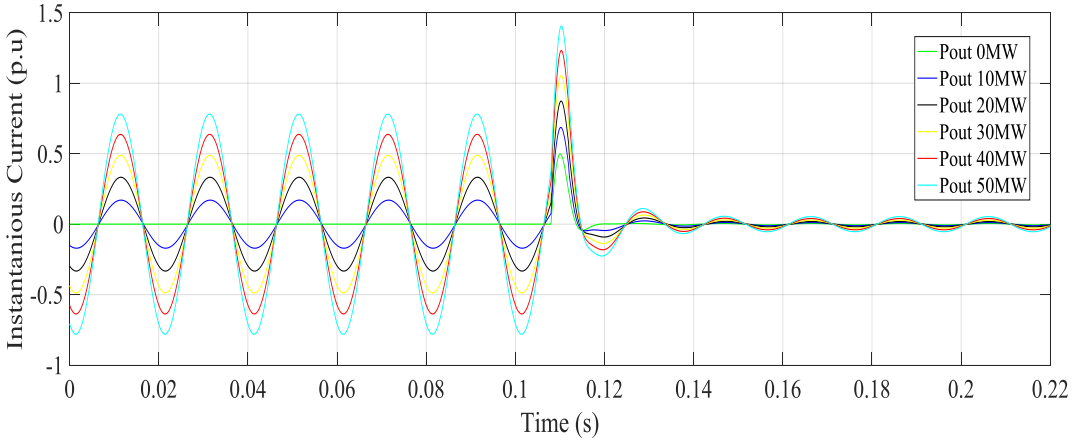

Fig.18: The SC current from the NSG during (FRT_{NQ} control) at different output power

Fig.18 shows that the initial transient has a significant relationship with the output power from the wind farm. It can be seen that the maximum instantaneous value, which occurs output power. Specifically, it ranges between (0.5 p.u. to 1.4 p.u.) corresponding to the minimum and maximum output power of the wind farm, respectively. However, the steady-state fault contribution is almost negligible after this first peak as shown in Fig.18.

3.2.1.2 Impact of the Voltage Dip Level (Fault Location)

On the other hand, Fig.19 also shows the NSG's fault contribution considering the impact of the voltage dip observed at the PCC (V_{PCC}). A wide range of values have been assigned to the fault impedance in order to produce different voltage dip levels (i.e. from 0.0 p.u. to 0.8 p.u.) to account for different fault locations. To observe the maximum fault contribution, it is assumed that the wind farm is operated at its maximum output power (i.e. 50 MW). The results show that voltage dip level has a remarkable influence on both the initial transient and steady-state fault components. Observe that the maximum instantaneous value of the fault contribution happens initially after the fault inception when (V_{PCC}=0.0 p.u.) of around 1.4 p.u. approximately.

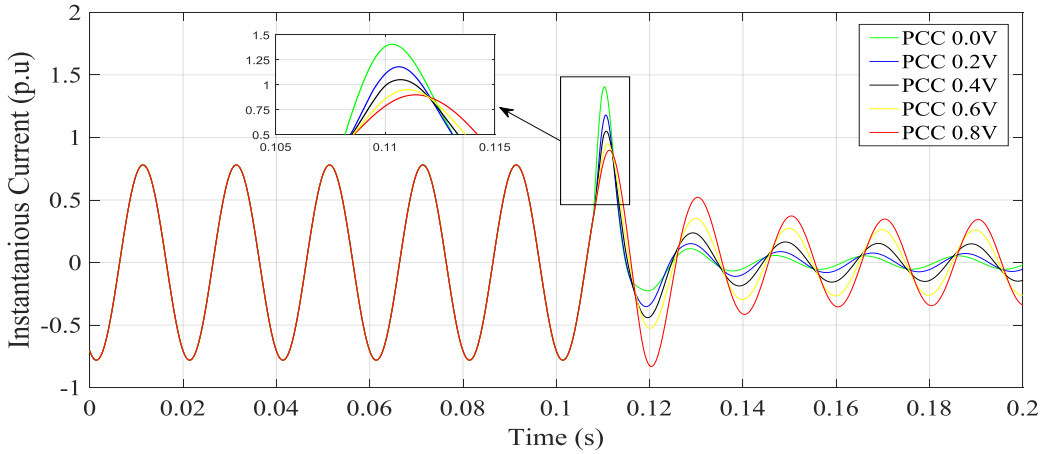

Fig.19: The SC current from the NSG during (FRT_{NQ} control) at different PCC voltage levels

However, this decreases with the increased fault impedance representing lower voltage dip at the wind farm PPC. For example, a minimum value of the instantaneous peak SC current of 0.9 p.u. is observed when a 0.8 p.u. voltage is seen at the PCC due to high fault impedance which represents a fault far from the generator. It is worth mentioning that the steady-state fault component is almost negligible (less than 0.15 p.u.) for cases where (V_{PCC}<0.4 p.u.), whereas, higher values can be observed in case of (V_{PCC}> 0.4 p.u.). For instance, steady-state fault currents of 0.28 p.u. and 0.37 p.u. have been measured for the cases V_{PCC} of (0.6 p.u. and 0.8 p.u.), respectively.

3.2.2 **Fault Response with an Immediate Reactive Current Injection (FRT_{IQ})**

Unlike the previous case, the FRT control of the NSG is adjusted to support the grid (i.e. to provide dynamic voltage support) by injecting reactive current. It is known than the injected reactive current mainly depends on the voltage dip level seen by the NSG. However, it might be affected by some other factors such as the operation condition, the overrating capabilities of the converter and the *k*-factor (i.e. proportional factor of the injected current). Therefore, the control of the NSG is amended to consider the immediate reactive current injection during the voltage dip. This aims to examine the SC current contribution of the NSG. Note that the

worst faulty condition (i.e. symmetrical three-phase bolted fault at the PCC) is considered again to observe the factors might affect this fault contribution rather than the impact of the voltage dip level. In contrast to the previous case (FRT_{NQ}), the results show that the fault contribution is only restricted to the steady-state contribution as no transient component is observed (almost negligible).

3.2.2.1 Impact of the Output Power under FRT_{IQ} Control

Observe Fig.20, where the impact of the NSG's output power is also investigated. It shows that the steady-state fault contribution is always fixed and limited to the maximum overrating capability of the converter (i.e. 1.2 p.u. in this study) regardless of the pre-fault operating point (i.e. output power of the wind farm). In other words, the steady-state fault contribution is independent of the output power of the converter during the normal condition before the fault. This might be denoted to the fact that this FRT control would prioritize the reactive current injection in response to the low voltage condition by only accounting for the voltage dip level without considering other factors.

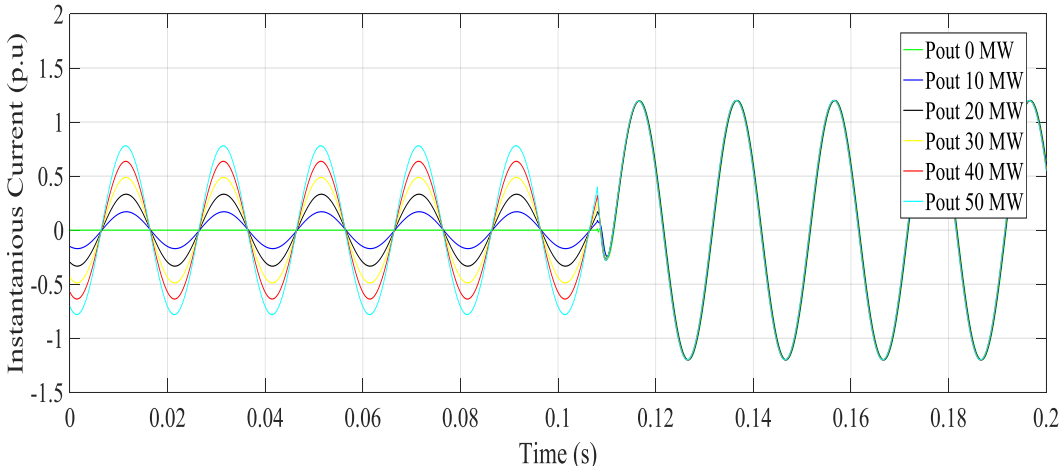

Fig.20: The SC current from the NSG during (FRT_{IQ} control) at different output power,

3.2.2.2 Impact of the k-Factor under FRT_{IQ} Control

It is already mentioned that the *k*-factor has a direct impact on the injected reactive current. The level of the injected current is also defined by this *k*-factor and the voltage dip level seen at the terminal of the NSG. However, in the case of severe faulty conditions, where a bolted fault occurs at the terminal of the PCC (see Fig.17), the voltage dip level will be severe and the fault current of the NSG might reach to its maximum for most of the values of the *k*-factor except the case where the k-factor equals 1,as shown in Fig.21. Observe that the fault current has a value of 0.9 approximately, in case of (*k*=1), while this has a fixed fault contribution equals its maximum overrating capability (i.e. 1.2 p.u.) in case of (k>1).

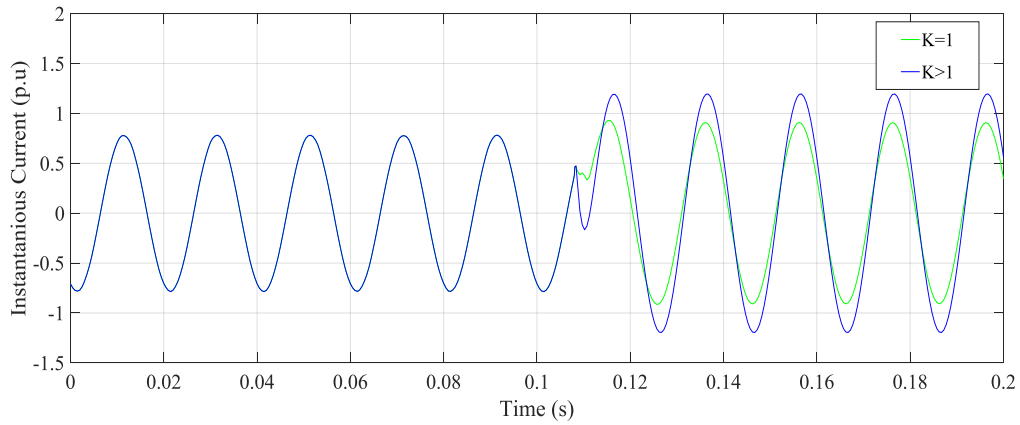

Fig.21: The SC current from the NSG during (FRT_{IQ} control) at different values of *k*-factor

3.2.2.3 Impact of the Maximum Overrating Capability under FRT_{IQ} Control

As it is expected, the maximum overrating capability of the converter, which is represented by the maximum combined current (i.e. I_{Max}), has a remarkable impact on the fault current contribution from the NSGs. To show this impact, the value of the maximum overrating capability of the converter is adjusted by multiplying the converter's rating current with a factor α, referred as an overrating factor, which ranges between (1.0 -1.4 p.u.). This means that the current I_{Max} , is also changing according to this factor as expressed in (3.5).

$$I_{\text{Max}} = \alpha I_{\text{Rating}} \tag{3.5}$$

Fig.22 shows the results obtained after initiating a bolted symmetrical three-phase fault at the PCC under the FRT_{IQ} control. It can be seen that the injected fault current from the NSG reaches its upper limit immediately according to the overrating factor α. This means that the NSG has injected its maximum reactive current in response to the severe fault which leads to reaching the maximum combined current (i.e. I_{Max}). In other words, the overrating factor α, has a great impact on the fault contribution of the NSG, especially in case of deep voltage dip levels resulted from severe faults near to the terminal of the NSG. It can be concluded that this factor is a very critical parameter for the design and operation of NSGs. Therefore, it should be carefully considered when studying the fault contribution of the NSG.

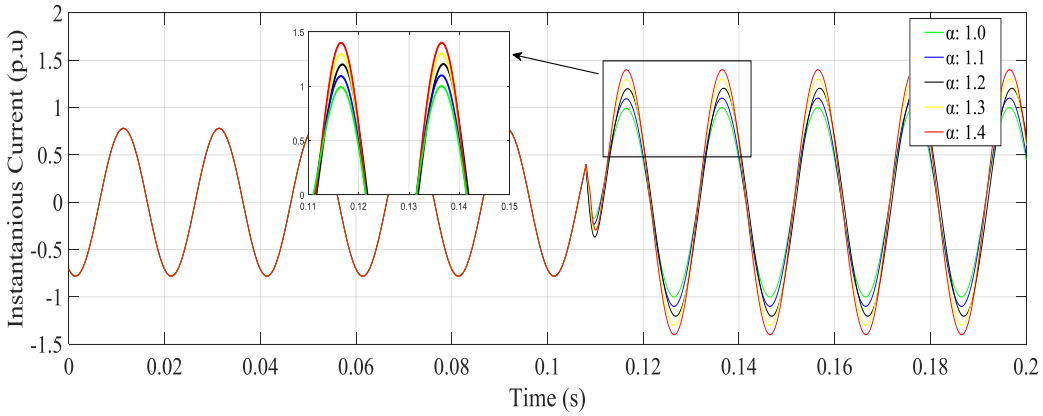

Fig.22: The SC current from the NSG during (FRT_{IQ} control) at different values of transient overrating factor α

3.2.3 **Fault response with a delayed reactive current injection (FRT_{DQ})**

On the basis of the aforementioned results, one can conclude that the transient behaviour of the SC current contribution is mainly determined by the pre-fault operating conditions as well as the level of the voltage dip seen during the fault as shown in Fig.18 and Fig.19. However, once in the immediate reactive current injection mode (i.e. FRT_{IQ}), the SC current is

determined by the injected reactive current which also depends on the maximum overrating capability and the *k*-factor. In addition, It can be observed from the previously shown results that the immediate transition to the FRT_{IQ} leads to override the transient fault current contribution. On the basis of that, the FRC can be simply modelled as a current source during the fault. Practically, this might not be accurate due to the delays in reactive current injection. In other words, not only the value of the injected reactive current by NSG has an impact on the fault current, but also to the speed of current injection after detecting the fault (i.e. reactive current injection time delay) [67, 101]. Furthermore, when such a delay appears, the steady-state SC current contribution can be delayed as well. Consequently, both transient and steady-state SC current contributions might be observed in the FRC SC current. Thus, investigating the influence of such a delayed reactive current injection on the SC current contribution of the NSG will be the focus of this section.

Many factors might govern the speed of the reactive current injection including: fault detection time, measurement and communication time, phase-locked loop (PLL) response time, and the injected current rise time. In grid codes defining the requirement for connecting NSGs, such delays are not explicitly determined [49]. These, however, might have significant impacts on the fault contribution of this generation to the grid, especially on the initial transient fault contribution. Table 6 shows the diversity of this requirement for the speed of reactive current injection in different grid codes. These requirements vary significantly in different countries. For instance, Great Britain grid code has mentioned an immediate SC current injection without a specific time delay [49, 59, 67]. In contrasts, the European Network of Transmission System Operators for Electricity (ENTSO-E) stated that the reactive SC current should be injected in between (10 ms to 60 ms) [57]. Specifically, in Germany, it is required that the SC current injection to take

Table 6: The requirement for the speed of reactive current injection according to different grid codes

Grid Code	Time	Comments
UK	Not specified	Immediate current injection (pure reactive).
Ireland	100 ms	Defined as a rise time.
German	20 ms	This doesn't include the time for fault detection according to: Transmission Code 2007.
	30 / 60 ms	Defined as Rise time/ transient time according to: VDE AR-N-4120.
ENTSO-E	60 ms	Current injection should not start before 10 ms

place within 20 ms after the fault detection, while 30 ms and 60 ms have been specified as SC current rise time and transient time, respectively. To clarify such an effect, a delay block is added to controller and the results have been re-generated considering two different values for the delayed reactive current injection:

- $\boldsymbol{FRT_{DQ20}}$ to represent a 20 ms delayed reactive current injection
- $\boldsymbol{FRT_{DQ50}}$ to represent a 50 ms delayed reactive current injection.

In both situations, it is assumed that the generator operates at its maxim power (i.e. 50 MW). Moreover, to only observe the impact of the reactive current injection time delay, the FRC overrating capability and the *k*-factor are also fixed to (1.2 and 2.0 p.u.), respectively. Then, the SC current fed from the NSG (phase A) is monitored and compared to the case where the reactive current is immediately injected without any delay (i.e. FRT_{IQ}). Note that a three-phase bolted fault has been initiated at the PCC where the voltage waveform crosses the zero axes to observe the maximum fault contribution. The resulted fault contributions for these three cases are shown in Fig.23. In the case of FRT_{IQ}, it can be seen that the SC current has

immediately reached the steady-state value with a maximum of (1.2 p.u.) of without transient component as shown in Fig.23a. However, the transient component is obvious in Fig.23b and Fig.23c due to the time delay of the reactive current injection. Observe that this transient shows a maximum peak of (1.4 p.u.) exceeding the maximum overrating capability of (1.2 p.u.). Then, it decays to a negligible level (e.g. around zero).

After a certain time delay, the SC current shows a steady-state contribution that reaches the maximum overrating capability of the converter (e.g. 1.2 p.u.). In fact, such new fault characteristics might be significantly altering the SC current waveforms, especially in future power systems. More specifically, in scenario with high penetration of NSGs, where the SC currents will be mainly fed by such sources.

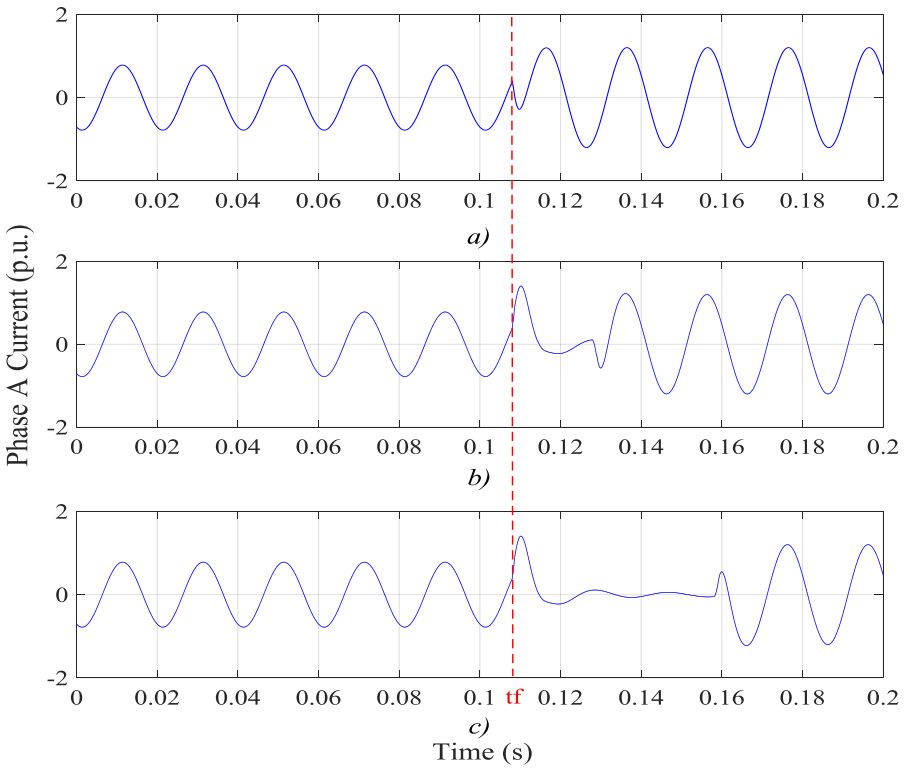

Fig.23: The SC current from the NSG in case of a) FRT_{IQ} b) FRT_{DQ20} c) FRT_{DQ50}

3.3 Characteristics of SC Current under Different Penetration Levels of NSGs

This section analyses the impact of the different penetration levels of NSGs on the SC current (characterised by $I_k^{"}$, I_p and I_b) considering the delayed reactive current injection during the FRT (i.e. FRT_{DQ}) as a main factor. The single machine system (see Fig.17) is adjusted and used again. The SG is gradually replaced by a NSG (represented by a type-4 wind) to investigate the sensitivity of the SC current to the penetration level of NSGs as shown in Fig.24. The penetration level is defined in (3.6).

$$Penetration\ level(\%) = \frac{NSG}{NSG + SG} \times 100\% \tag{3.6}$$

3.3.1 The Adjusted Single Machine System

Firstly, a conventional SG is only used to supply the total output power (i.e. 50 MW) without any NSG. Then, a NSG source (type-4 wind farm) is introduced partially to replace the de-tared portion of the SG starting from 20% up to 100% penetration scenario by a step of 20%. At the final step, the whole power supplied from the generation unit will be only generated from the wind farm. At all these steps, the fault contribution fed to the PCC from the resulted mixed generation unit (i.e. SG and the wind farm) is monitored.

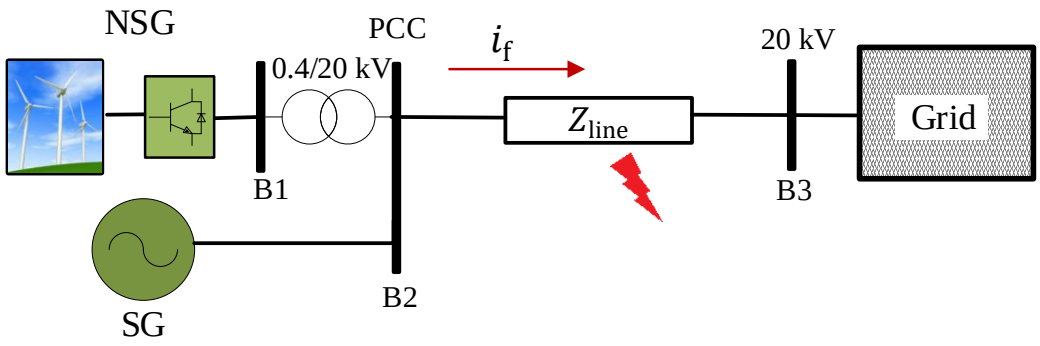

Fig.24: The adjusted single machine-infinite Bus test system

The maximum initial symmetrical SC current $I_k^{"}$, the peak instantaneous current, I_p, instantaneous SC current and the breaking current, I_b, are obtained at each penetration level considering the *FRT* control mode with the immediate and the delayed reactive current injection (i.e. FRT_{IQ} ,FRT_{DQ20} and FRT_{DQ50}). The resulted waveforms are presented in Fig.25, Fig.26and Fig.27 respectively. In addition, Table 7 presents the numerical results (value and time) for all fault currents ($I_k^{"}$, I_p and I_b).

3.3.1.1 Peak Instantaneous Current (I_p)

The results show the declined fault contribution with the increased penetration of NSG regardless of the speed of the reactive current injection during the *FRT* control. However, some differences can be observed as follows:

A) During the FRT_{IQ}

In the case of immediate reactive current injection, the maximum instantaneous current declines significantly from its highest value of (6.4 p.u.) at 0% NSGs' penetration scenario down to (1.2 p.u.) at 100% NSGs' penetration. This highlights the fact that the time decaying characteristics of the SC current can be still seen regardless of the penetration level of NSG. Moreover, the peak instantaneous current I_p gets to its maximum values at the initial contribution (i.e. first half cycle). However, this is not applied in the 100% scenario, where the fault contribution is only fed by the NSG. Note that the corresponding numerical results are also presented in Table 7, which shows both the value of I_p and the time at which has been observed in all the penetration levels of NSG.

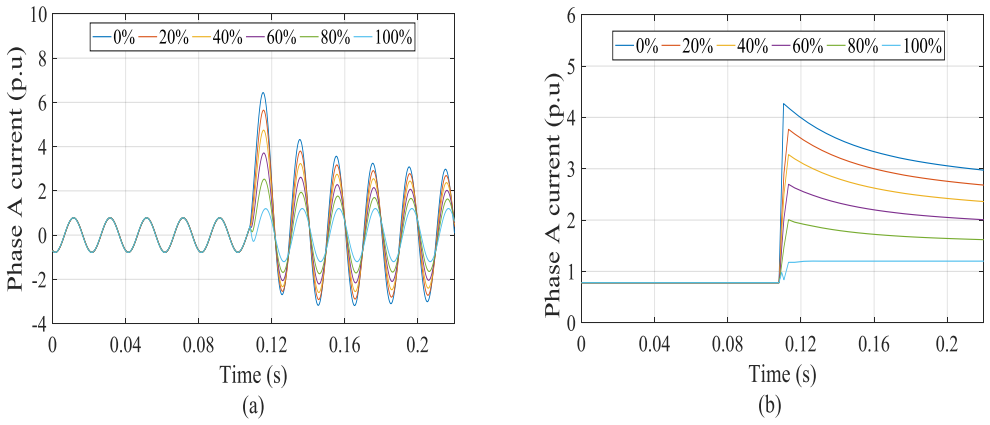

Fig.25: The SC current at different penetration levels (FRT_{IQ} control)

(a) Instantaneous, (b) RMS

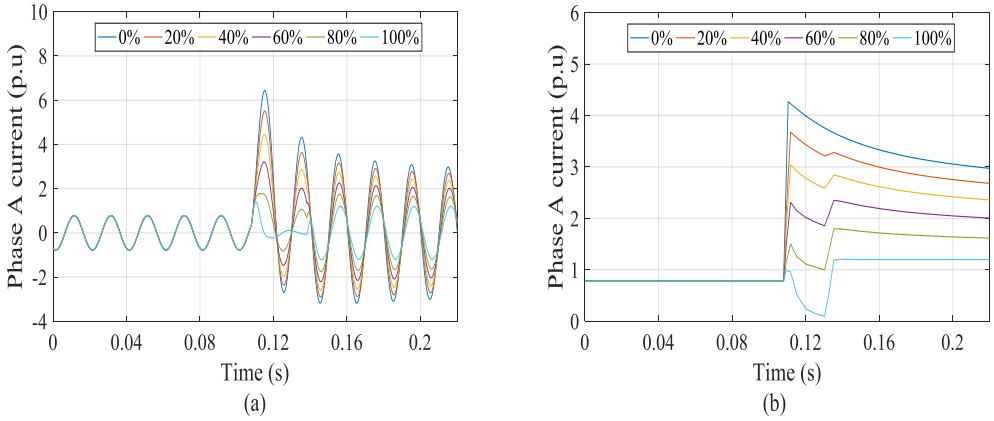

Fig.26: The SC current at different penetration levels (FRT_{DQ20} control

(a) Instantaneous, (b) RMS

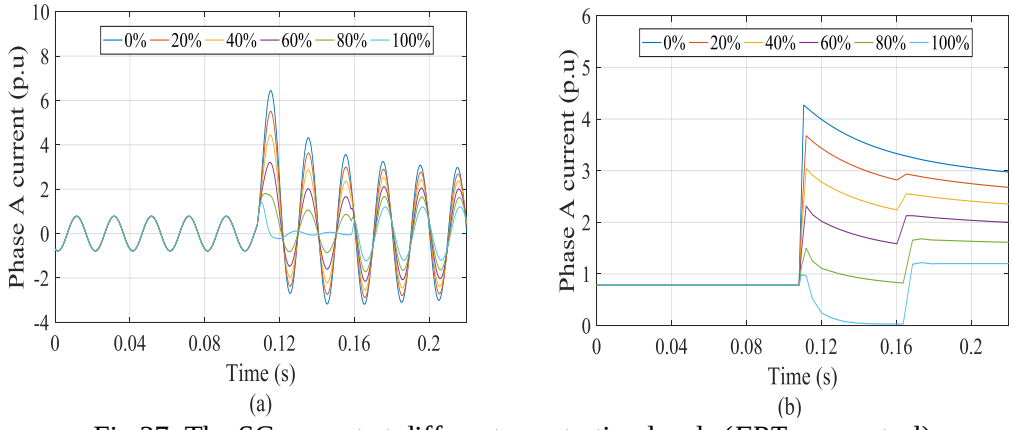

Fig.27: The SC current at different penetration levels (FRT_{DQ50} control)

(a) Instantaneous, (b) RMS

B) During the FRT_{DQ}:

In both FRT_{DQ20} and FRT_{DQ50}, it can be noted that the peak instantaneous current, I_p, has not only experienced a reduction with the increased penetration of NSGs, but also significant changes have been observed when the penetration of NSG has exceeded a specific level (e.g. 40% in this scenario) as shown in Fig.26 and Fig.27 respectively. This instantaneous SC current reaches its maximum in the first half cycle. However, it has not shown the same traditional decaying characteristics. More specifically, this peak value decays only for the first two cycles before it raises again to another local maximum value, which might show the same levels as the first peak (e.g. at 80% penetration: the initial peak of 1.77 p.u. and 5th peak of 1.75 p.u.) as shown in Fig.27.

Then, the current starts to decline again with another decaying level (i.e. different time constant) till the end of the fault period (i.e.100 ms). It is worth mentioning that peak instantaneous current I_p, has registered higher values during the FRT_{IQ} control mode compared to the FRT_{DQ20} and FRT_{DQ50}, for all penetration levels except at 100% scenario.

3.3.1.2 Initial Symmetrical SC Current ($I_k^{"}$)

The SC current waveform is monitored and the initial symmetrical current, $I_k^{"}$, is obtained for all the penetration levels similar to the previous case.

A) During the FRT_{IQ}

The initial symmetrical SC current, $I_k^{"}$, has reached its highest values immediately after the fault (4.3 and 1.2 p.u. at 0% and 100% respectively). This current also reaches its maximum value at the initial contribution (i.e. first cycle). This is due to the immediately injected

Table 7: Currents with different penetration levels at FRT_{IQ}

Penetration Level	**FRT_{IQ}**					
(%)	I_p (p.u.)	Time (s)	$I_k^{"}$ (p.u.)	Time (s)	I_b (p.u.)	Time (s)
0	6.42	0.115	4.27	0.110	3.02	0.208
20	5.7	0.115	3.77	0.113	2.72	0.208
40	4.74	0.115	3.28	0.113	2.40	0.208
60	3.71	0.115	2.69	0.113	2.03	0.208
80	2.51	0.115	2	0.113	1.63	0.208
100	1.20	0.115	1.2	0.121	1.20	0.208

reactive current in response to the voltage dip seen as a result of the fault. However, at 100% NSG penetration where the SC current is only fed by the NSG, it can be noted from the that the fault response shows a fixed limited contribution during the whole fault period Fig.25.b. The time instant at which $I_k^{"}$ occurs, also shows delays around 15 ms, as presented in Table 7.

B) During the FRT_{DQ}

In contrast to the previous FRT control (i.e. FRT_{IQ}), the maximum symmetrical RMS SC current $I_k^{"}$ has observed after a certain time delay. Fig.26.b and Fig.27.b show the RMS SC current during the FRT_{DQ} control mode. It can be seen that this maximum has been shifted in some scenario for almost one cycle (i.e. 20 ms) and three cycles (i.e. 60 ms) in the cases of FRT_{DQ20} and FRT_{DQ50} control modes, respectively. For example, at 60% penetration scenario and FRT_{DQ20}, $I_k^{"}$ has shown a maximum of 2.34 p.u. at 0.135 ms for a fault occurs at 0.108 s. This implies a 27 ms delay has been observed due to the 20 ms delayed reactive current

Table 8: Fault currents at the PCC with different penetration levels at FRT_{DQ20}

Penetration Level	**FRT_{DQ20}**					
(%)	I_p (p.u.)	Time (s)	$I_k^{"}$ (p.u.)	Time (s)	I_b (p.u.)	Time (s)
0	6.42	0.110	4.27	0.110	3.02	0.208
20	5.5	0.113	3.67	0.112	2.72	0.208
40	4.41	0.113	3.01	0.112	2.39	0.208
60	3.19	0.113	2.34	0.135	2.03	0.208
80	1.77	0.113	1.79	0.135	1.63	0.208
100	1.41	0.121	1.2	0.136	1.20	0.208

Table 9: Fault currents at the PCC with different penetration levels at FRT_{DQ50}

Penetration Level	**FRT_{IQ}**					
(%)	I_p (p.u.)	Time (s)	$I_k^{"}$ (p.u.)	Time (s)	I_b (p.u.)	Time (s)
0	6.42	0.115	4.27	0.110	3.02	0.208
20	5.50	0.115	3.67	0.112	2.72	0.208
40	4.42	0.115	3.04	0.112	2.39	0.208
60	3.21	0.115	2.31	0.112	2.02	0.208
80	1.80	0.112	1.68	0.174	1.62	0.208
100	1.41	0.110	1.20	0.174	1.20	0.208

injection as shown in

Table 8. On the other hand, at 80% penetration scenario and FRT_{DQ50}, $I_k^{"}$ has illustrated the lower maximum of 1.68 p.u. at 0.174 ms for a fault occurs at the same inception time (i.e. 0.108 s). In other words, a 66 ms delay has been observed as shown in Table 9.

3.3.1.3 Symmetrical Breaking SC Current (I_b)

In all scenario, it is assumed that the breaking current is measured 100 ms after the fault inception time. It can be noticed that the results for the breaking current I_b, are almost coincided. They have shown the same decline level with the increased penetration of NSGs, as demonstrated in Fig.25.b, Fig.26.b and Fig.27.b regardless of the FRT control mode. In other words, the different time delays during the reactive current injection have not influenced the level of the SC current at the breaking time. This might be due to the fact that at the breaking time (i.e. after 100 ms), the FRCs will be already injecting its maximum capability of reactive current regardless the starting time of this current injection.

3.3.2 **Case Study Using IEEE 9-Bus Test System**

To confirm the results on a bigger test system, IEEE 9-Bus test system [102] is used considering different penetration scenario and the previously discussed FRT controls as well. As can be shown in Fig.28, three NSG's penetration scenario where type-4 wind farms

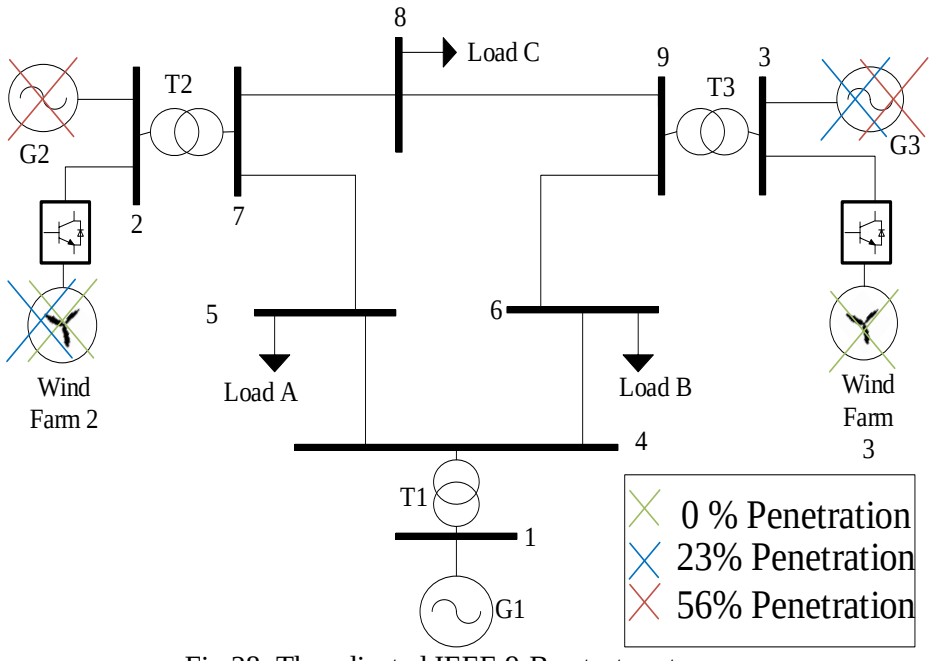

Fig.28: The adjusted IEEE 9-Bus test system

equipped with FRCs have replaced the traditional synchronous generators. These scenario are assumed as follows: Zero NSG's penetration (i.e. base case scenario with synchronous generation units only), 23%NSG's penetration scenario (i.e. G3 is replaced with type4-based wind farm), and 56% NSG's penetration scenario (i.e. both G2 and G3 are replaced). A symmetrical three-phase bolted fault has been initiated at Bus 6 which lasts for 100 ms. The obtained results from the IEEE 9-Bus test system are considered for FRT_{DQ20} and FRT_{DQ50} controls as shown in Fig.29 and Fig.30, respectively.

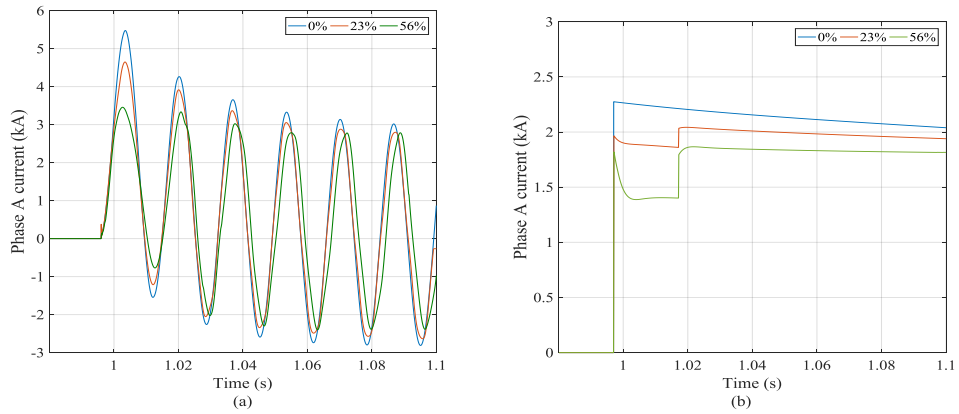

Fig.29: The SC current of Bus-6 at different penetration levels (FRT_{DQ20} control)
(a) Instantaneous, (b) RMS

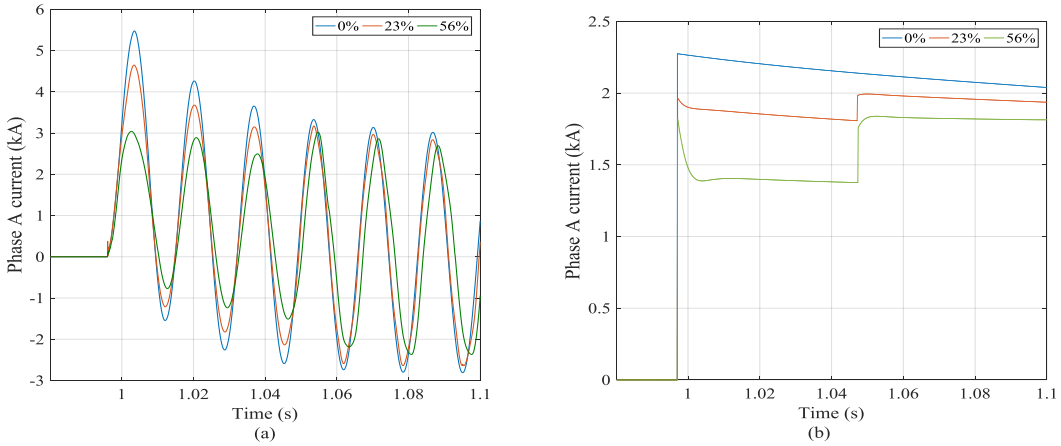

Fig.30: The SC current of Bus-6 at different penetration levels (FRT_{DQ50} control)
(a) Instantaneous, (b) RMS

Note that this fault has been created at the voltage zero-crossing to observe the maximum instantaneous fault current component. It can be seen that the obtained results confirmed the previously concluded results in the single-machine infinite Bus system. Also, all fault currents ($I_k^{"}$, I_p and I_b) are monitored and listed in Table 10 and Table 11 for FRT_{DQ20} and FRT_{DQ50} controls respectively. Note these Tables which show the value and the time of each current component. These results illustrate the impact of the delayed reactive current injection as well. These results are discussed in details below.

Table 10: Fault currents at Bus 6 with different penetration levels for FRT_{DQ20}

Penetration Level	**FRT_{DQ20}**					
(%)	I_p (p.u.)	Time (s)	$I_k^{"}$ (p.u.)	Time (s)	I_b (p.u.)	Time (s)
0	5.43	1.004	2.27	0.997	2.04	1.100
23	4.65	1.004	2.03	1.017	1.94	1.100
56	3.03	1.004	1.861	1.020	1.82	1.100

Table 11: Fault currents at Bus 6 with different penetration levels for FRT_{DQ50}

Penetration Level	**FRT_{DQ50}**					
(%)	I_p (p.u.)	Time (s)	$I_k^{"}$ (p.u.)	Time (s)	I_b (p.u.)	Time (s)
0	5.43	1.004	2.27	0.997	2.04	1.100
23	4.63	1.004	1.98	1.048	1.93	1.100
56	3.02	1.054	1.83	1.051	1.81	1.100

3.3.2.1 Peak Instantaneous Current (I_p)

The instantaneous fault current has shown a declined behaviour with the increased penetration level of NSG regardless of the FRT control. It is worth pointing out that this peak current has been observed in the first half cycle for all cases under the FRT_{DQ20} as shown in Fig.29.a. However, a noticeable delay can be observed in the case of 56% of NSG's penetration under the FRT_{DQ50}. Notice the shifted instantaneous peak current I_p, from the first cycle to the fourth cycle at the 56% scenario as shown in Fig.30.a. This implies that the time-decaying characteristic of the instantaneous fault current is sensitive not only to the FRT control but also to the penetration level of NSGs. In other words, the traditional SC response is not observed anymore in high NSG's penetration scenario.

3.3.2.2 Initial Symmetrical SC Current ($I_k^{"}$)

This fault current component has also shown a declined behaviour with the increased penetration of NSG. However, this contribution is no longer the maximum as shown in Fig.29.b and Fig.30.b. In other words, the maximum symmetrical SC current is shifted in cases other than zero NSG's penetration scenario. Notice that a decaying RMS SC current can be observed immediately after the initial component. Nevertheless, the RMS SC current witnesses a jump due to the injected reactive current where the maximum symmetrical current might be observed. For example, Tables 10 and 11, illustrate that the maximum symmetrical SC current has been shifted at 23% penetration scenario from (0.997 ms at zero penetration) to 1.017 ms and 1.02 ms under the FRT_{DQ20} and FRT_{DQ50}, respectively.

3.3.2.3 Symmetrical Breaking SC Current (I_b)

The results for the breaking current I_b, have shown declined values proportionally to the penetration level of NSG. However, the delayed injection of reactive current (i.e. different FRT_{DQ}) has not influenced this current in a similar pattern as those observed in the single-

machine test system. Fig.29.b and Fig.30.b demonstrate that the values of the symmetrical breaking current at the same penetration scenario have shown the same declined levels under both cases FRT_{DQ20} and the FRT_{DQ50}.

3.4 Conclusion

In this chapter, the new dynamic response of Short Circuit (SC) currents in power systems including high penetration of NSGs is analysed. While the SC current from the conventional Synchronous Generators (SGs) is determined by the inherited physical characteristics of the generator as well as the grid nature, the results show a controlled response with a limited SC current contribution from the NSGs. This depends on the size of the power electronic interface utilised for NSG. In this chapter, a wide range of factors that might influence the SC current contribution of NSG utilising Fully Rated Converter (FRC) was studied in details. The results have shown that transient SC contribution from the NSGs, connected through FRCs, is mainly determined by the pre-fault operation conditions, the voltage dip seen during the fault and the speed of reactive current injection. On the other hand, the steady-state contribution is only affected by the inverter's overrating capability as well as the proportional gain for the reactive current injection (i.e. *k*-factor). Then, the sensitivity of the SC current characteristics to the resulted generation mix (SGs and NSGs) has been presented considering different NSG penetration levels. The simulation results demonstrated that the SC currents in high NSGs' penetration scenario may witness some significant changes compared to the one observed in conventional power systems on the basis of SGs.

Also, the SC current response may show a delayed maximum contribution (i.e. very low initial contribution), multiple peak values and different levels of current decaying after exceeding some levels of NSGs penetration in the grid (i.e. 40% in this study). However, in cases where the NSGs can ride though the fault immediately without any delays, the traditional time-decaying response might be observed as far as the penetration level is less than 100%.

Finally, One of the major findings which can be observed from these results, is that the breaking current converges to the same level of the initial symmetrical SC current ($I_k^{"}$) with the increased penetration of NSGs until they coincide at 100% scenario.

4 Evaluating the Accuracy of Steady-State Fault Calculation Methods with High Penetration of NSGs

4.1 Introduction

This chapter investigates the performance of steady-state fault calculation (SSFC) methods in power systems with a high penetration of non-synchronous generation (NSG), i.e. generation connected to the grid over fully rated converter (FRC) technologies. The chosen SSFC methods include those previously described methods: i) equivalent voltage source, and ii) complete (superposition). In particular, the performance of the up-to-date IEC60909 standard, which belongs to the former SSFC method, and the complete method are studied here using modified single machine-infinite Bus test system including NSG utilising FRC in DIgSILENT PowerFactory. The estimated fault currents from these methods are compared with those calculated using dynamic simulations in response to different voltage dip levels resulting from faults at different locations. This allowed us to identify issues and challenges of the existing SSFC methods planned to be applied for future networks with a high penetration of NSG utilising FRC. These findings are confirmed using the IEEE 9-Bus test system.

4.2 Modelling of NSG Utilising FRC in Steady-State Fault Calculations

4.2.1 According to IEC60909 Standards

Traditionally, the IEC60909 standard has not provided explicit modelling for NSG utilising FRC. Hence, their fault currents have been usually either ignored similarly to other passive elements or considered as static converter-fed drives. Recently, due to the increased penetration of NSGs (i.e. mainly RESs), some augmentation was made into the IEC60909 to enable better estimation of the fault currents from such resources. The latest version of the

IEC60909:2016 standard has suggested a current source model for NSG, assuming a predefined limited fault current contribution from FRC according to its maximum overrating capability [35]. In DIgSILENT PowerFactory, static generator model is used for representing most NSG utilising FRC [103]. That model assumes that rotating machines are entirely decoupled from the system for such calculations (i.e. non-synchronously connected to the grid). The modelling details for FRC available in the IEC60909:2016 standards are discussed and investigated below.

1) *Static Converter-Fed Drive:*

NSG utilising FRC is considered as a static converter-fed drive that only contributes to three-phase SC faults in here. The SC current is calculated using the voltage behind an impedance model, as shown in Fig.31. The impedance of the converter, Z_C, is assumed to be one-third of the nominal impedance which is calculated using the rated values of the converter as given in (4.1).

$$Z_C = \frac{V_N^2}{3S_N} \tag{4.1}$$

Where V_N,S_N are nominal values of the voltage and apparent power of the NSG, respectively.

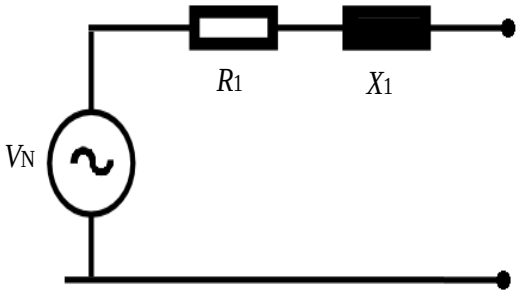

Fig.31: Voltage behind impedance used for FRC modelling in the static converter-fed drive method

The impedance in (4.1) is decomposed to an inductance, X_C, in series with a resistance, R_C, as shown in Fig.31. These two components are calculated by assuming $R_C/X_C = 0.1$ and $X_C = 0.995 \times Z_C$.

2) *Equivalent Synchronous Generator Model:*

NSG utilising FRC is modelled as a SG (voltage source behind impedance) for both the sub-transient and transient fault contributions. The impedance of NSG in the equivalent circuit is calculated on the basis of predefined maximum fault contribution. This assumes a bolted symmetrical fault at the low voltage side of the step-up transformer connecting the grid-side converter of NSG to the PCC. The equivalent circuit of this methodology is the same as Fig.31, but with different values for the resistance, R_1, and reactance, X_1, as given below:

$$X_1 = \frac{c_{\max}}{S_K^{''}\sqrt{1+(R/X^{''})^2}} \tag{4.2}$$

$$R_1 = (R/X^{''}) \times X_1 \tag{4.3}$$

Where $c_{\max}$, $S_K^{''}$, and $R/X^{''}$ are the voltage factor *c*, the maximum initial sub-transient SC power in MVA as given from the manufacturer, and the ratio of resistance to the sub-transient reactance. Note that for calculating both transient $(I_k^{'})$ and breaking (I_b) currents, the same model is used with the sub-transient impedances assuming they are equal to the initial sub-transient current $(I_k^{''})$.

3) *Full-Size Converter (Current Source Model)*

In this modelling methodology, a NSG utilising FRC is modelled as a current source (with infinite parallel impedance) that contributes to an inductive fault current according to a

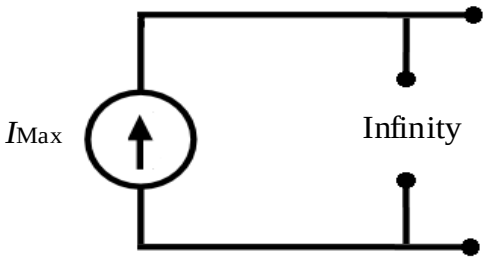

Fig.32: The current source model with infinite impedance

pre-defined limited value, as shown in Fig.32. This model considers a maximum fixed contribution from FRC in the fault current regardless of the fault location. This maximum fault contribution is limited by its overrating capability at the grid-side, as previously shown in chapter 3. Moreover, this approach only considers the positive sequence current even in the case of unbalanced faults such as single- or double-line faults. In the IEC 60909 standard, the same fault contribution is assumed for sub-transient, transient and steady-state fault currents of this approach. More detail on the way of calculating the fault current according to the latest IEC 60909 standards using a current source method will be furnished in chapter 5.

4.2.2 **According to the Complete Method**

This method can represent the fault current supplied from NSG using two different approaches including: 1) equivalent synchronous generator, and 2) dynamic voltage support. They represent NSG on the basis of the SG model or current source for fault current calculation as well as considering the load flow initializations, respectively. In the dynamic voltage support approach, where the NSG is modelled as a current source, it is assumed that NSG has the capability to inject a reactive current during the fault (i.e. FRT capability) to comply with the grid code requirement. Note that these methods distinguish between two different contributions in system fault currents (i.e. sub-transient and transient). Therefore, they assume two different models accordingly.

4.2.2.1 Equivalent Synchronous Generator

- **Sub-transient model:** The voltage source behind a series impedance is used again for this model. The values of the resistance, R_1, and reactance, X_1, are calculated as previously described in (4.2) and (4.3). However, this method considers the impact of load flow currents in the fault calculation by using the actual values of the pre-fault load flow voltages instead of the correction factors.
- **Transient model: The** sub-transient model is employed here assuming a new value for the transient fault level, $S_K^{'}$.

4.2.2.2 Dynamic Voltage Support

- **Sub-transient model:** The sub-transient circuit is similar to the one used in the equivalent synchronous generator model.
- **Transient model:** To consider the fault contribution of FRC in the transient interval, the static converter is replaced by its equivalent current source in this model. An iterative method is used for this purpose to define the injected fault current. This method is already incorporated in the complete method to consider the dynamic voltage support according to several grid codes. Note that the additional reactive current value, which has a priority over the active current, in this transient model is also dependent on the grid code defining the dynamic voltage support and the relationship between the reactive current and the voltage drop (as explained earlier in chapter 2). In other words, the iterative algorithm tries to priorities the reactive current injection during the voltage dip considering the *k*-factor and the maximum overrating capability of the converter. More details on the way of implementation in DIgSILENT PowerFactory can be found in [104].

4.3 Results and Discussion

In order to simplify the comparison process and presenting the results, the different modelling approaches adopted by the IEC60909 standards and the complete methods, which are explained above, are abbreviated and listed in Table 12.

4.3.1 Assessment of SSFC Methods Performance Using the Single Machine-Infinite Bus Test System

At first, the single-machine infinite Bus system (previously shown in Fig.17) is used as a test system to evaluate the performance of various SSFC methods explained in (section 4.2) for fault current estimation in response to different levels of voltage dip seen from the NSG utilising FRC due to different fault locations.

The results from the SSFC methods (also listed in Table 12) are then compared with those obtained from dynamic simulations, i.e. for the initial sub-transient current ($I_{\mathrm{k}}^{''}$), breaking current (I_{b}), and the peak instantaneous current (I_{p}).

Table 12: Different SSFC Methods

Abbreviation	Method
IEC1	No contribution
IEC2	Static Converter-Fed Drive
IEC3	Equivalent Synchronous Generator
IEC4	Full Size Converter (Current Source Model)
Complete1	Equivalent Synchronous Generator
Complete2	Dynamic Voltage Support

4.3.1.1 Initial Sub-Transient Contribution ($I_k^{"}$)

As it can be shown in Fig.33, the initial sub-transient fault current from the NSG utilising FRC is dependent on the voltage dip level (assuming the same pre-fault operating condition). Observe that the initial sub-transient current declines (see Fig.33) with the increased voltage seen at the PCC. As can be seen, the IEC1 does not consider ($I_k^{"}$), current from FRC (i.e. zero fault current). On the other hand, the IEC2, which employs the static fed-drive model, shows the maximum fault current in response to a bolted three-phase fault (V_{pcc} =0 V), and this declines proportionally with the increased voltage dip. It can be seen that the IEC2 method overestimates the fault current, while the opposite trend can be seen for other values of PCC voltage (i.e. V_{pcc} >0.25 p.u.). Further, see that the IEC2 method provides a reasonable estimation of the ($I_k^{"}$), when (zero<V_{pcc}<0.5) compared to the dynamic simulation results. In contrast, there is a significant difference in the estimated values when (V_{pcc} >0.5 p.u.).In the IEC3 method, where the equivalent SG model is used, the fault current ($I_k^{"}$), is under-estimated in all voltage dip cases. Note that the fault current calculated from the IEC3 is less

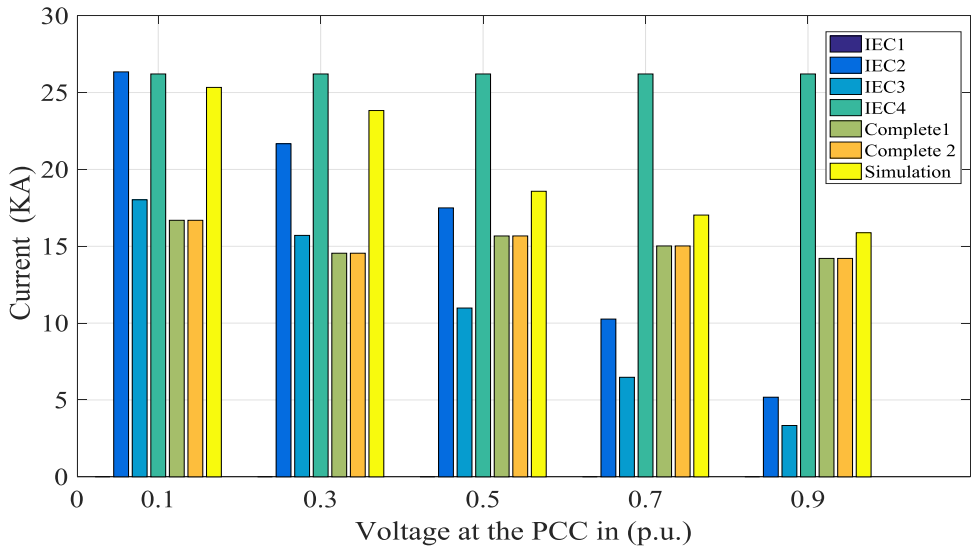

Fig.33: Results for ($I_k^{"}$) at different voltage dip levels seen by the NSG

than the one calculated using the IEC2. In addition, a higher error between results obtained from the IEC3 and the one obtained from dynamic simulations can be seen for faults far away from the generator. Using the current source model (i.e. IEC4), resulted in overestimated fixed fault current regardless of the level of a voltage dip, as can be seen in Fig.6. However, the fault currents estimated from the IEC4 appear to be one of the best approximates of the initial sub-transient fault current when the voltage (V_{pcc} >0.5 p.u.). Moreover, where the complete method (superposition with load flow initialization) is considered, both Complete1 and Complete2 approaches have coincided with each other for all cases. This is expected as they both use the same sub-transient equivalent circuit, as previously explained in (section 4.2) in more detail. These methods underestimate the fault current, for cases where (V_{pcc}<0.5 p.u.). However, for other cases, they provide the best fault current estimation compared to other SSFC methods, as shown in Fig. 33.

4.3.1.2 Breaking Current (I_b)

Similar to initial sub-transient fault current, SSFC methods provide different estimation for the breaking current of NSG utilising FRC as shown in Fig.34. This occurs at the instant where the fault has been cleared (i.e. after 100 ms in our example). As illustrated in Fig.34, for instance, the IEC1 method has completely neglected the fault current, as expected. On the other hand, the estimated FRC breaking current by the IEC2 is similar to the ($I_k^{"}$), estimated with it. These results in a significant error between the results obtained from the IEC2 method and the one obtained from dynamic simulations for power systems including NSG utilising FRC, as shown in Fig.34.

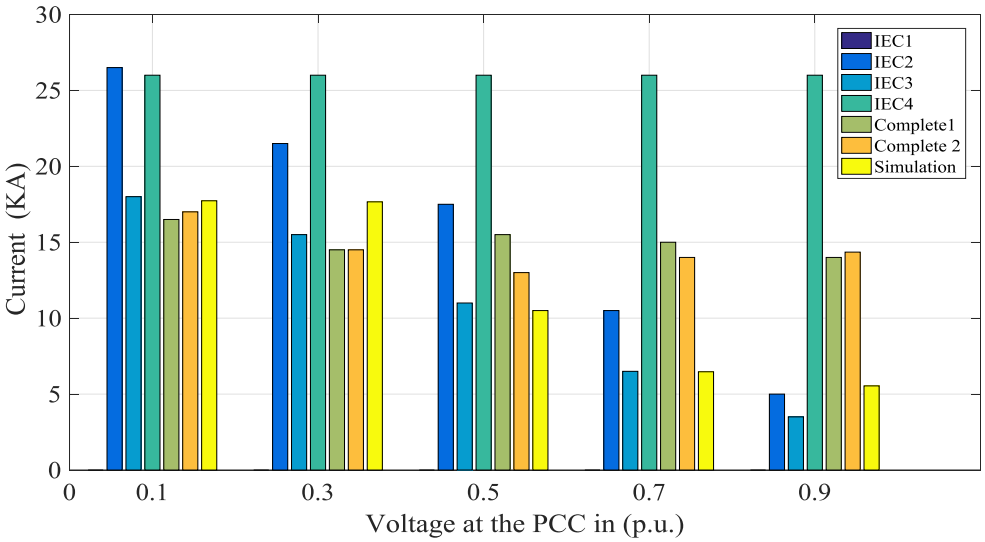

Fig.34: Results for (I_b) at different voltage dip levels seen by the NSG

Further, it can be seen that similar to initial sub-transient fault current, SSFC methods provide different estimation for the breaking current of NSG utilising FRC at the instant where the fault has been cleared (i.e. after 100 ms in our example), as illustrated in Fig.34. The IEC1 has completely ignored the fault current, as expected. On the other hand, the estimated FRC breaking current by the estimated breaking current with the IEC3 changes with different levels of voltage dip at the V_{pcc}. It is noted that the fault current is overestimated in the case of strong voltage dip (V_{pcc}<0.25 p.u.), otherwise it is underestimated. However, this method provides the best estimation of breaking current for cases where (V_{pcc}>0.5 p.u.). The IEC4 is approximated an overestimated fixed fault current regardless of the voltage dip level. This leads to the worst approximations of the breaking current, specifically for cases where (V_{pcc}>0.5 p.u.).

4.3.1.3 The Maximum Peak Fault Current (I_p)

As for the maximum instantaneous peak fault current from NSG utilising FRC, a reduction is observed with the increased voltage level at the PCC, as shown in Fig.35. However, it is noted that the declined trend is almost negligible for cases where (V_{pcc}>0.5 p.u.). This implies

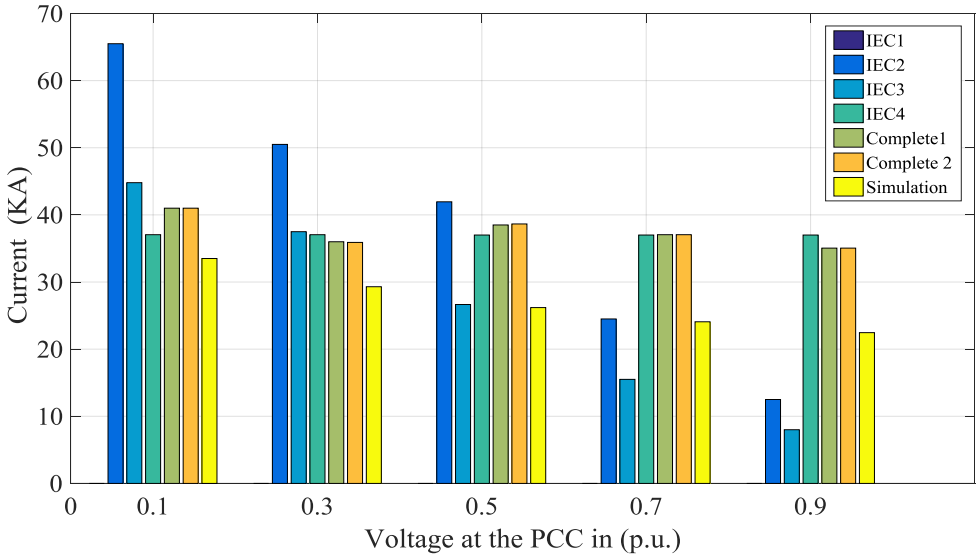

Fig.35: Results for I_p at different voltage dip levels seen by the converter

that the FRC may provide a fixed instantaneous peak fault current for Vpcc>0.5 p.u. Similar to other fault current components, the IEC1 method ignores the fault current, so it is the worst SSFC method for fault current estimation of NSG utilising FRC. In contrast, both IEC2 and IEC3 have overestimated the maximum instantaneous fault current where (V_{pcc}<0.7 p.u.), followed by the IEC3 which has less error compared to dynamic simulation. In terms of the current source model (IEC4), it can observe a fixed maximum instantaneous peak fault regardless of the level of voltage dip. This method has overestimated maximum instantaneous peak fault component in all cases. Also, observe in Fig.35 that complete methods have overestimated the maximum instantaneous peak fault current for most voltage dip cases. It is worth mentioning that the results obtained from these are almost the same as the one obtained from the IEC4 method. However, the IEC4 method has less error compared to other methods in some cases (e.g. V_{pcc}= 0.1 and 0.5 p.u.).

Table 13, summarizes the above results and provides a guideline for the most accurate SSFC methods that can be used for power systems including high penetration of NSG utilising FRC. As illustrated in Table 13, the recommendations are on the basis of two different

Table 13: The recommended SSFC methods besed on the location of the fault

Fault Current	***Near to the NSG*** ***(V_{pcc} < 0.5 p.u.)***	***Far from the NSG*** ***V_{pcc} > 0.5 p.u.***
Sub-transient Current	IEC4	Complete1 & Complete2
Breaking Current	Complete1 Complete2	IEC3
Peak instantaneous Current	IEC3 &IEC4 Complete1 & Complete2	None

voltage dip levels: i) for cases where (V_{pcc}<0.5 p.u.) to represent faults near to NSG; and ii) for cases where (V_{pcc}>0.5 p.u.) to represent faults far away from the NSG.

4.3.2 **Assessment of SSFC Methods Performance Using the IEEE 9-Bus Test System**

In order to examine the accuracy of the above SSFC methods in a larger power system with high penetration of NSG utilising FRC, the IEEE 9-Bus test system is used in this section. Firstly, the SSFC methods are used to identify the fault current level on Bus 8 at 23% and 56% penetration of NSG utilising FRC as shown in the previous chapter in Fig.28. Secondly, the obtained results are compared with the ones obtained from dynamic simulations. Note that these penetration levels are associated with the replacement of the SG-G2 and SG-G3 with NSG utilising FRC, respectively.

The penetration of NSG is defined as a percentage of their capacity to the total installed capacity in the system, as given in (3.6). Both Fig.36 and Fig.37 compare the three fault current components calculated using the SSFC methods with those obtained from the dynamic simulation on Bus 8 at different penetration of NSG. Note that these present the 23% and 56% NSG's penetration scenario, respectively.

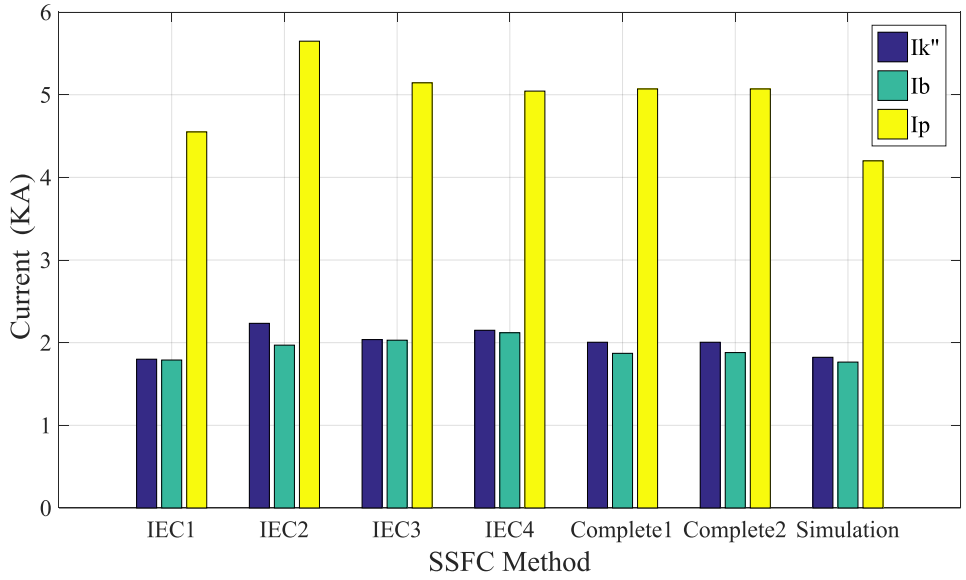

Fig.36: Fault currents on Bus 8 with 22% penetration of NSG in the grid

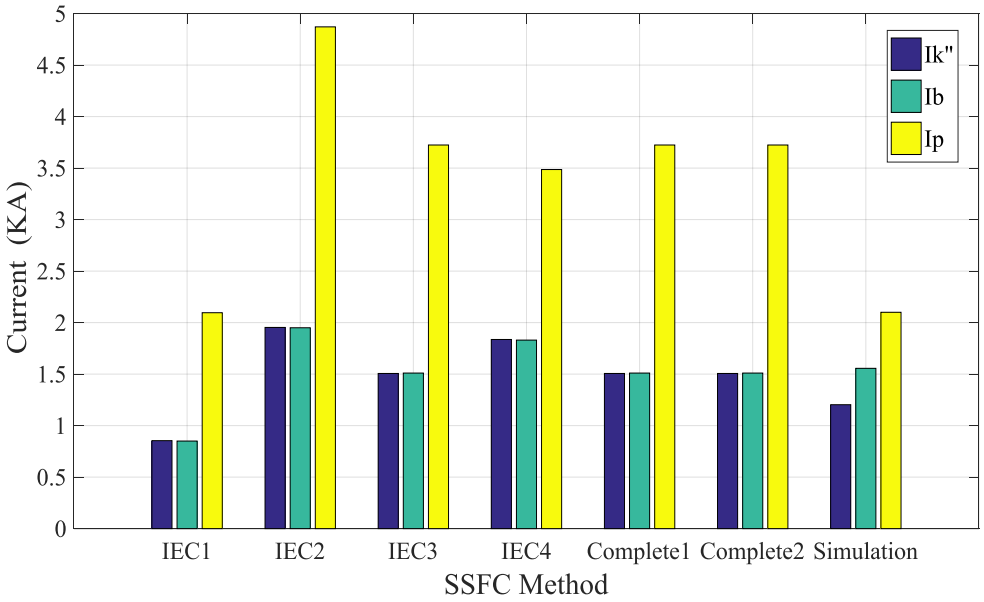

Fig.37: Fault currents on Bus 8 with 55% penetration of NSG in the grid

Similar to the results in the single-machine infinite Bus test system, the results obtained from the SSFC methods lead to different estimations for fault currents. Observe an error gap between the dynamic simulation results (i.e. the actual fault current) and the estimated ones using various SSFC methods. Further, note that this error gap becomes more tangible with the increased penetration of NSG, as shown in Fig.36. It is worth mentioning that at the 56%

penetration scenario for NSG (i.e. Fig.37), the change in the system fault currents due to NSGs is significant, and hence the impact of those generations cannot be neglected. Besides, as can be shown in Fig.37, all SSFC methods overestimated the sub-transient fault current except for the IEC1. This is expected as IEC1 does not account for the fault contribution of NSGs. Note that this might be accepted in cases where the penetration level of NSGs is small as seen in the 23% scenario. However, using this method leads to a high error when compared to dynamic simulation results as shown in the second scenario (i.e. 56%), as depicted in Fig.37.

As for the breaking current (I_b), the simulation results show that in high penetration scenario, all SSFC methods estimate the same contribution for both breaking and sub-transient fault current, as shown in Fig.37. However, on the basis of dynamic simulation results, the breaking current can be higher than the sub-transient current. This might happen due to FRT controller initiation that injects the maximum fault current leading to higher fault current contribution for NSG compared to sub-transient period. This also implies that the initial sub-transient current depends on the pre-fault currents more than the converter capability. Finally, it can be shown from Fig.36and Fig.37 that the contribution from the NSGs to the peak fault current is almost negligible in both penetration scenario compared to other components (i.e. $I_k^{"}$ and I_b).

4.4 Conclusion

This chapter has investigated the performance of steady-state fault calculation (SSFC) methods in power systems including high penetration of non-synchronous generation (NSG) on the basis of fully rated converter (FRC) technologies. In particular, we investigated the performance of updated versions of the IEC60909 as well as complete methods. The estimated fault currents from these SSFC methods are compared with the dynamic simulation results considering a wide range of voltage dip levels accounting for faults near and far from NSGs (i.e. different fault locations).

The simulations are conducted using single machine-infinite Bus and the IEEE 9-Bus test systems. It was shown that complete methods can provide the best estimation for breaking current (I_b). However, most SSFC methods showed poor performance in estimating of sub-transient ($I_k^{''}$) and maximum peak (I_p) currents in power systems with high penetration of NSG utilising FRC. Further, it was observed that all SSFC methods have tangible error gaps for estimating fault currents compared to actual fault levels calculated using dynamic simulations in power systems with high penetration of NSG utilising FRC. These necessitate a need to augment the existing modelling methodologies used in the SSFC methods to better represent the dynamic behaviour of NSG utilising FRC for such an analysis, which is the focus of the two following chapters.

5 Proposed Modification of the Latest Version of IEC60909 Standards to Consider the Fault Contribution of NSGs

5.1 Introduction

As mentioned above, the latest version of the IEC60909 standards has suggested a current source model for the representation of the FRC-based NSGs in steady-state fault calculation in the positive-sequence system. This assumes an ideal current source without any impedance (i.e. infinite impedance), as previously shown in Fig.32. Such a modelling method might be appropriate considering the fast response of the inner controller of the converter. However, this assumes a fixed maximum fault current contribution, which should be provided by the manufacturer, regardless of the voltage dip level resulted during the fault. In other words, this model does not consider the impedance of the fault path (i.e. fault impedance). As discussed earlier in chapter 4, the results obtained from this method (i.e. IEC4) have demonstrated an effective way for calculating the fault currents in some scenarios. However, it overestimates the fault currents for most scenarios, especially those scenarios with high penetration of NSGs. More specifically, for cases where the fault occurs far away from the RES (i.e. shallow voltage dip levels are seen at the generation terminal). This over-estimation might be denoted to the previous assumption and considering the maximum fault contribution regardless of the severity of the fault. Therefore, this chapter will present a proposed modification for this method to consider the fault contribution from the NSGS more accurately. Such an improvement will be on the basis of the FRT principle accounting for the various levels of reactive current injection proportionally to the voltage level seen during the fault. At first, the way of calculating the fault currents including NSGs according to the latest version of IEC60909 standards will be presented. Then, the proposed modification considering the reactive current injection according to the FRT and grid code will be

explained. Finally, the results of the current IEC60909 standards, as well as the proposed methods, will be validated against the actual fault currents obtained from the RMS simulations. For this purpose, the adjusted 14-Bus test system is modelled with high penetration of NSGs (e.g. PV systems) in DIgSILENT PowerFactory.

5.2 Fault Calculation According to IEC60909 Standards

The IEC60909 standard calculates the fault current in power systems on the basis of the Thevenin equivalent method. It represents the system during the fault condition by the equivalent impedance seen by the faulty point connected to a voltage source. Note that this does not consider the impact of RESs in such calculations. However, in the presence of FRC-based RESs, their fault contribution will be calculated using the current source model and then the sum of both contributions from SGs and RESs will represent the total fault current. It is worth pointing out that the IEC60909 standards only calculate the initial symmetrical fault current, then the other fault currents (such as I_p and I_b) are calculated by applying special multiplying factors to the initial symmetrical current ($I_k^{"}$). Therefore, the following calculations will be only restricted to the initial symmetrical current in this chapter. The IEC60909 standard has adopted the superposition principle to consider the fault contribution from NSGs. Therefore, the fault currents are calculated firstly assuming that the SGs are the only sources contributing to the fault. In other words, the NSGs are neglected (open-circuited). Then, these NSGs are considered only in the circuit while the SGs are neglected at this stage (short-circuited). Then, the superposition is used to calculate the total fault current from both types of generators. The calculation procedure for the initial symmetrical fault current according to the IEC60909 standards can be summarised as follows:

5.2.1 **Calculating the Fault Current without Considering the NSGs**

1) Calculate the equivalent impedance at the faulty point Z_k.

This will be accomplished either by using the *Z-Bus* matrix or by using network reduction. Consider the *Z-Bus* matrix of an n-Bus system as expressed in (5.1), with a case where the fault occurs at Bus *i*, the value of the equivalent impedance ($Z_k = Zii$).

$$\mathbf{Z} = \mathbf{Y}^{-1} = \begin{bmatrix} \mathbf{Z_{11}} & . & \mathbf{Z_{1i}} & . & \mathbf{Z_{1n}} \\ . & . & . & . & . \\ \mathbf{Z_{i1}} & . & \mathbf{Z_{ii}} & . & \mathbf{Z_{in}} \\ . & . & . & . & . \\ \mathbf{Z_{n1}} & . & \mathbf{Z_{ni}} & . & \mathbf{Z_{nn}} \end{bmatrix} \tag{5.1}$$

2) Apply a voltage at the faulty point.

According to the IEC60909 standards, this voltage equals the nominal pre-fault value (phase voltage) multiplied by a correction factor *c*, as expressed in (5.2). Such correction factor is considered to account for pre-fault operating conditions and the loaded network.

$$V\mathrm{n} = \frac{c \times V_{\mathrm{L\text{-}L}}}{\sqrt{3}} \tag{5.2}$$

3) Calculate the initial symmetrical current of the grid to the faulty point by applying the following formula (5.3).

$$I''_{K\_Grid} = \frac{Vn}{Z_K} = \frac{Vn}{\sqrt{R_K^2 + X_K^2}} \tag{5.3}$$

5.2.2 **Calculating the Fault Current of the NSGs**

1) Obtaining the maximum value of the *j*-th current source, I_{Maxj} representing the NSG from the manufacturer. Where *j*, represents the Bus connecting the NSG to the grid.

2) Calculating the transfer impedance between the faulty Buses *i*, and *j*, where the NSG is connected, Z_{ij}.

3) Applying the following equation shown in (5.4).

$$I''_{K\_RESs} = \frac{1}{Z_K} \sum_{j=1}^{j=N} Z_{ij} \times I_{Maxj} \tag{5.4}$$

Where,

- N: Number of the connected NSGs.
- I_{Maxj} : The maximum fault current contribution of the NSG connected to the j-th Bus.
- I''_{k_RESs} : The total fault current contribution of all connected NSGs.
- Z_{ij}: The transfer impedance between the j-th Bus and the faulty Bus-i.
- Z_k: The equivalent impedance at the faulty point.

5.2.3 **Calculating the Total Fault Current** I''_{K_Total}

$$I''_{K\_Total} = I''_{K\_Grid} + I''_{K\_RESs} \tag{5.5}$$

This total current represents the total fault current considering both SGs and NSGs contributing to the fault current. Note that this calculated current represents the initial symmetrical fault current during the sub-transient period as mentioned earlier, while the other currents such as the breaking current and the peak instantaneous currents will be calculated by applying some multiplication factors according to the IEC60909 standards.

5.3 The Proposed Modification Method

As illustrated earlier, this method might be considered a straightforward and simplified method to account for the fault contribution from the NSGs connected to the grid. However, the results for several scenario, where this method has been used for fault calculation, show that this method over-estimates the fault currents due to neglecting the impact of the voltage level during the fault and the reactive current injection during the FRT control which varies according to the grid code. Therefore, this part proposes an adjustment for the fault calculation procedure shown in the previous section. More specifically, a different way of calculating the value of the current source representing the fault current contribution from the NSG-based RESs in the IEC60909 standards, I_{RESj}. Instead of assuming a pre-defined fixed fault contribution (i.e. the value of the current source), a variable value will be assigned to each NSG on the basis of the voltage dip level and the grid code requirement. In other words, the aim is to consider the reactive current injection and the dynamic voltage support more precisely. This modified method can be summarised in the following sections.

5.3.1 Calculating the Fault Current without Considering the NSGs

As per the original IEC 90606 standards-based method, the initial symmetrical fault current ($I_k^{"}$), is calculated using the Z-Bus matrix, using the steps mentioned in section (5.2.1) by applying equations (5.1), (5.2) and (5.3).

5.3.2 Calculating the Fault Current of the NSGs

The current source model will be used but the fault current contribution of RESs will not equal the maximum overrating capability of the NSG, I_{Maxj}, anymore. This will have different values according to the voltage dip level seen during the fault and the FRT parameters. The

new value of the fault contribution (i.e. the value of the current source representing the NSG), I_{RESj}, will be calculated as follows:

1) Use the Bus matrix to calculate the voltages distribution at each Bus during the fault as follows (5.6).

$$\begin{bmatrix} \mathbf{v_1} \\ . \\ \mathbf{v_i} \\ . \\ \mathbf{V_n} \end{bmatrix} = \begin{bmatrix} \mathbf{V_1} \\ . \\ \mathbf{V_i} \\ . \\ \mathbf{V_n} \end{bmatrix} - \begin{bmatrix} \mathbf{Z_{11}} & . & \mathbf{Z_{1i}} & . & \mathbf{Z_{1n}} \\ . & . & . & . & . \\ \mathbf{Z_{i1}} & . & \mathbf{Z_{ii}} & . & \mathbf{Z_{in}} \\ . & . & . & . & . \\ \mathbf{Z_{n1}} & . & \mathbf{Z_{ni}} & . & \mathbf{Z_{nn}} \end{bmatrix} \begin{bmatrix} \mathbf{0} \\ . \\ \mathbf{I''_K} \\ . \\ \mathbf{0} \end{bmatrix} \tag{5.6}$$

Where, $\boldsymbol{V}_i$ and $\boldsymbol{v}_i$ are the *i*-th Bus voltages before and after the fault respectively.

2) Obtain the values of the proportional gain (*k*-factor) and threshold voltage ($V_{Threshold}$) from the grid code defining the FRT requirements for reactive current injection, in addition to the maximum combined current of the converter interface, I_{Max}, from the manufacturer.

3) Calculate the value of each connected current source, I_{RESj}, by applying (5.7). Note that V_j in (5.7) represents the calculated voltage at the *j*-th Bus, which is replacing the corresponding measured value at the Bus connecting the NSG in case of dynamic simulation, as explained previously in (i). Note that the calculated value of the calculated current (I_{RESj}) should not exceed the maximum combined current (I_{Max}).

$$I_{RESj} = k \times \left| V_{Threshold} - V_j \right| \quad \text{for } I_{RESj} < I_{Max} \tag{5.7}$$

Otherwise, the maximum current (I_{Max}) will be considered, which means that the NSG is injecting its maximum overrating capability. Note that in such case, the results of the proposed modification method are expected to match with the IEC60909-based

method which always assumes a fixed maximum contribution. In other words, the IEC 6099-based method can be considered as a special case of this proposed method.

4) Use the transfer impedance between the faulty Buses *i*, and *j*, where the NSG is connected, Z_{ij}. Then re-call the (5.4) considering the calculated values of each connected current source, I_{RESj}, in the previous step. By doing so, the new value of the total fault contribution from the RESs considering the new values $I_{\mathrm{RES}j}$ Instead of $I_{\mathrm{Max}j}$ will be given as shown in (5.8).

$$I''_{\mathrm{K\_RESs\_New}} = \frac{1}{Z_K} \sum_{j=1}^{j=N} Z_{ij} \times I_{\mathrm{RES}j} \tag{5.8}$$

5.3.3 **Calculating the New Total Fault Current** $I''_{\mathrm{K\_Total\_New}}$

Now, as we have the new fault current fed from those NSG-based RESs, the same procedure previously explained in section (5.2.3) will be followed again to calculate the total fault current. This is simply the summation of (5.3) and (5.8) as previously expressed in (5.5).

5.4 Results and Discussions

In this section, the performance of our proposed method in section IV for steady-state fault calculation in a power system including FRC-based RESs is evaluated. First, the response of a Photovoltaic (PV) system to different levels of voltage dip (i.e. different fault impedances) considering the impact of the *k*-factor on the injected fault current is investigated. Second, the IEEE 14-Bus test system is used to examine the accuracy of the proposed method. In the test system, PV units are used to replace some SGs to represent a high RESs penetration scenario. The fault currents are calculated at specific Buses using the proposed method. Finally, the

results are compared with those obtained from both IEC60909 standard and the dynamic simulations (i.e. RMS) in DIgSILENT PowerFactory.

5.4.1 **Single-Machine Infinite Bus Test System**

A single machine infinite Bus test system shown in Fig.38 is modelled in DIgSILENT PowerFactory. It represents a PV system (10 MW) connected to a grid (132 kV). A three-phase fault is created at the point of common coupling with the grid considering different values of the fault impedance to represent various levels of voltage dip. This test system is used to show the sensitivity of the fault current to the voltage dip level and the k-factor during the fault. The reactive current injection has been considered using two different values for the proportional gain (i.e. *k*-factor). The maximum combined current is limited to (I_{Max}=1.3 p.u.) in both cases. Fig.39 and Fig.40 show the results for the injected reactive current during the fault for the cases (*k*=2) and (*k*=10), respectively. Observe the difference between the two responses in spite of the same fault conditions (i.e. same fault impedances, voltage dip levels and the fault type).

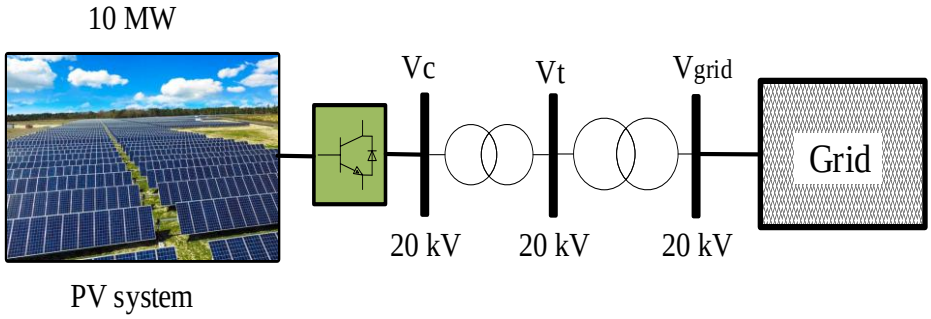

Fig.38: A 10 MW PV system connected to a 132 kV external grid

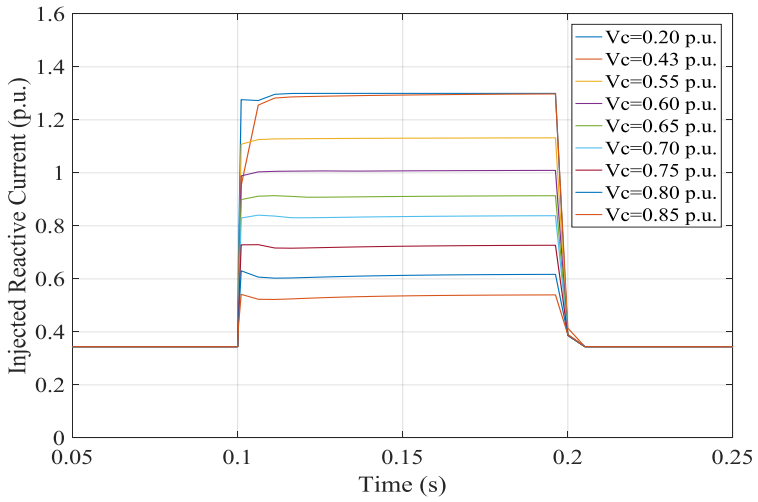

Fig.39. Injected currents in response to a different voltage dip levels for the case (*k*=2)

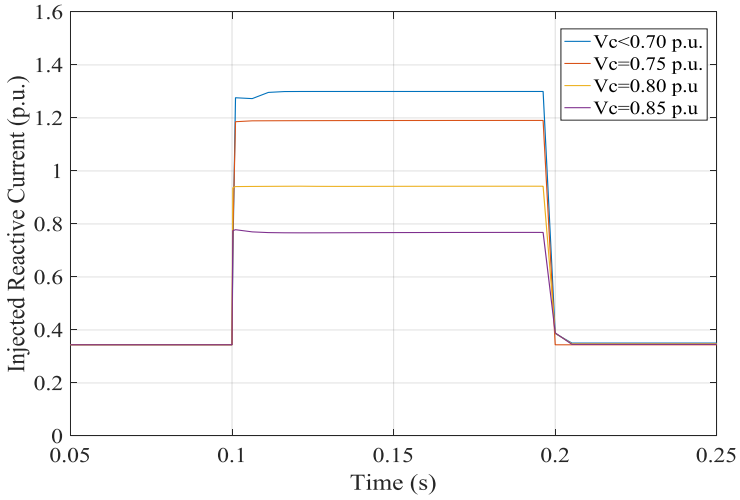

Fig.40. Injected currents in response to a different voltage dip levels for the case (*k*=10)

The results show that the injected reactive current in the case of (*k*=2) only reaches the maximum combined current, I_{Max}, when the voltage at the converter terminal voltage is less than 0.5 p.u. (i.e. V_C <0.5 p.u.), as shown in Fig.39. This implies that the PV system only injects a maximum current for deep voltage dip levels resulted from faults close to the PV system. On the other hand, where *k*-factor is equal to 10, the injected reactive current reaches its maximum (i.e. $I_{Reactive}$= I_{Max}) even when a shallow voltage dip is observed.

Table 14: The injected Current from PV System at Different Voltage Dip Levels

Injected Current	**Converter Voltage V_C (p.u.)**								
(p.u.)	**0.20**	**0.43**	**0.55**	**0.60**	**0.65**	**0.70**	**0.75**	**0.80**	**0.85**
Case 1 (*k*=2)	1.30	1.30	1.12	1.00	0.91	0.83	0.72	0.61	0.53
Case 1 (*k*=10)	1.30	1.30	1.30	1.30	1.30	1.30	1.20	0.95	0.76

Observe in Fig.40 that the injected reactive current reaches the maximum combined current (e.g. 1.3 p.u.) for all cases where (V_C <0.7 p.u.). These results are also listed in Table 14. Those results demonstrate the impact of the proportional gain (i.e. *k*-factor) on the value of the injected reactive current during the fault. Consequently, considering the influence of the *k*-factor in the steady-state fault calculation would potentially enhance the accuracy of the calculated fault currents fed from the NSG-based RESs. This will be also examined in the following section using a larger system.

5.4.2 **IEEE 14-Bus Test System**

In this part, the accuracy of the proposed method for considering the NSG-based RESs in the steady-state fault calculations is evaluated using the adjusted IEEE 14-Bus test system. The system originally includes five SGs but three of them are used as synchronous condensers (synchronous condensers). It is worth mentioning that the Synchronous condensers show response to the fault the same as SGs, therefore synchronous condensers are treated/modelled as SGs according to IEC60909 standard for fault calculations. Fig.41 shows the modified IEEE 14-Bus test system with the PV systems. Observe that three PV systems (100 MVA each) have displaced the original units (SG at Bus 2, Synchronous condensers at Buses 3 and 6). Note that the installed capacity of the PV systems is equal to 300 MVA, which represents a total penetration level of (37.5%). This is calculated using the previously explained capacity-based penetration level metric as expressed in (3.6).

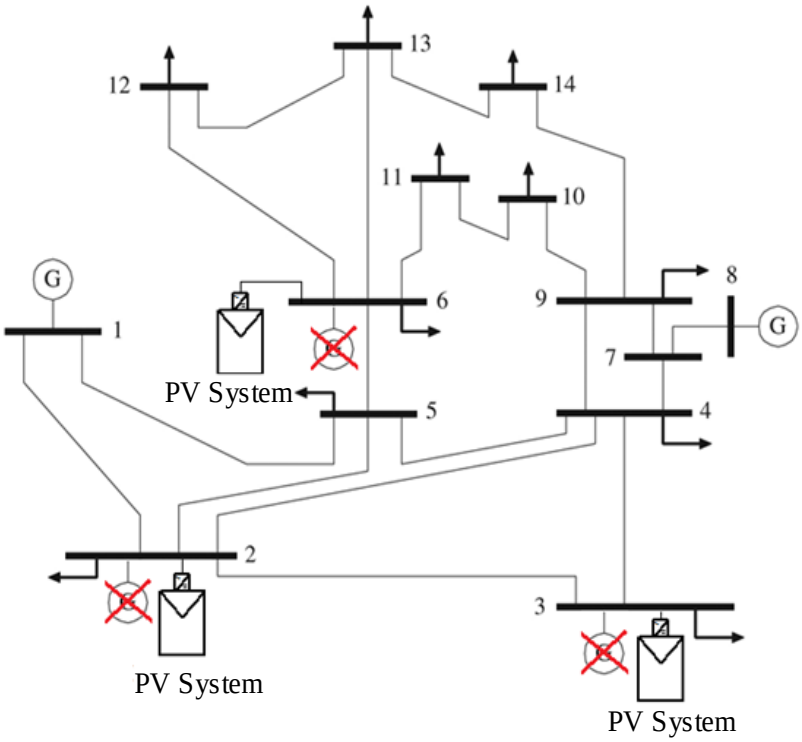

Fig.41: The modified IEEE 14-Bus test system

The initial symmetrical fault currents have been calculated at three different locations in the system (i.e. at Buses 5, 9 and 13) assuming a bolted three-phase fault. The calculation process has been conducted using both the IEC60909 standard and the proposed modification method in section 5.3. Then, the obtained results have been compared with those obtained from RMS simulations for validation purposes. This has been done considering two values of the proportional gain (*k*-factor) to validate the accuracy of the proposed method at different levels of reactive current injection.

At first, a value of (k=2) is used which represents the requirement from various grid codes such as German grid code. Second, a value of (k=10), is used which represents some grid codes which require a maximum reactive current injection during the fault such as UK grid code. It is worth pointing out that a maximum overrating capability of the converter interface of (1.3 p.u.) is used for both cases.

5.4.2.1 Case 1 (k=2)

Fig.42 compares the values of the initial symmetrical fault current calculated on Buses 5, 9 and 13 for the case where (k=2). Observe the superior performance of the proposed method when compared to the IEC60909 standard. It can be noted that the IEC60909 standard tends to overestimate the fault currents regardless of the location of the faulty point. The difference between the estimated values and the actual ones (i.e. RMS simulations) should not be neglected anymore, as it exceeds 20% in some cases. For instance, the absolute error on Bus 13, is equal to 22.20% as shown in Table 13. On the other hand, a noticeable enhancement of the fault currents calculation procedure is observed using the proposed method.

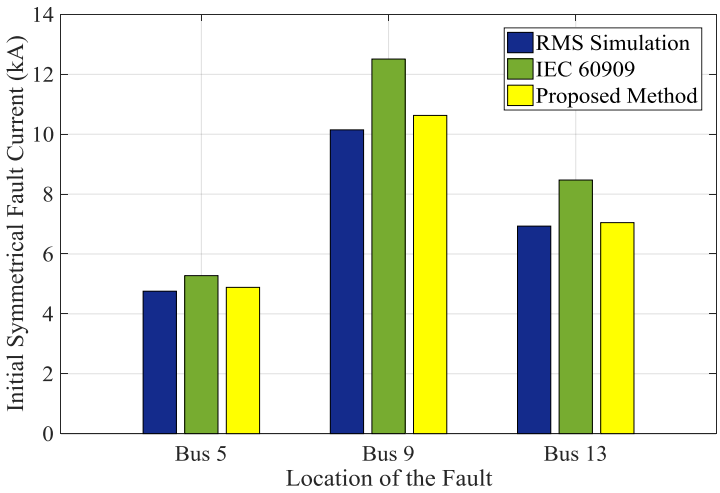

Fig.42: The resulted values of the fault currents from different methods for the case (k=2)

Opposing the IEC60909 standard, the results obtained from the proposed method has a negligible error, as it is less than 5%. It is worth mentioning that the maximum absolute error has been registered on Bus 9. This equals to 23.31% and 4.75%, for the IEC60909 standard and the proposed method respectively. The results are also listed in Table 15, which compares between the calculated fault currents (i.e. initial symmetrical fault currents ($I_k^{"}$). obtained from both the IEC60909 method and the proposed one in section 5.2 and 5.3 respectively. The absolute errors, compared to the RMS simulation results, are also calculated and listed in Table 15.

Table 15: Fault currents on the adjusted IEEE 14-Bus test system (k=2)

Bus	***RMS Simulation***	***IEC60909***		***Proposed Method***	
Num.	I_K'' ***(kA)***	I_K'' ***(kA)***	***Error (%)***	I_K'' ***(kA)***	***Error (%)***
Bus 5	4.75	5.27	10.93	4.88	2.69
Bus 9	10.15	12.51	23.31	10.63	4.75
Bus 13	6.93	8.47	22.20	7.05	1.67

5.4.2.2 Case 2 (k=10)

Fig.43, shows the fault currents at the same locations (i.e. Buses 5, 9 and 13) which have been re-calculated using both the IEC60909 and the proposed method, considering a different value for the injected reactive current proportional gain (*k*-factor =10). As it can be shown in Fig.43, the results show that the calculated currents using the IEC60909 standard overestimate the actual values shown by the RMS simulation results, but with less absolute error compared to the Case 1 (*k*=2). For example, the absolute error on Bus 5, has decreased from 10.93% with *k*=2 down to 6.60% with *k*=10.

Moreover, the proposed method has shown a higher error margin for the calculated fault currents compared to those calculated when in Case 1 (*k*=2). For instance, the absolute error of 1.67%, which has been noted in Case 1 (*k*=2), is increased up to 4.12% in Case 2 (*k*=10). Note that both the IEC60909 standard and the proposed method show the same estimated fault currents on Bus 5 in Case 1 (*k*=2). This demonstrates that calculated fault currents from both methods converge to the same values for faults near the RESs and high *k*-factor.

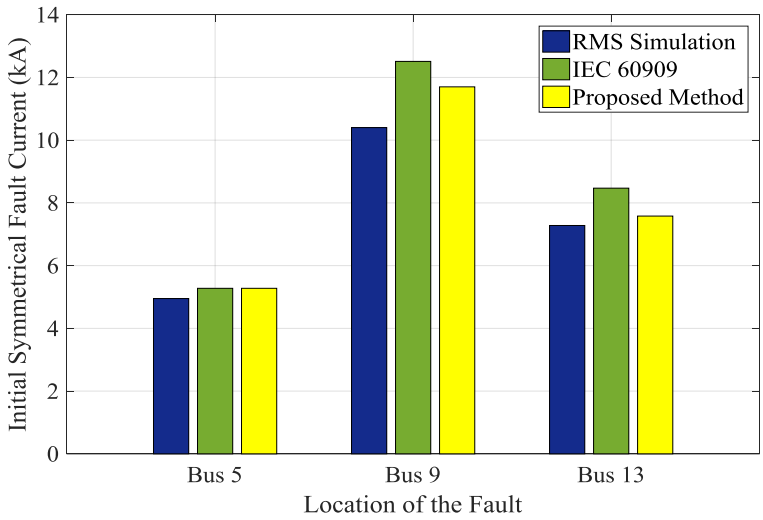

Fig.43: The resulted values of the fault currents from different methods for the case (*k*=10)

Table 16: Fault currents on the adjusted IEEE 14-Bus test system (k=10)

Bus	***RMS Simulation***	***IEC60909***		***Proposed Method***	
Num.	I_K'' ***(kA)***	I_K'' ***(kA)***	***Error (%)***	I_K'' ***(kA)***	***Error (%)***
Bus 5	4.95	5.27	6.60	5.277	6.60
Bus 9	10.4	12.51	20.29	11.7	12.50
Bus 13	7.28	8.47	16.35	7.58	4.12

In other words, the performance of the IEC60909 standard-based fault currents calculation method can be acceptable depending on the location of the fault and on the proportional gain for reactive current injection (k-factor). For example, the results of the calculated fault current at Bus 5 for case 2 (k=10) has the same accuracy with the proposed method as illustrated in Table 16. Note that both have calculated the fault current with a 6.6% error, which might be accepted.

5.5 Conclusion

An enhancement on the steady-state fault calculations according to the IEC60909 method is proposed and evaluated in this chapter. While the up-to-date IEC60909 standard has proven its accuracy for conventional power systems dominated by synchronous generators (SGs), the results have shown poor accuracy in estimating the fault currents in systems with high penetration of NSG-bases RESs. The latest version of the IEC60909 standard has modelled the fully rated converter (FRC)-based NSG as a current source with a maximum fixed pre-defined fault current contribution. This neglects many factors such as the variety of grid code requirement, FRT control and the voltage dip level during the fault. This proposed method has augmented the methodology in the latest version of the IEC60909 standard by improving the reactive current injection modelling for NSG-based RES during the fault. The simulation

results show that the proposed method can provide better estimates for the fault currents with smaller error margins compared to the IEC60909. In particular, the proposed method has shown a maximum absolute error of 4.75% and 12.5% using the modified IEEE 14-Bus system for the cases when (k=2) and (k=10) respectively. On the other hand, the IEC60909 standard illustrated a maximum absolute error of 23.31% and 20.9% for the same cases. Hence, it can be concluded that the error margin in steady-state fault calculation of power systems with high penetration of NSG-based RES can be reduced at least by 50% using the proposed method.

6 Novel MVA-based Fault Level Calculation Method in Future Grid Scenario with High Penetration of NSGs

6.1 Introduction

This chapter proposes a novel method for quantifying fault level in FG scenarios with various penetrations of NSG-based RESs. In this chapter, these sources will be also referred to as PE-based sources. As it is known, the information about the fault level is critically important for designing protection schemes, different control loops, understanding voltage profile in the grid. This new method is focused on the steady-state fault level calculation (FLC) and it can be used to analyse a wide range of different FG scenario including uniform and non-uniform penetration of PE-based generation displacing all, or just specific conventional synchronous generation in the grid. Due to different possibilities for type, size and location of PE-based RES generation in FGs, it is required to analyse an unprecedented scale of PE-based penetration scenarios.

This method considers the MVA representation of the fault level, which is widely used in power systems calculations [105-107]. The MVA method, which is considered a modification of the ohmic and per-unit methods, is applied for symmetrical faults calculations where the circuit components can be separated and represented by their corresponding SC power in (MVA) [105]. Also, this method has been used to calculate the SC capacity at different faulty points for various feeders in distribution system for its simplicity [106]. The authors have applied this MVA method to develop curves representing the SC capacity along feeders to evaluate the increments of SC capacity resulted from upgrading the distribution network. In [107], the MVA representation of the fault level has been used for another application. It has

been considered to propose a screening tool for predicting fault-induced low voltages problems on bulk transmission systems.

In this thesis, the novel proposed method for FLC employs the MVA representation to consider the fault contribution from NSGs in large networks benefiting from the ability to decompose the fault level into different MVA values according to the circuit components too. This MVA representation is augmented in such a way to represent the fault level at the faulty point by an arrangement of two MVA components, a variable component related to the fault level MVA at the generation Bus, besides a fixed component representing the rest of the network. This allows dealing with the generation Buses in a separated way from the network and enables to reflect the impact of integrating PE-based generation and quantify the fault level as a function of the penetration level of these sources at both the generation Buses and the faulty points.

Such augmentation of the MVA method provides a quick and efficient tool to assess the system fault level for a large number of FG scenarios without a need for a detailed system modelling or dynamic simulations. Moreover, the simple generic modelling of the NSGs would be adequate in our FLC method, as it only requires the maximum contribution from these NSGs in response to a severe fault at their terminal. This information is usually available or easy to obtain by knowing the maximum overrating capability of the converter utilised in these NSGs. Details and steps of the proposed FLC method will explain and show the novelty more clearly.

The obtained results demonstrated the suitability of the proposed FLC method for various penetration levels of PE-based RESs in three different test systems which include the 2-area, the IEEE 9-Bus and the IEEE 39-Bus test systems. These results are compared with the actual

fault level calculated based on the time-domain simulations as well as those results obtained from the IEC60909 standards performed in DIgSILENT PowerFactory, where the efficacy of the proposed methodology is demonstrated.

6.2 Fault Level Contribution from SG and its MVA Representation

As stated earlier in chapter 2, the MVA representation of the fault level can be expressed by multiplying the SC current flowing at the faulty Bus, by the corresponding nominal voltage at that Bus as expressed previously in (1.1). However, in order to do so, the SC current should be calculated first. The fault contribution from any connected SG in the grid can be determined using an equivalent circuit shown in Fig.44.a and Fig.44.b.

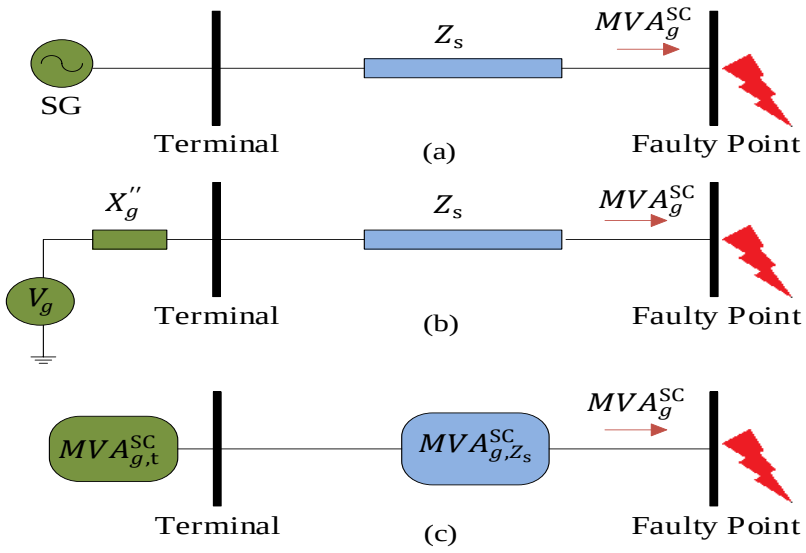

Fig.44. SG fault contribution (a) single line diagram, (b) equivalent circuit, and (c) its MVA representation.

Using the SG voltage source, V_g, behind the equivalent impedance observed from the faulty point, Z_g^{eq}, the SC current can be calculated as follows:

$$I_g^{SC} = \frac{V_g / \sqrt{3}}{Z_g^{eq}} \tag{6.1}$$

The equivalent impedance, Z_g^{eq}, includes the internal sub-transient reactance of the SG, X_g'', in series with the total equivalent series impedance of the elements connecting the generator terminal to the faulty point, Z_g^s, as shown in Fig.44.b. The fault level associated with the SG can be calculated by substituting (6.1) in (1.1), as given in (6.2):

$$MVA_g^{SC} = \sqrt{3}V_g \frac{V_g / \sqrt{3}}{Z_g^{eq}} = \frac{V_g^{\,2}}{Z_g^{eq}} = \frac{V_g^2}{X_g^{"} + Z_s} \tag{6.2}$$

By re-arranging (6.2), the fault level contribution of SG can be represented as follows:

$$MVA_g^{SC} = \frac{1}{\frac{1}{(V_g^2 / X_g^{"})} + \frac{1}{(V_g^2 / Z_s)}} \tag{6.3}$$

Two MVA components associated with the fault level contribution of a SG can be derived from (6.3), as follows:

- $(V_g^2/X_g^{"})$: Fault contribution associated with the SG sub-transient reactance that represents its maximum fault capability in response to symmetrical three-phase SC fault at its terminal, referred as $MVA_{g,\mathrm{t}}^{\mathrm{SC}}$.
- (V_g^2/Z_s): Fault contribution associated with the impedance of the connecting elements between the SG terminal to the faulty point including the impedance of the step-up transformer and connecting lines, referred to as $MVA_{g,Z_s}^{\mathrm{SC}}$.

The equation (6.3) can be also re-written using $MVA_{g,\mathrm{t}}^{\mathrm{SC}}$ and $MVA_{g,Z_s}^{\mathrm{SC}}$ terms as:

$$MVA_g^{SC} = \frac{1}{\frac{1}{MVA_{g,\mathrm{t}}^{SC}} + \frac{1}{MVA_{g,Z_s}^{SC}}} = \frac{MVA_{g,\mathrm{t}}^{SC} \times MVA_{g,Z_s}^{SC}}{MVA_{g,\mathrm{t}}^{SC} + MVA_{g,Z_s}^{SC}} \tag{6.4}$$

On the basis of (6.4), the fault level contribution associated with SG, MVA_g^{SC}, can be defined using combinations of $MVA_{g,t}^{SC}$ and MVA_{g,Z_s}^{SC}, as shown in Fig. 45c.

6.3 Augmenting FLC Method Including the Impact of PE-Based Generation

6.3.1 Penetration Level Metric

The penetration level, P, is defined to represent the portion of supplied power from a PE-based generation, MVA_{PE} , out of the total generation capacity of the generation unit, MVA_T, as shown in Fig.45. The penetration of PE generation can be given as follows:

$$P = \frac{MVA_{PE}}{MVA_T} = \frac{MVA_{PE}}{MVA_g + MVA_{PE}} \tag{6.5}$$

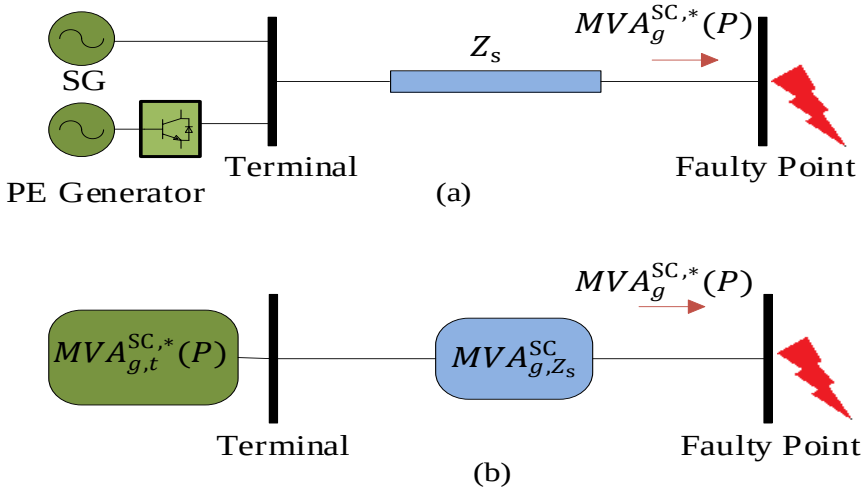

Fig.45. Fault level contribution from the compound generation unit
(a) single line diagram, and (b) its MVA representation.

6.4 Main Steps of the Proposed Methodology

This proposed methodology integrates the impact of PE-based generation in (6.4) by augmenting $MVA_{g,\mathrm{t}}^{\mathrm{SC}}$ term as a function of penetration level of this PE-based generation at the SG terminal, i.e. $MVA_{g,\mathrm{t}}^{\mathrm{SC},*}(P)$. Note that the star notation (*) is used for the compound generation unit including SG and PE-based generation. The representation of the fault level in (6.5) the impact of newly added PE-based generation alongside de-rated SG unit, as shown in Fig.45. This new FLC method allows to study the impact of any FG scenario with various penetration of PE-based generation at all/specific SG locations, as explained below in more details. It is worth mentioning that the scope of previous related studies was limited to particular networks and/or scenarios due to the use of time-consuming methodologies such as time-domain simulations. On the other hand, our FLC method can be used as a fast scanning tool for analyzing large numbers of FG scenario. Note that we augmented (6.4) benefiting from unchanged $MVA_{g,Z_s}^{\mathrm{SC}}$ (i.e. the fault level contribution associated with the connecting elements up to the faulty point does not change), as given in (6.6).

$$MVA_{g}^{\mathrm{SC},*}(P)=\frac{MVA_{g,\mathrm{t}}^{\mathrm{SC},*}(P)\times MVA_{g,Z_s}^{\mathrm{SC}}}{MVA_{g,\mathrm{t}}^{\mathrm{SC},*}(P)+MVA_{g,Z_s}^{\mathrm{SC}}} \tag{6.6}$$

Note that this is the initial step made towards the formulation of the effect of displacement of the SG by PE-based generation on the system fault level. This methodology for FLC including the impacts of PE-based generation is summarised in the following steps:

- ***Step1**-Calculating $\boldsymbol{MVA_{gi,Z_s}^{SC}}$ for each displaced SG from the base case[1]:*

As mentioned earlier, this methodology assumes that both the fault level contribution from the *i*-th generator to the faulty point, MVA_{gi}^{SC}, and to its terminal, $MVA_{gi,\mathrm{t}}^{\mathrm{SC}}$, are initially known either by using simulations or the steady-state fault calculation programs. In this paper, the results for the initial bases scenario, which are used as inputs for our methodology, are obtained from the steady-state fault calculation using the complete method in DIgSILENT PowerFactory. Using these values, the term, $MVA_{g,Z_s}^{\mathrm{SC}}$, can be calculated by rearranging (6.4) as follows:

$$MVA_{gi,Z_s}^{\mathrm{SC}} = \frac{MVA_{gi,\mathrm{t}}^{\mathrm{SC}} \times MVA_{gi}^{\mathrm{SC}}}{MVA_{gi,\mathrm{t}}^{\mathrm{SC}} - MVA_{gi}^{\mathrm{SC}}} \tag{6.7}$$

In the proposed FLC method, once calculated, $MVA_{gi,Z_s}^{\mathrm{SC}}$ is assumed to be fixed regardless of changes that might occur at the generation side, as explained above.

- ***Step 2**-Calculating of the updated terminal fault level $MVA_{gi,t}^{SC,*}(P_i)$ as a function of the PE-based generation penetration:*

The maximum available fault level, at the terminal of the generation unit at any penetration level of PE-based generation, is equal to sum of the fault level supplied from both de-rated SG, $MVA_{g,\mathrm{t}}^{\mathrm{SC}}(P)$, and PE-based generation, $MVA_{PE,\mathrm{t}}^{\mathrm{SC}}(P)$, as given in (6.8).

$$MVA_{gi,\mathrm{t}}^{\mathrm{SC},*}\left(P_i\right) = MVA_{gi,\mathrm{t}}^{\mathrm{SC}}\left(P_i\right) + MVA_{PEi,\mathrm{t}}^{\mathrm{SC}}\left(P_i\right) \tag{6.8}$$

[1]Note that the base case is referred to the existing power systems before analysing FG scenario including further uptake of PE-based generation.

Where, the terms $MVA_{gi,\mathrm{t}}^{\mathrm{SC}}(P)$ and $MVA_{PEi,\mathrm{t}}^{\mathrm{SC}}(P)$ can be calculated as follows:

Step 2.1- Updated fault contribution from SG at its terminal, $MVA_{gi,t}^{SC}(P)$: The maximum fault level of a SG at its terminal can be determined using its rating voltage and internal sub-transient reactance, as given in (6.9):

$$MVA_{gi,\mathrm{t}}^{\mathrm{SC}} = \frac{MVA_{gi}}{x_{gi}^{"}} \tag{6.9}$$

Where, $x_{gi}^{"}$ is the sub-transient reactance in per unit.

In displacement scenario, which are the focus of most FG scenario studies, it is assumed that the SG rating is reduced to (1-P_i) due to the increased penetration of PE-based generation to (P_i). In such a case, the terminal fault level in (6.9) also will be decreased by the same factor, as follows:

$$MVA_{gi,\mathrm{t}}^{\mathrm{SC},*}\left(P_i\right) = \frac{\left(1-P_i\right)\times MVA_{gi}}{x_{gi}^{"}} = \left(1-P_i\right)\times MVA_{gi,\mathrm{t}}^{\mathrm{SC}} \tag{6.10}$$

Step 2.2- Fault contribution from PE-based generator at its terminal, $MVA_{PEi,t}^{SC}(P_i)$: It is assumed that the PE-based generator complies with the grid code requirement by injecting reactive current during the fault. Hence, a proportional gain (*k*-factor) of 2 is chosen, according to the German grid code. This means that the injected reactive current is twice proportional to the voltage dip resulting from the fault. The maximum contribution of the PE-based generator to a SC at its terminal depends on the overloading capability represented by (α_{PE}) in (6.11).

$$MVA_{PEi,\mathrm{t}}^{\mathrm{SC}} = \alpha_{PEi}\times MVA_{PEi} \tag{6.11}$$

Using (6.5), the rating of PE-based generation, MVA_{PE}, can be defined on the basis of total installed generation capacity, MVA_{T}, which is assumed to be equal to the synchronous generator rating before decommissioning (i.e.$MVA_{Ti} = MVA_{gi}$)**,** hence MVA_{PE} can be represented as shown in (6.12).

$$MVA_{PEi} = P_i \times MVA_{\mathrm{Ti}} \tag{6.12}$$

By substituting (6.12) in (6.11), the fault level contribution at the terminal of the PE generation can be given as follows:

$$MVA_{PEi,\mathrm{t}}^{\mathrm{SC}} = \alpha_{PEi} \times P_i \times MVA_{\mathrm{Ti}} \tag{6.13}$$

Considering the fault contributions from both the SG and the PE-based generator, which are given in (6.10) and (6.13) respectively, the maximum fault level from the compound generation at its terminal can be written as:

$$MVA_{gi,\mathrm{t}}^{\mathrm{SC},*}\left(P_i\right) = \left(1-P_i\right) \times MVA_{gi,\mathrm{t}}^{\mathrm{SC}} + \alpha_{PEi} \times P_i \times MVA_{\mathrm{Ti}} \tag{6.14}$$

- ***Step 3*-** Calculating the updated fault level contribution $\boldsymbol{MVA_{gi}^{\mathrm{SC},*}(P)}$ as a function of the PE-based generation:

The total fault level contribution from both de-rated SG and PE-based generation, $MVA_{g}^{\mathrm{SC},*}(P)$, can be obtained by substituting (6.14) in (6.6), as follows:

$$MVA_{gi}^{\mathrm{SC},*}\left(P_i\right) = \frac{[\left(1-P_i\right) \times MVA_{gi,\mathrm{t}}^{\mathrm{SC}} + \alpha_{PEi} \times P_i \times MVA_{\mathrm{Ti}}] \times MVA_{gi,Z_s}^{\mathrm{SC}}}{[\left(1-P_i\right) \times MVA_{gi,\mathrm{t}}^{\mathrm{SC}} + \alpha_{PEi} \times P_i \times MVA_{\mathrm{Ti}}] + MVA_{gi,Z_s}^{\mathrm{SC}}} \tag{6.15}$$

- ***Step 4***-Calculating of the updated total fault level $\boldsymbol{MVA_{SC}(P_T)}$ as a function of the total PE-based generation:

The equation (6.15), which is valid for a single compound machine considering the corresponding local penetration level at generation Bus (i.e. P_i), can be used for each displaced SG. By doing so, the FLC can be extended to consider various displacement scenario. This will enable representing the fault level as a function of the total system-scale penetration level (i.e. P_T). Note that the total penetration level at a system scale, P_T, and the local penetration level at a certain generation Bus, P_i are correlated as follows:

$$P_T = \frac{\sum_{i=1}^{N} MVA_{PEi}}{\sum_{i=1}^{N} MVA_{Ti}} = \frac{\sum_{i=1}^{N} P_i \times MVA_{Ti}}{\sum_{i=1}^{N} MVA_{Ti}} \tag{6.16}$$

By using these metrics, the total fault level as a function of the total penetration level, P_T, can be represented by summing up the contributions from all the connected generation units formulated on the basis of the local penetration level, Pi, as follows:

$$MVA_{SC}(P_T) = \sum_{i=1}^{N} MVA_{gi}^{SC,*}(Pi) \tag{6.17}$$

6.5 Non-Numerical Case Study

For better understanding, let us to consider an example where a PE-based generator displaces the conventional generator SGg_1, as shown in Fig.46. By following the proposed FLC method, the only variable here will be the fault level contribution from the displaced SGg_1 (e.g. MVA_{g1}^{SC}). In other words, the total fault level at the faulty point before decommissioning

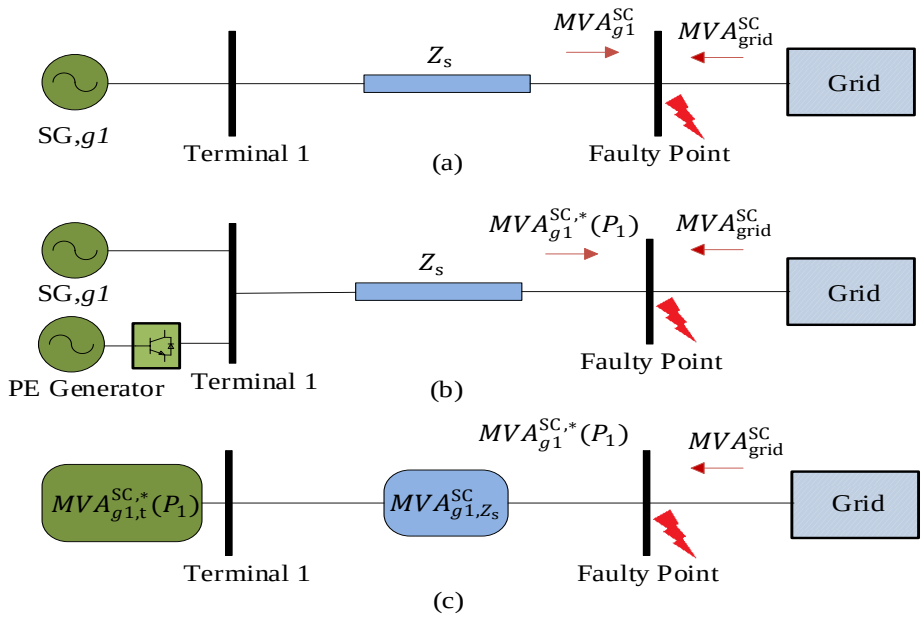

Fig.46: The representation of the fault level at non-uniform penetration scenario.

of the SGg_1, MVA_{SC}, is re-calculated as a function of the penetration level of PE-based generator. This total fault level at the faulty point, MVA_{SC}, is divided into two parts: i) variable fault contribution from the SGg_1, MVA_{g1}^{SC}, and ii) fixed fault contribution from the other connected generators in the grid (i.e. P_i=0, for i≠1). Therefore, (6.17) is re-written as follows:

$$MVA_{SC}(P_T) = MVA_{g1}^{SC,*}(P_1) + \sum_{i=2}^{N} MVA_{gi}^{SC,*}(0) \tag{6.18}$$

The second fixed term can be represented by an equivalent grid, as given in (6.19).

$$MVA_{SC}(P_T) = MVA_{g1}^{SC,*}(P_1) + MVA_{grid}^{SC} \tag{6.19}$$

Then, the equations (6.6)-(6.15) should be used for calculation of the fault level as a function of PE-based generation penetration, $MVA_{g1}^{SC,*}(P_1)$, as given in (6.15). In other words, at this

stage, we include the impact of PE-based generation and decommissioned SG g_1 in the FLC method. Finally, the calculated $MVA_{g1}^{\mathrm{SC},*}(P_1)$, given in (6.15), should be added to the fixed fault level contribution from the rest of the grid, $MVA_{\mathrm{grid}}^{\mathrm{SC}}$, as shown in (6.20).

$$MVA_{\mathrm{SC}}\left(P_T\right)=\frac{[(1-P_1)\times MVA_{g1,\mathrm{t}}^{\mathrm{SC}}+\alpha_{PE1}\times P_1\times MVA_{\mathrm{T1}}]\times MVA_{g1,Z_s}^{\mathrm{SC}}}{[(1-P_1)\times MVA_{g1,\mathrm{t}}^{\mathrm{SC}}+\alpha_{PE1}\times P_1\times MVA_{\mathrm{T1}}]+MVA_{g1,Z_s}^{\mathrm{SC}}}+MVA_{\mathrm{grid}}^{\mathrm{SC}} \tag{6.20}$$

6.6 Special Case (uniform PE penetration scenario)

In these scenario, PE-based generation penetration is evenly increased at all generation Buses (i.e. P_1=P_2=…=P_{N}). Although this scenario might not be a practical in real power systems currently, it will help to understand the impact of the uniform distribution of the NSGs in the system. Moreover, such an assumption would be beneficial for assessing some future scenario in power systems where most of the classical generation units will be replaced by RESs. In this special case, the value of the total penetration level is equal to the local penetration level, (i.e.$P_T = P_i$). In order to apply our FLC method to such scenario, it is assumed that the fault level MVA_g^{SC} is decomposed into two aggregated components: i) fault contribution associated with the aggregated SGs at its terminal, $MVA_{g,\mathrm{t}}^{\mathrm{SC,Agg}}$, and ii) fault level associated with the aggregated impedance Z_s^{Agg}, represented by $MVA_{g,Z_{\mathrm{s}}}^{\mathrm{SC,Agg}}$. These imply that the SC current is fed from one aggregated source, through aggregated impedance that is connected in series between the generation unit and the faulty point, Z_s^{Agg}. This is similar to the schematic diagram shown in Fig.45. Terms, $MVA_{g,\mathrm{t}}^{\mathrm{SC,Agg}}$ and $MVA_{g,Z_{\mathrm{s}}}^{\mathrm{SC,Agg}}$, can be calculated using (6.21) and (6.22) respectively.

$$MVA_{g,\mathrm{t}}^{\mathrm{SC,Agg}} = \sum_{i=1}^{i=N} MVA_{gi,\mathrm{t}}^{\mathrm{SC}} \quad (22) \tag{6.21}$$

$$MVA_{g,Z_s}^{\mathrm{SC,Agg}} = \frac{MVA_{g,\mathrm{t}}^{\mathrm{SC,Agg}} \times MVA_{g}^{\mathrm{SC}}}{MVA_{g,\mathrm{t}}^{\mathrm{SC,Agg}} - MVA_{g}^{\mathrm{SC}}} \quad (23) \tag{6.22}$$

Using (6.14), the value of the aggregated terminal fault level in (6.21) can be updated, as follows:

$$MVA_{g,\mathrm{t}}^{\mathrm{SC,Agg}}\left(P_T\right) = \left(1-P_T\right) \times MVA_{g,\mathrm{t}}^{\mathrm{SC,Agg}} + \alpha_{PE} \times P_T \times MVA_{\Gamma}^{\mathrm{Agg}} \tag{6.23}$$

Finally, by substituting (6.22) and (6.23) in (6.6), the fault level for uniform penetration of PE-based generation will be given in (6.24):

$$MVA_{SC}\left(P_T\right) = \frac{[\left(1-P_T\right) \times MVA_{g,\mathrm{t}}^{\mathrm{SC,Agg}} + \alpha_{PE} \times P_T \times MVA_{\Gamma}^{\mathrm{Agg}}] \times MVA_{g,Z_s}^{\mathrm{SC,Agg}}}{[\left(1-P_T\right) \times MVA_{g,\mathrm{t}}^{\mathrm{SC,Agg}} + \alpha_{PE} \times P_T \times MVA_{\Gamma}^{\mathrm{Agg}}] + MVA_{g,Z_s}^{\mathrm{SC,Agg}}} \tag{6.24}$$

Note that all the FLC steps are also described the flow chart shown in Fig.47.

6.7 Flow chart of the proposed FLC Method

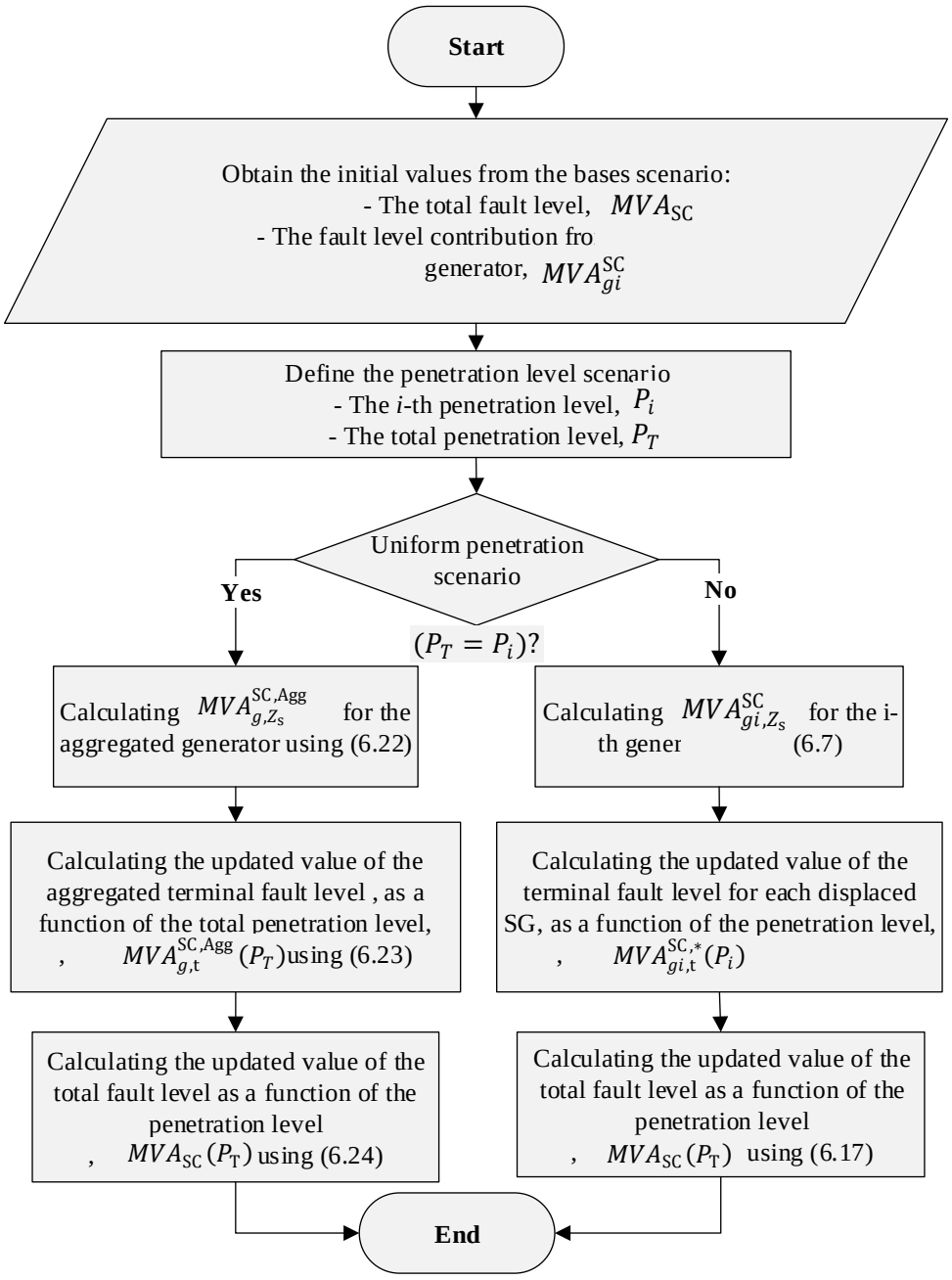

Fig.47: The flow chart of the proposed FLC

6.8 Results and Discussion

Our FLC method in section (6.7) is used for fault level calculation in three test systems: the 2-area test system [108], IEEE 9-Bus test system [102] and the IEEE 39-Bus test system [109]. The proposed method is tested under different scenarios with the increased penetration of PE-based generation, and the obtained results are compared with the simulations performed in DIgSILENT PowerFactory, where the accuracy of our methodology is proven. The following sections discuss the simulation results obtained from those test systems in more details.

6.8.1 **Two-Area System**

6.8.1.1 Scenario1 (Non-uniform penetration of NSG at G2)

In this scenario, a wind power plant utilising FRC technology (i.e. Type 4) has gradually displaced SG-G2 up to a penetration level of 100% (i.e. P*2*=1) of PE-based generation as shown in Fig.48. This represents a maximum total PE penetration level of 25% (i.e. P_T =0.25).

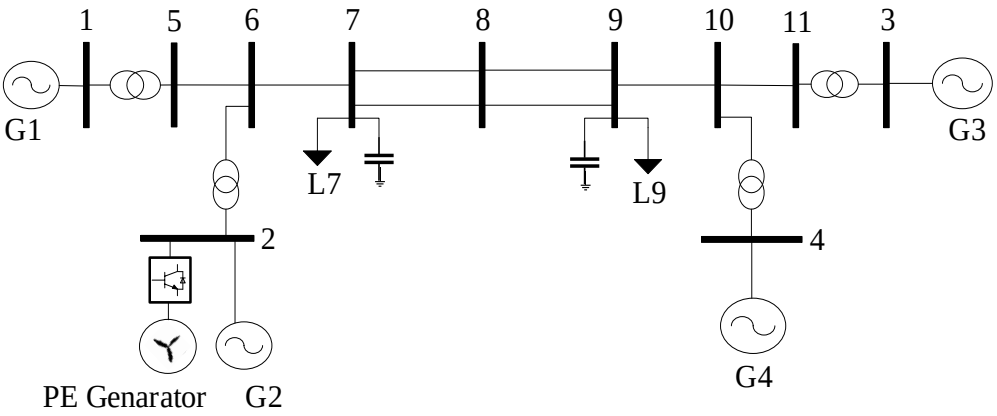

Fig.48: The two-area test system with a PE-based generation on Bus 2.

As can be shown in Fig.49, the system fault level tends to decrease with the increased penetration of PE-based generation in the system. This is due to the fact that the maximum fault level of PE-based generation is limited to its MVA rating of FRC (e.g. $\alpha_{PE} = 1.1$ is considered here). In addition, Fig.49 compares the results obtained from our FLC method (section 6.3) and the one obtained from dynamic simulation carried out in DIgSILENT. It can be seen that the results obtained from our method are almost the same as the time-domain simulation results. For this scenario, the maximum absolute error between our FLC method and time-domain simulations is less than 3.1%. Note that the results in Fig.49, are demonstrated for two typical Buses in the system, while the same trend was observed for other Buses in the grid. Further, the fault levels on Buses 6 and 7 are reduced from (4375 MVA and 3328 MVA at P_2=0) to (2907 MVA and 2706 MVA at P_2=1), respectively. This implies 33% and 18% reductions in the fault level on Buses 6 and 7 at 100% penetration of PE-based generation, respectively.

6.8.1.2 Scenario 2 (Non-uniform penetration of NSG at all Generators)

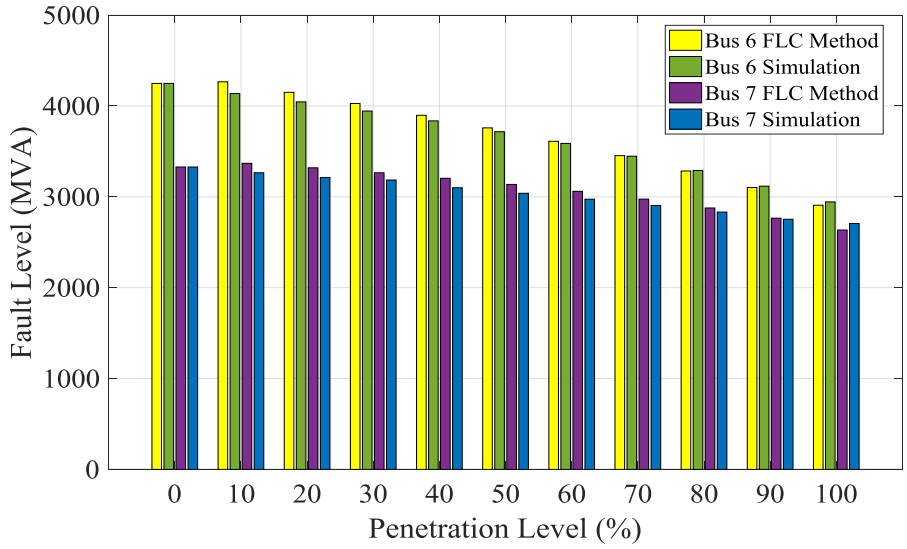

Fig.49: The fault level on 2-area test system with different levels of P_2 (*scenario 1)*

In this scenario, PE-based generation units (wind power plants) are connected to all SG locations. The penetration level, $P_{T,}$ is increased gradually from 0%to 70%. The fault level is then calculated for all the Buses, as depicted in Fig.50. Similar to the observed pattern in Fig. 50, reductions in the fault levels for Buses 6 and 7 are noted with the increased penetration of PE-based generation in the grid. The maximum reduction in the fault level is occurred at the highest penetration level (i.e. 70%), as expected. The fault level on Buses 6 and 7 are reduced from (4248 MVA and 3328 MVA at P_T=0) to (3093 MVA and 2667 MVA at P_T=0.7), respectively. This indicates 18% and 20% reductions in the fault level on Buses 6 and 7, respectively.

It is worth mentioning that the error in this scenario is slightly higher than the non-uniform penetration scenario, which is due to higher numbers of PE-based generation in the grid. Nevertheless, the maximum absolute error is still less than 4%. The simulation results showed the efficiency of our FLC methodology for analyzing large numbers of FG scenario in a short period.

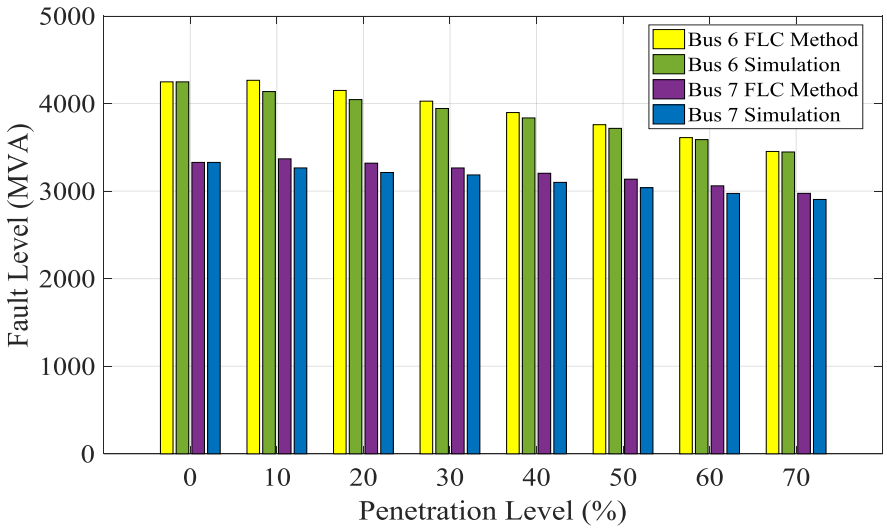

Fig.50: The fault level on 2-area test system with different levels of P_T (*scenario 2)*

6.8.2 **IEEE 9-Bus Test System**

In this section, another test system is used to validate the accuracy of the proposed FLC method. Specifically, the IEEE 9-Bus test system is modelled in DIgSILENT PowerFactory with different NSG's penetration scenario. Like the previous case where the 2-area test system is used, the studied scenario covers both uniform and non-uniform scenario of NSG-based RESs. At first, the system is adjusted to consider a non-uniform penetration of NSGs represented by a type-4 wind farm connected at Bus 2. Then, the uniform penetration scenario is considered, where three wind farms (type-4) are evenly introduced to partially displace the SGs at all generation locations.

6.8.2.1 Scenario1 (Non-uniform penetration of NSG at G2)

The PE-based generation has gradually replaced conventional SG-G2, as shown in Fig.51. The total installed capacity the resulted compound power plant is always remained fixed (i.e. 192 MVA) during the displacement scenario.

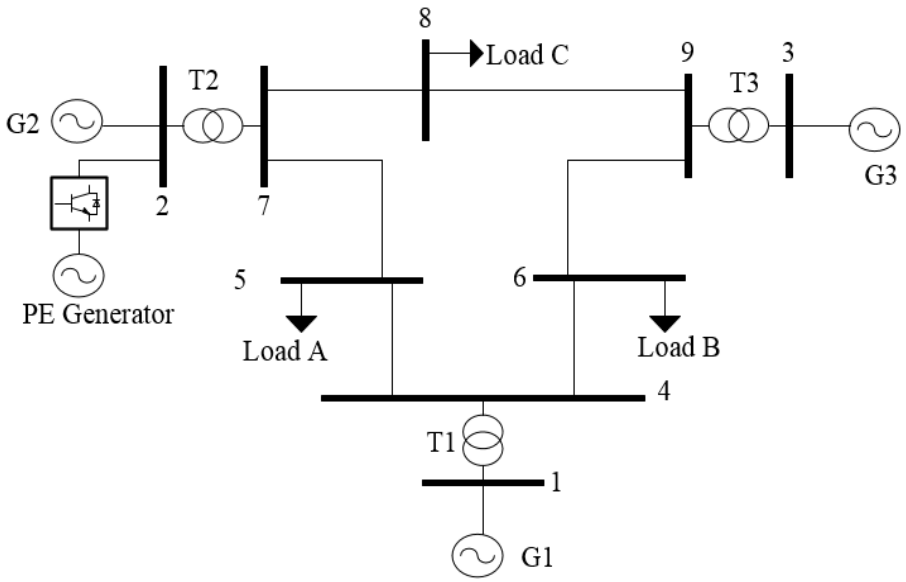

Fig.51: The adjusted IEEE 9-Bus test system with a PE-based generator on Bus 2

Note that the maximum local PE penetration level is 100% (i.e. P_2=1) for this scenario represents a 33.8% penetration of the total generation capacity in the system (i.e. P_T=0.338). As can be shown in Fig.52, the system fault level is reduced with the increased penetration of PE-based generation in the system, similar to the observed trend in Fig.52. The fault levels on Buses 5 and 8 are reduced from (914 MVA and 905 MVA) to (815 MVA and 740 MVA), respectively (i.e. 21% and 35%, respectively). Hence, the reduction of fault level on Bus 8 is more sensitive to the displacement scenario compared to Bus 5. This might be denoted to the fact that SG at Bus 2 (i.e. G2) has had initially more contribution to the fault level on Bus 8 more than Bus 5. Note that Fig.52 also provides a comparison between the results obtained from our FLC method and those obtained from time-domain simulations. It is worth mentioning that the maximum absolute error between the proposed FLC method and the actual results of the time-domain simulations is almost negligible, as only a maximum absolute error of 2.4% is observed.

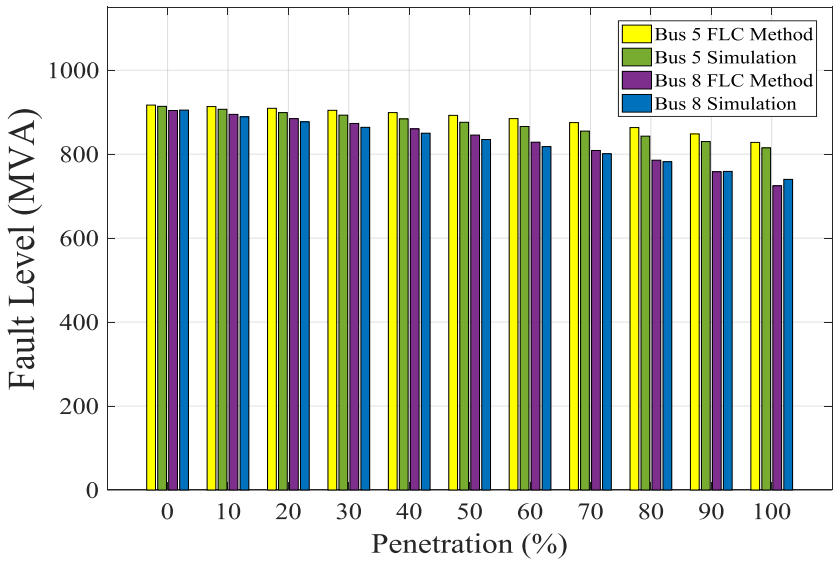

Fig.52. Fault level in the modified IEEE 9-Bus test system with different levels of P_2 (*scenario1*)

6.8.2.2 Scenario2 (Uniform penetration of NSG at all Generators)

For uniform penetration scenario in the IEEE 9-Bus test system, the PE-based generators are evenly increased at all generation Buses to partially displace the conventional SGs. Similar to the previous scenario, the total generation capacity is kept fixed and the total PE penetration level is gradually increased from 0% up to 70%. The fault level on Buses 5 and 8 is shown for this scenario in Fig.53, where again a reduction in the system fault level can be observed from (914 MVA and 905 MVA at P_2=0) to (689 MVA and 667 MVA at P_T=0.7), respectively. These values represent a reduction of 25% and 27% on Buses 5 and 8, respectively. This is a different pattern compared to the one observed in the two-area system indicating that different system configurations may lead to various fault level reduction trends in response to the increased penetration of PE-based generation. Finally, note that the maximum absolute error between the results of our FLC method and those obtained from time-domain simulations is 2.3%. This is almost the same error observed in the previous scenario (i.e. scenario 1), which also confirms the efficiency of this proposed FLC method.

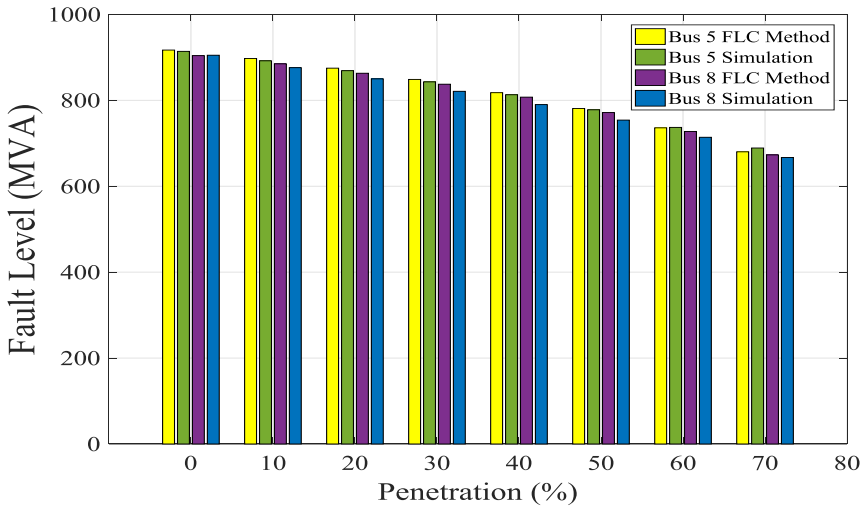

Fig.53. Results from the adjusted 9-Bus test system with different levels of P_T (*scenario 2*)

6.8.3 **The IEEE 39-Bus Test System**

To demonstrate the accuracy of the proposed FLC method on a large test system, the adjusted IEEE 39-Bus test system, shown in Fig.54, is used. In this part, the proposed FLC method is validated against the actual results obtained from the dynamic simulations (RMS) which uses detailed modelling and small simulation steps to account for the dynamics of the fault currents. Also, it is compared with the IEC60909 standard for steady-state fault calculation. For this purpose, the IEEE 39-test system is adjusted in DIgSILENT PowerFactory to consider two different penetration scenarios of NSGs which are described as follows:

- ***Scenario 1*** (P_1=0.5, P_3=1, P_6=0.5, P_2=P_4=P_5=P_7=P_8=P_9=P_{10}=0).
- ***Scenario 2*** *(P_1=0.7, P_3=P_4=P_6=P_7=1, P_2=P_5=P_8=P_9=P_{10}=0).*

Note that these represent a total penetration of (36%) and (59%) respectively. The fault level at Buses 9 and 16 are calculated and compared with both the actual values represented by

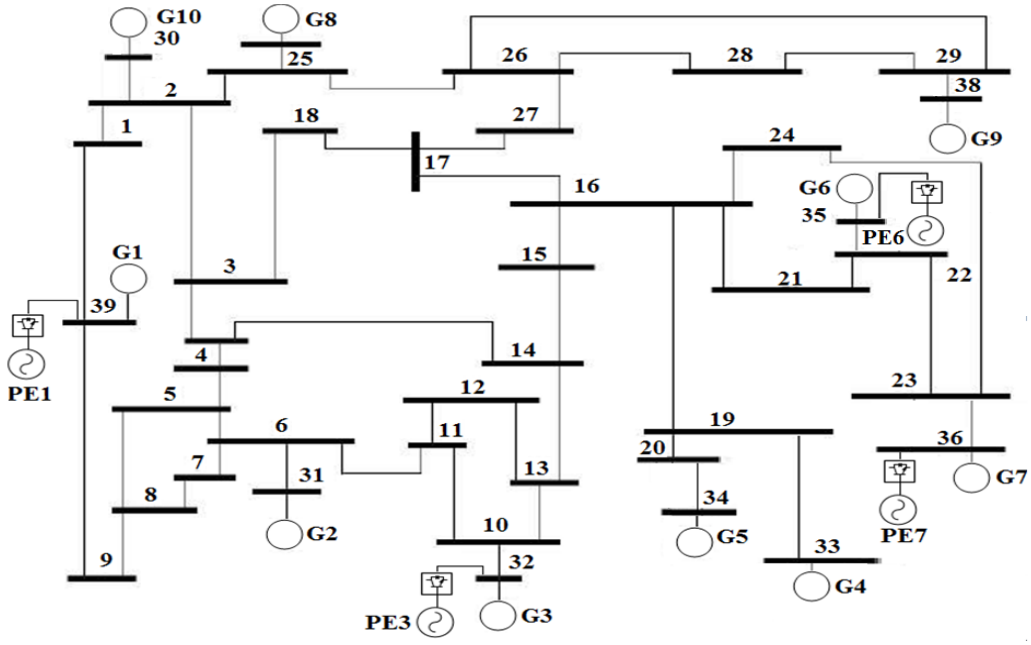

Fig.54: The adjusted IEEE 39-Bus system with PE-based generators (*scenario 1*)

the results obtained from RMS simulations and the steady-state fault calculations on the basis of the IEC60909 standards as shown in Fig.55 and Fig.56, respectively. It can be shown that the system fault level is falling with increasing the penetration of PE-based generation on both studied Buses. Observe Bus 9 in Fig.55, where the fault level has reduced from (4758 MVA) at the bases scenario (i.e. P_T=0%), down to (4481 MVA and 4182 MVA) at a total Penetration level of NSGs, P_T, of (36% and 59%) respectively.

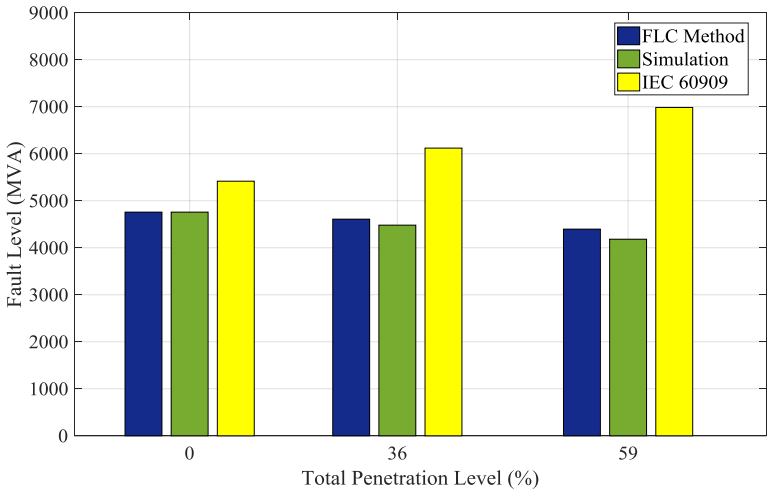

Fig.55: The fault level on Bus 9 at different penetration levels of NSGs

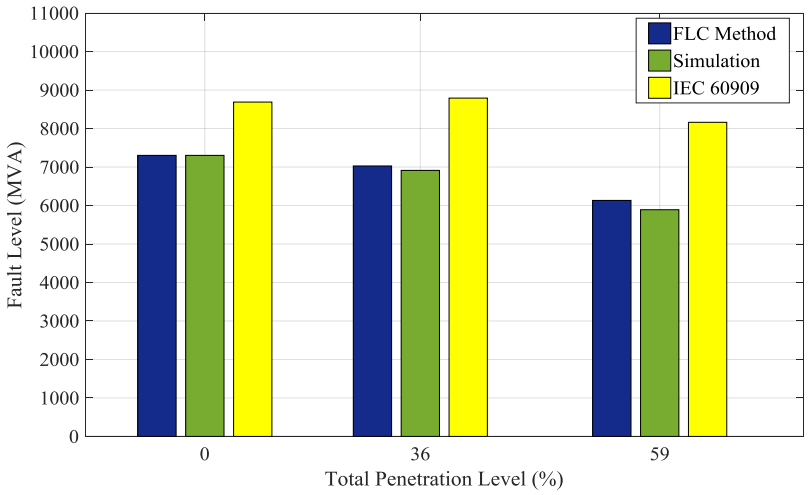

Fig.56: The fault level on Bus 16 at different penetration levels of NSGs

On the other hand, Fig.56 shows that the fault level at Bus 16 has reduced from (7303 MVA) at the base scenario (i.e. P_T =0%), down to (6913 MVA and 5891 MVA) at a total Penetration level of NSGs, P_T, of (36% and 59%), respectively. Table 17 and Table 18, also list the results obtained from our FLC method and IEC60909 standards, which are compared with the actual values of the fault level obtained from RMS simulations. The results verify the accuracy of the proposed FLC method in predicting the trend of the decreasing fault level and providing results very close to the actual fault level (i.e. RMS simulations) on both Buses (maximum absolute error of 5.1%).

Table 17: Bus 9 Fault level on the adjusted IEEE 39-Bus test system

Penetration Level	***RMS Simulation***	***IEC60909***		***FLC Method***	
(%)	***Fault Level (MVA)***	***Fault Level (MVA)***	***Error (%)***	***Fault Level (MVA)***	***Error (%)***
0	4758	5416	13.8	4758	0.0
36	4481	6120	36.6	4609	2.9
59	4182	6985	67.0	4396	5.1

Table 18: Bus 16 Fault level on the adjusted IEEE 39-Bus test system

Penetration Level	***RMS Simulation***	***IEC60909***		***FLC Method***	
(%)	***Fault Level (MVA)***	***Fault Level (MVA)***	***Error (%)***	***Fault Level (MVA)***	***Error (%)***
0	7303	8688	19.0	7303	0.0
36	6913	8791	27.2	7028	1.7
59	5891	8162	38.6	6133	4.1

In contrasts, the IEC60909-based fault calculation has provided misleading results in some cases, as it has shown an increasing fault level on Bus 9. Observe from Fig.55 and Fig.56, the increasing error gap between the IEC60909 standards and the simulation results. This error has registered very high values especially at 59% penetration of NSGs (i.e. P_T=0.59). For example, a maximum absolute error of 67.0% and 38.6% has registered at Bus 9 and Bus 16.

In this chapter, a new method for steady-state fault level calculation (FLC) including the impact of high penetration of NSGs-based RES, referred here as PE-based generation, is proposed. Our proposed method is formulated based on the correlation between the fault level and the penetration of PE-based generation in the power system. Our generic modelling method can assist in estimating/predicting of the system fault level in a wide range of future grid scenarios without a need for a detailed system modelling or time-domain simulations. The proposed new FLC method has been tested using three representative test systems, i.e. a) 2-area test system, b) IEEE 39-bus test system, c) IEEE 39-bus test. The proposed FLC method has demonstrated adequate applicability, with small absolute errors, smaller than 5.1%, when compared to the full-scale dynamic simulation results on the basis of detailed network modelling.

Furthermore, the results obtained have shown that the proposed FLC method has superior accuracy when compared with the IEC60909-based fault calculations. It was noted that the IEC60909 standard may result in conservative/inaccurate outcomes in some cases. For example, in the case of the IEEE 39-bus test system, the IEC60909-based fault calculation demonstrated an increasing fault level on Bus 16 with increased PE-based penetration, which was opposite to the actual results obtained from dynamic simulation. In contrast, our proposed FLC method demonstrated an accurate trend of fault level with the increased penetration of PE-based generation, as confirmed by dynamic simulations.

Although the simulation results showed that the transmission system fault level may decrease with the increased penetration of PE-based generation, these reductions may show different trends in different power systems, depending on the fault location and the synchronous generation (SG) displacement scenario. For instance, it can be noted that those Buses which are closer to the displaced SGs, may experience lower fault levels, compared to the remote ones. On the other hand, an approximately homogeneous fault level reduction may be experienced in the network when the SGs are uniformly replaced by PE-based generation. This implies the impact of PE-based generation location on the fault level reduction, and our FLC method can assist researchers and system operators to analyse large numbers of FG scenario with different possibilities for type, size and location of PE-based RES.

7 Possible Solutions to Substitute the Low Fault Level in Future Power Systems with High Penetration of NSGs

This chapter aims to propose some solutions to substitute the low fault level resulted from the increased penetration level of NSGs. At first, it examines the negative impact of the low fault level on the system strength resulted from the increased penetration of NSGS. This is done by monitoring the voltage dip propagation during the fault as well as the voltage change due to a switching event at high and low fault level conditions. Then, some of the possible solutions to the problem of low fault level are discussed and analysed too. This includes optimizing the of the FRT capability of the NSGs by maximizing the *k*-factor, enhancement of the capability of NSGs by maximizing the transient overrating and installation of synchronous condensers in low fault level systems. Finally, it shows the efficiency of the suggested solutions in improving the fault level profile and mitigating the negative implications of the low fault level on the system due to the increased penetration of NSGs.

7.1 Maximizing the *k*-Factor

The relation between the injected reactive current and the severity of the fault (i.e. the resulted voltage dip level during the fault), is already defined and explained in chapter 3. It has been shown that according to most grid codes, this injected current is defined by the proportional gain (i.e. *k*-factor) as expressed in (3.1). In other words, the higher the value of the *k*-factor, the higher the injected current during the fault. However, some grid codes define a specific range for the values of this k-factor such as the German grid code where a range of (k=2 to k=10) is suggested with a default value of (k=2) [53]. This means that the converter will provide different levels of reactive current depending on the severity of the fault. In other words, the higher the *k*-factor, the higher the injected current during the fault in proportional

to the voltage dip level seen at the grid-connected side of the NSG. For example, faults near to the converter terminal see deeper voltage dip and therefore the NSG injects almost the maximum capability of the converter. However, the converter might only inject some limited values of reactive current for faults far from the converter terminal. Therefore, higher levels of reactive currents can be injected by using higher values of the *k*-factor. The converter control should have the capability to maximize the reactive current injection during the faults with higher *k*-factor (e.g. *k*=10). This chapter will examine the effectivity of this solution in more details in the results section.

7.2 Maximizing the Overrating Capability of the NSGs

As state earlier, the injected reactive current is determined by both the voltage dip and the *k*-factor. However, this will be limited by the transient overrating capability of the converter during the voltage dip conditions. In literature, this transient capability is ranged between (1.1 -1.5 p.u.) according to [8, 59, 72]. This includes the maximum limit for the combined current of both (active and reactive) currents might be injected during the faulty condition as expressed in (7.1).

$$I_{\text{Max}} = \sqrt{I_{\text{Active}}^2 + I_{\text{Reactive}}^2} = \alpha I_{\text{Rating}} \tag{7.1}$$

Usually the FRT control limits the active current to a minimum level (e.g. almost zero) to prioritize the reactive current injecting without violating the maximum limit of the converter. This upper limit is determined by the maximum currents that the power electronic switches (e.g. IGBTs) can carry. So, an enhanced overrating capability will allow for more fault current injection (i.e. higher I_{Max}) during the low voltage conditions. Although such solution adds extra cost to produce switches with higher current-carrying capability, it might be an

effective alternative to provide the required fault currents. This will be examined and evaluated more in the results section.

7.3 Installation of Synchronous Condensers

Synchronous condensers have been used in traditional power systems for many purposes such as voltage support, reactive power compensation and power factor improvement [110-113]. These synchronous condensers are modelled as unloaded synchronous machines which either supply reactive power when it is overexcited or absorb reactive power when it is under-excited. In other words, it can function as a capacitor or an inductor according to the excitation status [111]. Recently, synchronous condensers have been strongly proposed as a solution for some system strength challenges (e.g. low inertia and low fault level) which might accompany the increased integration of PE-based generation (i.e. mainly RESs which are connected through converters to the grid) [114-117]. Likewise synchronous generators, these synchronous condensers have the capability to inject high fault current during low voltage conditions (i.e. SC faults), therefore they are modelled using the same way in steady-state fault calculations as well [35]. This capability of providing high fault currents makes the synchronous condensers a promising alternative to substitute the fault level decline in future energy systems with high penetration of NSG-based RESs.

7.4 Simulation Results

7.4.1 Impact of the Increased Penetration on the Fault Level

In order to achieve a better understanding of the impact of the increased penetration of NSGs on the fault level of large systems, the IEEE 39-Bus test system is used again and modelled in DIgSILENT PowerFactory. In this part, the IEEE 39-Bus test system is divided into two areas as shown in Fig.57. Two scenarios have been considered as follows:

- ***Scenario 1:*** *All generators in both areas are SGs*
- ***Scenario 2:*** *Area-2 generators are replaced by NSGs (i.e. type-4 wind farms)*

Note, that scenario 2 represents the case where Area-2 has a 100% penetration level of NSGs. However, the maximum penetration level of NSGs in the whole system considering both areas equals to 23% using the same metric in (3.6).

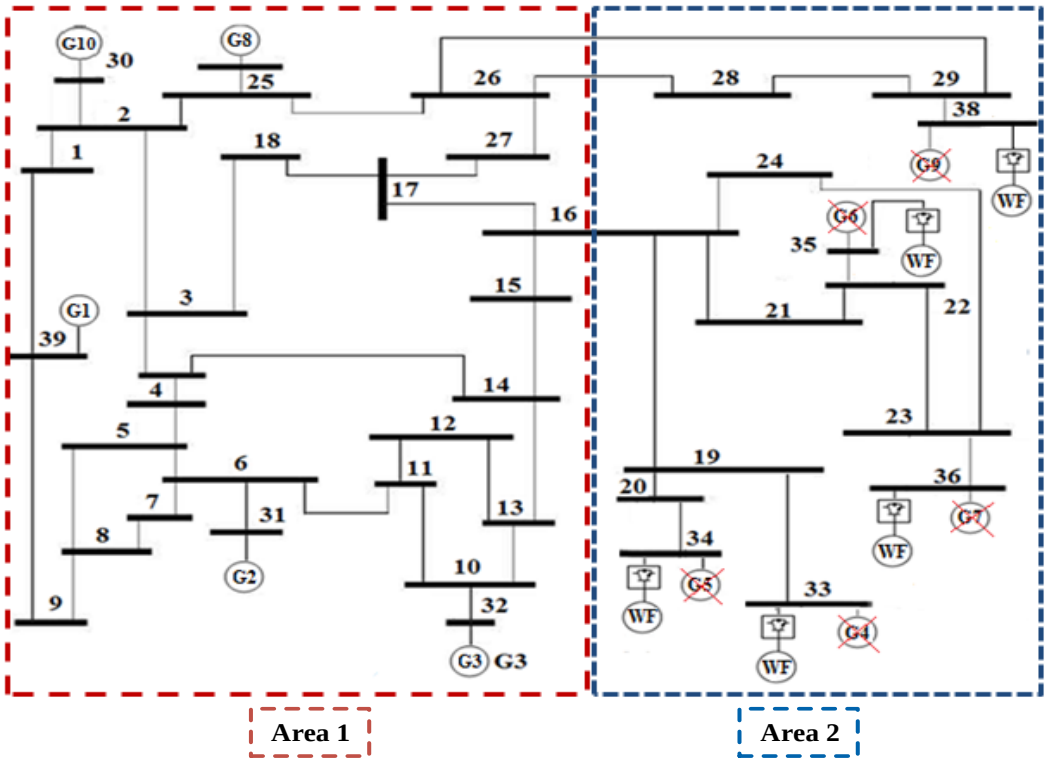

Fig.57: The adjusted IEEE 39-Bus test system

In both scenarios, the fault level is calculated using the results obtained from dynamic simulations (i.e. RMS simulations). The results are obtained for several locations (i.e. Buses) in the system covering both areas in the test system considering the two already defined scenario. The results show a significant decline in the fault level at all of Area-2 Buses with the NSGs (i.e. *scenario 2*) compared to the original fault level in the original system with SGs only (i.e. *scenario 1).*

For instance, the fault level on Buses 23 and 29 have registered a reduction of 33.2% and 48.2% of their original values, respectively. On the other hand, those Buses of Area-1 have witnessed a marginal decline in the fault level as shown in Fig.58. For example, Buses 2 and 8 have registered a reduction of 6.6% and 5% of their original value respectively. In other words, Buses which are close to the SGs (e.g. mainly Buses in Area-1) are less affected by the increased penetration level of NSGs, whereas those far Buses (e.g. mainly Buses in Area-2) are significantly affected by the increased penetration level of NSGs. This is somehow expected due to the limited fault contribution to the total fault level from the NSGs, which is

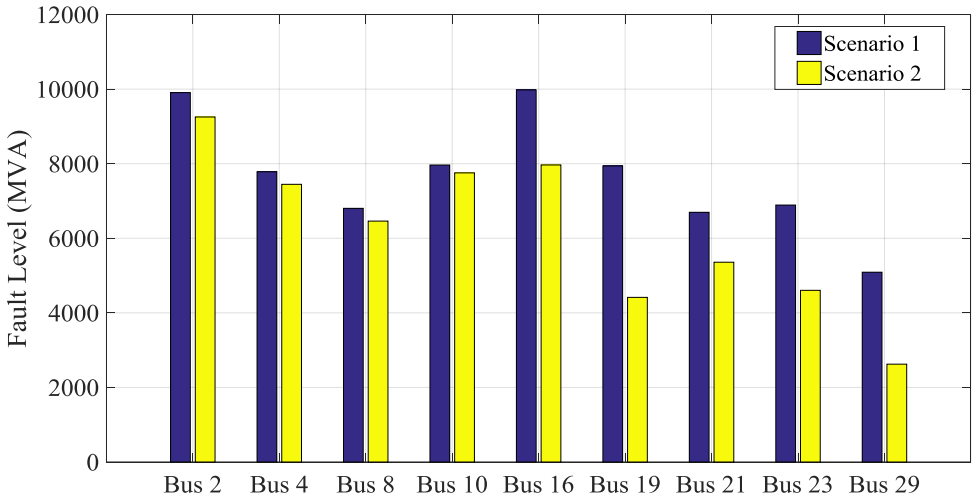

Fig.58: The fault level in the adjusted IEEE 39-Bus test system

the dominated sources in Area-2, while Area-1 Buses are mainly fed by SGs which contributes to higher levels of fault currents in compared to the NSGs. Note that the average fault level reduction of 33% of the original values has been observed at Buses in Area-2 due to the 23% penetration level of NSGs.

On the other hand, an average reduction of 4.7% from the original values of the fault level has been observed at Buses in Area-1. Table 19, shows the fault level at both NSG's penetration scenario in addition to the reduction percentage comparted to the original fault level.

Table 19: The fault level of adjusted IEEE 39-Bus test system

Location	Fault Level (MVA)		Decrement %
	(Scenario 1)	(Scenario 2)	
Bus 2	9906	9253	6.6
Bus 4	7784	7447	4.3
Bus 8	6803	6461	5.0
Bus 10	7965	7754	2.6
Bus 16	9979	7966	20.2
Bus 19	7940	4415	44.4
Bus 21	6697	5358	20.0
Bus 23	6891	4604	33.2
Bus 29	5090	2624	48.4

7.4.2 **Impact of the Low Fault Level on the System Strength**

To examine the impact of the fault level reduction on the system strength, which is characterised by the voltage stiffness, both the voltage dip propagation during the fault as well as the voltage change due to a switching event are studied. This has been conducted using the same IEEE 39-Bus test system considering the same scenario in the previous section (i.e. scenario 1 and scenario 2).

7.4.2.1 Voltage Dip Propagation

Considering a bolted three-phase symmetrical fault at Bus 16 of the system Fig.57, the resulted voltage dip propagation through the system during the fault is monitored in both scenarios. Observe Fig.59 that shows the during-fault voltage (DFV) on different Buses (Buses 2, 4,8 and 10 from Area-1) and (Buses 19,21,23,29 from Area-2). In addition, the numerical results are listed in Table 20. These results indicate that the fault at Bus 16, which is located at the middle of the system between Area-1 and Area-2, has affected most of the other Buses in the system.

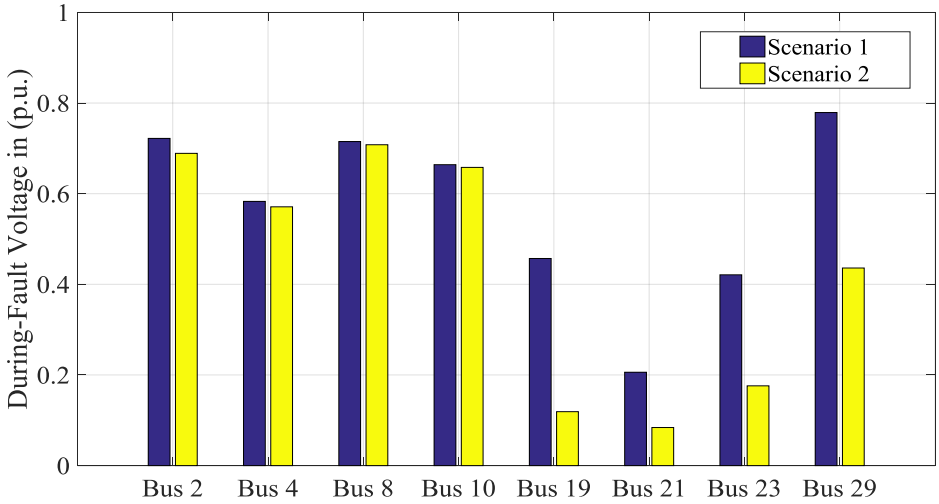

Fig.59: Voltage dip propagation due to a fault at Bus 16

Note the wider voltage dip propagation in Area-2 Buses (more specifically Buses 19, 21 and 23), opposing the less impacted Area-1 in both 0% and 23% NSG's penetration scenario.

- ***Scenario 1 (0% NSGs' penetration)***

Buses in Area-1, are less influenced by the fault at Bus 16. It can be observed from Fig.59 that all Buses in Area-1 have shown a DFV of more than 0.5 p.u. (i.e. DFV > 0.5 p.u.). Note that the lowest DFV has been registered at Bus 4, which equals to 0.583 p.u. On the other hand, most Buses in Area-2, apart from Bus 29, have shown a during-fault voltage of less than 0.5 p.u. (i.e. DFV < 0.5 p.u.). It can be noted that the lowest DFV has been registered at Bus 21, which equals to 0.206 p.u.

- ***Scenario 2 (23% NSGs' penetration)***

Buses in Area-1 have approximately shown the same interaction with the fault at Bus16 with an almost negligible difference in DFVs in compared with those observed in scenario 1. In other words, the values of the DFVs are more than (0.5 p.u.) as it can be shown in Table 20. In contrast, all Buses in Area-2 have witnessed significant low values of DFVs, more specifically those Buses which are closer to the faulty point (i.e. Bus 16). For example, DFVs of (0.084 p.u. and 0.119 p.u.) have been registered at Buses 21 and 19 respectively. On the basis of the results, it can be confirmed that the voltage dip propagation represented by the DFVs is strongly correlated to the strength of the Bus under study, which is characterised by the fault level. In other words, strong Buses, which have witnessed a marginal decline in fault level due to the NSGs' penetration (e.g. Buses in Area-1), have also shown a marginal decline of their DFVs. Accordingly, weak Buses, which have witnessed a significant decline in the fault level (e.g. Buses in Area-2), have shown a significant decline of their DFVs.

Table 20: During-fault voltage due to a bolted fault at Bus 16

Location	Before-fault voltage	Scenario 1	Scenario 2
Bus2	1.043	0.722	0.689
Bus4	0.98	0.583	0.571
Bus8	0.973	0.715	0.708
Bus10	0.976	0.664	0.658
Bus16	1.021	0	0
Bus19	0.989	0.457	0.119
Bus21	1.024	0.206	0.084
Bus23	1.041	0.421	0.176
Bus29	1.047	0.779	0.436

7.4.2.2 Voltage Change due to Capacitor Banks Switching

This part studies the impact of the system strength characterised by the fault level on the voltage change due to a capacitor bank switching at the transmission level. To do so, a 100 MVAr capacitor bank is connected at Bus 21 in Area-2. The change in the voltage level is monitored in the previously explained scenarios (scenario 1 and scenario 2) which represent (0% and 23%) of NSGs' penetration respectively as shown in Fig.60.

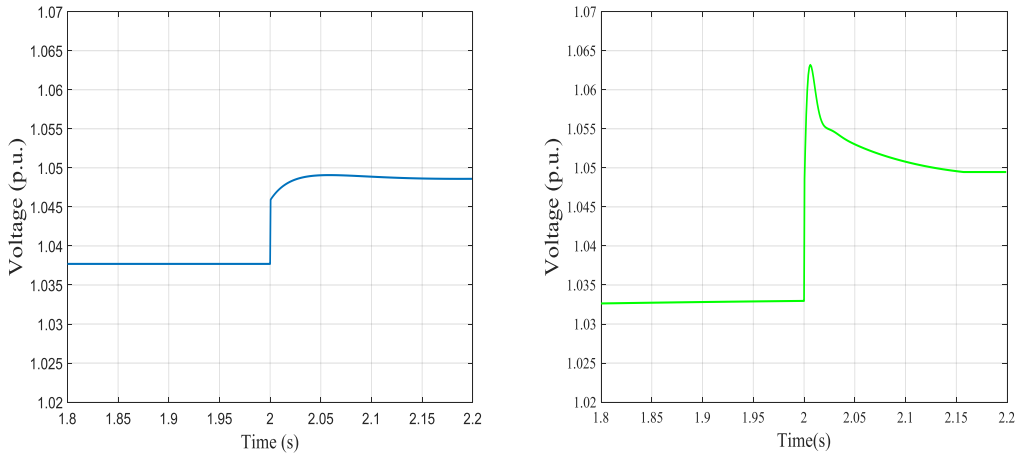

(a) Scenario 1 (b) Scenario 2

Fig.60: Voltage change due to a 100 MVAr capacitor bank switching at Bus 21

Observe Fig.60, where the voltage change due to the capacitor bank switching is presented, it can be noticed that a higher voltage level is observed in both cases after switching on the capacitor bank at (t=2 s).

While a smooth step change in the voltage can be observed in scenario 1 when a fault level equals to 6697 MVA, an overshoot is observed in scenario 2 when the fault level is reduced to 5358 MVA. Note that the resulted steady-state voltage change (i.e. ΔV) equals to 0.01 p.u. and 0.017 p.u. in scenario1 and scenario 2 respectively. It is worth mentioning that the transient overshoot observed in scenario 2 exceeds 0.03 p.u. These results justify the need for a minimum fault level in order to ensure a certain level of system strength, and to avoid violating the voltage limits during switching events. In view of the previous results, it is obvious that the decline in the fault level has a negative impact on the system strength.

Hence, it is required to substitute the fault level to ensure the system stability and to provide the minimum requirement of system strength too. Therefore, this section discusses some possible remedies by proposing several doable solutions to enhance the fault level profile and substitute the low fault level. Three main alternatives are proposed and discussed as follows: Maximizing the gain for reactive current injection during the faults (i.e. *k*-factor), maximizing the overrating capability of the converters utilised in the NSGs, and installation of synchronous condensers.

7.4.3 **Maximizing the *k*-Factor**

As stated earlier, grid code requirements for connecting NSGs to the electrical grid as well as the FRT control strategy have a strong impact on the fault current contribution from the NSGs. For instance, the proportional gain of reactive current injection during the fault plays a key role in determining the level of the fault current from such sources.

This part examines the influence of using high values of this gain (i.e. *k*-factor) on maximizing the fault current contribution from NSGs. The fault level is also calculated on the same Buses considering scenario 2 which represents a 100% penetration of NSGs in Area-2. The sensitivity of the system fault level to the value of the *k*-factor has been tested considering two values (i.e. *k*=2 and *k*=10) as shown in Fig.62. The results show an enhanced fault level profile by maximizing the k-factor with decent levels of fault level improvement in all Buses. Note that not only the Buses in Area-2 have witnessed an improved fault level but also those Buses in Area-1.

An average of increment of the fault level profile at all Buses equals to 19% whereas a maximum fault level increment of 31% is observed at Bus 29 as shown in Fig.61. This can be interpreted as the maximum *k*-factor ensures that the converter will see the faults and inject the maximum reactive current regardless of the fault location even for those Buses far from the NSGs. In other words, the higher the *k*-factor the more the capability of the NSG to support the grid during the faulty conditions.

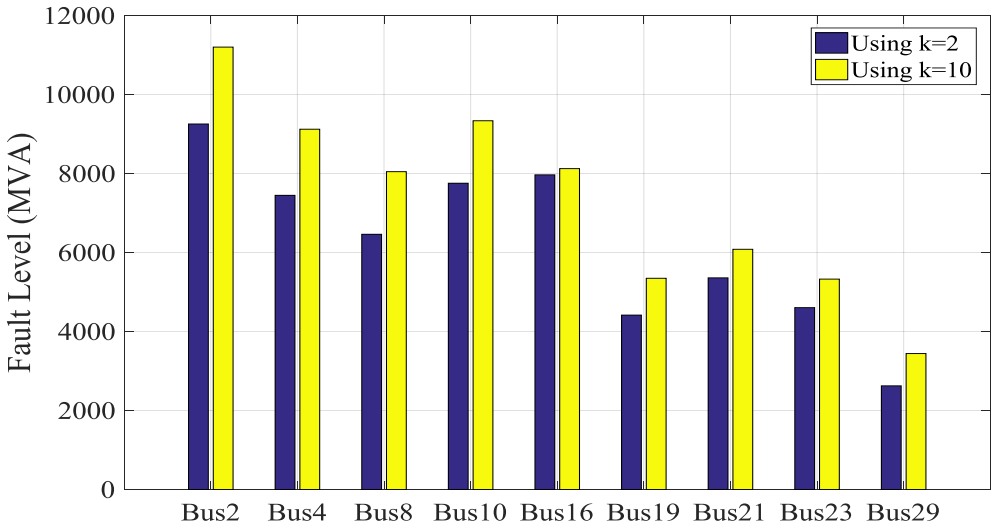

Fig.61: The enhanced fault level using higher vlues of *k*-factor

Table 21:Impact of increasing the *k*-factor on the fault level

Location	Case 1 (*k*=2)	Case 2 (*k*=10)	Increment (%)
Bus 2	9253	11200	21
Bus 4	7447	9121	22
Bus 8	6461	8046	25
Bus 10	7754	9335	20
Bus 16	7966	8123	02
Bus 19	4415	5347	21
Bus 21	5358	6081	13
Bus 23	4604	5326	16
Bus 29	2624	3441	31

Table 21 shows the fault level (MVA) for both cases (*k*=2 and *k*=10), in addition to the percentage of the fault level increment resulted from maximizing the *k*-factor (i.e. *k*=10) compared to the original fault level when (*k*=2). Observe that by using this solution, the fault level profile has been improved without any requirement to enhance the overrating capability of the converters. In other words, this solution helps to utilise most of the available converter capability perfectly without adding any extra cost.

7.4.4 **Maximizing the Overrating Capability of the NSG**

This part examines the effectiveness of maximizing the transient overrating capability of the converter utilised in NSG on enhancing the system fault level. For this purpose, the same test system (IEEE 39-Bus test system) with all generators in Area-2 replaced by NSGs, scenario 2, is used again. The fault level has been obtained using dynamic simulations considering three different values for the maximum converter current (i.e. I_{Max} =1.1, 1.5 and 2 p.u.).

Having increased the maximum overrating capability of the converter, the fault level has been improved at all Buses in the system as shown in Fig.62. Observe the different levels of the fault level in Fig.62, which shows the sensitivity of the fault level to the changing value of the maximum overrating capability of the NSGs. In compared with the base case where (I_{Max}=1.1 p.u.), it can be noticed that the fault level at all Buses has experienced an increase with an average of (13.8% and 35.8%) for the cases (I_{Max} = 1.5 p.u. and I_{Max} =2 p.u.) as shown in Table 22, respectively.

It is worth mentioning that the maximum increase in the fault level has been observed at Bus 16 in both cases. For example, the fault level of Bus 16 has increased from 8123 MVA up to 11335 MVA when the (I_{Max}) changed from 1.1 p.u. to 2 p.u., which represents a significant increase of 45%. Note that all numerical results including the fault level and the increment percentages are also presented in Table 22.

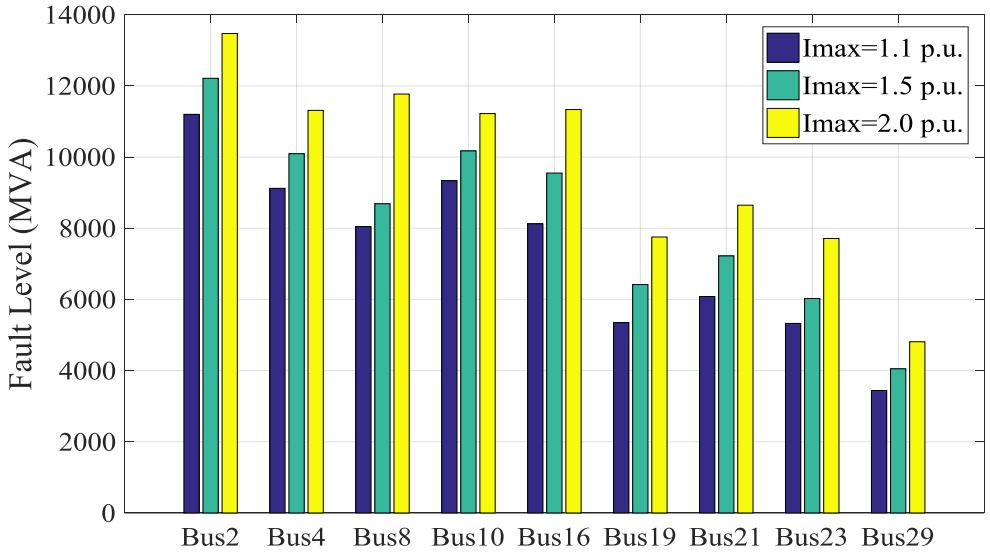

Fig.62: The enhanced fault level using higher overrating capability

Table 22: The impact of increasing the overrating capability on the fault level

Location	(base) Imax=1.1	Imax=1.5	Increment (%)	Imax=2	Increment (%)
Bus2	11200	12213	9.0	13470	20.3
Bus4	9121	10094	10.7	11311	24.0
Bus8	8046	8688	8.0	11770	46.3
Bus10	9335	10173	9.0	11221	20.2
Bus16	8123	9551	17.6	11335	39.5
Bus19	5347	6417	20.0	7754	45.0
Bus21	6081	7222	18.8	8648	42.2
Bus23	5326	6026	13.1	7713	44.8
Bus29	3441	4050	17.7	4810	39.8

These results indicate the effectiveness of increasing the overrating capability of the converter interface of NSGs in improving the fault level profile in the whole system in scenarios with high penetration of NSGs.

7.4.5 **Installation of Synchronous Condensers**

As far as synchronous condensers are concerned, three synchronous condensers of the same ratings are installed (at Buses 15, 23 and 28) to substitute the low fault level observed in Area-2. The ratings of these installed synchronous condensers are changed at three different values (100 MVAr, 200 MVAr and 300 MVAr). The fault level has been calculated at all Buses for each case using the dynamic simulation results for each value of the synchronous condensers. Generally, it can be seen that the fault level increases at all system Buses with the increased rating of the installed synchronous condensers as shown in Fig.63. This has improved the fault level profile and substituted the low fault level especially in Area-2, where the NSGs are installed to displace the SGs.

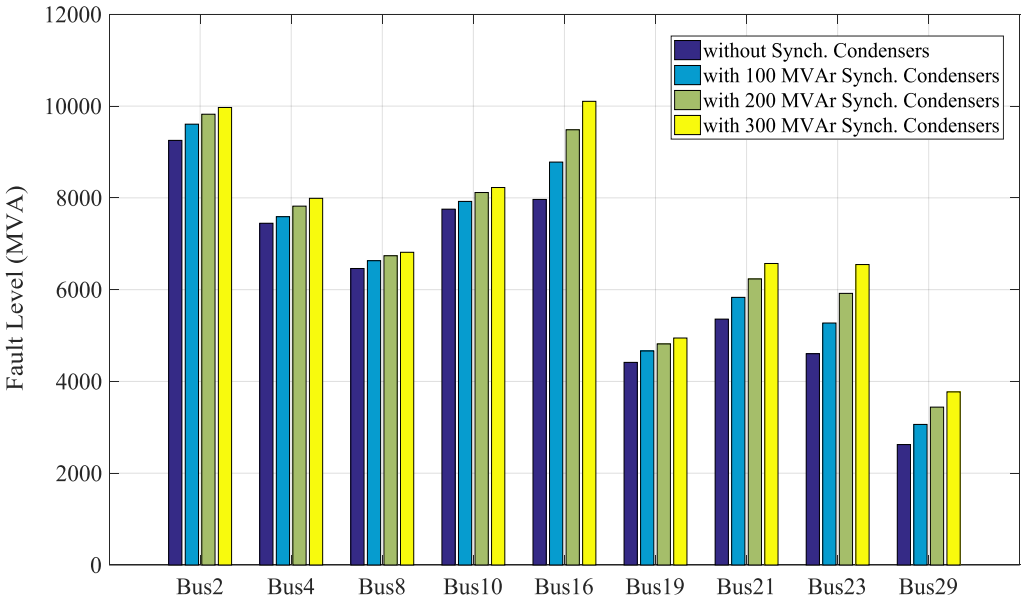

Fig.63: The enhanced fault level using Synchronous condensers

Unlike the impact of the increased overrating capability of the converters, it can be noticed that the installed synchronous condensers have mainly influenced the fault level on the nearby Buses (i.e. Area-2 Buses). On the other hand, a marginal impact can be noticed on Area-1's Buses as shown in Fig.63. Observe the maximum fault level increase, which has been experienced on Buses 23 and 29. It can be seen that fault level at Bus 23 has increased from 4604 MVA at the base case without synchronous condensers, up to (5273MVA , 5919 MVA and 6547 MVA) for the synchronous condensers ratings of (100 MVAr, 200 MVAr and 300 MVAr) respectively.

Note that these represent fault level increments from the original fault level at the bases case without synchronous condensers of 14.5%, 28.6% and 42.2% respectively. On the other hand, a higher increment of fault level has been experienced on Bus 29 from 2624 MVA without s, up to (3063 MVA , 3440 MVA and 3772 MVA) for the synchronous condensers ratings of (100 MVAr, 200 MVAr and 300 MVAr), which represent 16.7%, 31.1% and 43.8% respectively, as listed in Table 23.

Table 23:Impact of installation of synchronous condensers on the fault level

Location	Original Fault Level	Fault Level with the Synchronous Condensers					
		(100 MVAr)		(200 MVAr)		(300 MVAr)	
		MVA	(%)	MVA	(%)	MVA	(%)
Bus2	9253	9606	3.8	9823	6.2	9970	7.7
Bus4	7447	7590	1.9	7820	5.0	7990	7.3
Bus8	6461	6631	2.6	6739	4.3	6814	5.5
Bus10	7754	7923	2.2	8117	4.7	8226	6.1
Bus16	7966	8780	10.2	9484	19.1	10104	26.8
Bus19	4415	4664	5.6	4817	9.1	4946	12.0
Bus21	5358	5832	8.8	6233	16.3	6570	22.6
Bus23	4604	5273	14.5	5919	28.6	6547	42.2
Bus29	2624	3063	16.7	3440	31.1	3772	43.8

Taken together, these results suggest that the synchronous condensers can form an effective solution to improve the fault level profile. However, the location and the ratings of the installed synchronous condensers should be considered carefully.

7.5 Conclusion

The main goal of this chapter was to propose some possible solutions for substituting the low fault level resulted from the increased penetration level of NSGs. Primarily; the impact of the low fault level on the system strength was studied and evaluated in scenarios of high penetration levels of NSGs. Then, three different solutions have been suggested to improve the fault level profile and to avoid the negative implications might result from the fault level decline accompanied by the increased penetration levels of NSGs. These three proposed solutions include: optimizing the of the FRT capability of the NSGs by maximizing the *k*-factor, enhancement of the capability of NSGs by maximizing the transient overrating and installation of synchronous condensers in low fault level systems.

Apart from the significant fault level decline, which has been witnessed in scenarios with high penetration of NSGs, the results presented in this chapter have shown that the strength of the system is negatively affected by the low fault level. For instance, the results have shown that the voltage stiffness at the system Buses is strongly dependent on the fault level of those Buses as the higher fault level Buses have shown more stiffness and a less voltage change in response to switching events or to faults occurred at other Buses in the system.

This research has found that generally an average fault level increment of 19% has been achieved by maximizing the *k*-factor (i.e. k=10) in compared to the original case (i.e. k=2). Furthermore, some Buses in the system has experienced higher increments depending on the Bus location and how close to the NSGs. For example, the fault level at Bus 29 has registered an increment of 31% higher than the of the original fault level observed before changing the k-factor. This confirms the importance of this parameter in optimizing the FRT control during

the faulty conditions and in improving the fault level profile in the system with the high share of NSG-based RESs.

Regarding the second proposed solution represented by maximizing the overrating capability of the converter interface utilised by the NSG, the results have shown a general fault level increment at all the system Buses, as well. These increments are (13.8% and 35.8%) for the cases (I_{Max} = 1.5 p.u. and I_{Max} =2 p.u.) compared to the original system fault level when (I_{Max} = 1.1 p.u.). Although this solution might achieve a better fault level increment compared to what increment resulted from maximizing the k-factor, it requires oversizing the converters utilised by the NSGs to be able to provide higher levels of fault currents. In other words, new design and additional capability are required which is considered a defect in the solution as it would lead to extra costs.

Considering the results obtained by using the third suggested solution characterised by synchronous condensers' installation, it can be concluded that the fault level at all Buses in the system has risen in response to the installation of the synchronous condensers. This might be expected as the synchronous condensers contribute to higher levels of fault currents same as SGs as mentioned earlier. However, the results of this investigation show that thee synchronous condensers mainly affect the fault level at those Buses close to them, while the far Buses from the installed synchronous condensers are marginally affected. For example, average increments of (7.4%, 13.8 % and 19%) have been observed in the system fault level considering all Buses after installation of 100 MVAr, 200 MVAr and 300 MVAr respectively. Nevertheless, this increment was not uniformly observed at all Buses. For example, considering the case where 300 MVAr synchronous condensers are installed, Area-1 Buses and Area-2 Buses have experienced very different levels of increments of (6.6%) and (29.5%) respectively. This is somehow opposing the first two suggested solutions where the

fault level increments were almost uniform at all Buses with minor differences. Note that installation of synchronous condensers would lead to an additional cost which is considered a drawback of this suggested solution same as the overrating capability solution.

Taken together, these results show the effectiveness of the suggested solutions in improving the fault level profile and mitigating the negative implications of the low fault level on the system due to the increased penetration of NSGs.

8 Thesis Summary

This chapter summarizes the whole research undertaken in the thesis. Firstly, it provides some general conclusions about the main tasks have been conducted and presented in the thesis (section 8.1). Secondly, the main contributions as well as the key findings of the research will be presented in (section 8.2). Finally, it suggests some interesting new ideas and recommendations for further development of the work in the future, which might be launched, on the basis of the outcome of the

8.1 Conclusions

This thesis was undertaken to assess the fault level in future power systems with high penetration of NSGs. A comprehensive assessment has been provided about the theme of fault level in systems with high penetration of NSG-based RESs. This has included broad investigation of the new characteristics of SC currents fed by the NSGs, understanding the impact of the increased penetration of NSGs on the transient response of the SC current and the fault level in future systems, evaluating the accuracy of the available steady-state methods for fault calculation with the presence of NSGs and defining the negative implications which might appear when operating systems with low fault levels.

Initially, a comprehensive review of the related literature that covers all studied aspects which have been undertaken and presented. Several simulation studies have been conducted to understand the fault current contribution from NSGs-based RESs, as well as to monitor the SC current response in power systems with the variable fault level in future scenarios with increased penetration of NSGs. The results have shown a very different SC current characteristics represented by a limited and controlled SC current contribution from the

NSGs. Generally, it can be concluded by analysing the transient followed by a steady-state SC current. This created a motivation to precisely understand the factors behind such characteristics and how the new characteristics might affect the SC response in future scenarios with high penetrations of these NSGs. Therefore, a wide range of factors that might influence the SC current contribution of NSGs utilising FRCs was studied in details. The results have shown that the transient SC contribution from the NSGs, connected through FRCs, is mainly determined by the pre-fault operation conditions, the voltage dip seen during the fault and the speed of reactive current injection. On the other hand, the steady-state contribution is only affected by the inverter's overrating capability as well as the proportional gain for the reactive current injection (i.e. *k*-factor).

On the other hand, the sensitivity of the SC current response to the generation mix (SGs and NSGs) in future scenarios has demonstrated that the SC currents in high NSGs' penetration scenario will decrease to lower levels with the increased penetration of NSGs and displacing the traditional SGs. It was also shown that the SC current response may witness some significant changes compared to the one observed in conventional power systems on the basis of SGs. For instance, the SC current response may show a delayed maximum contribution (i.e. very low initial contribution), multiple peak values and different levels of current decaying after exceeding some levels of NSGs penetration in the grid, more specifically after exceeding (40% penetration of NSGs). However, in cases where the NSGs can ride though the fault immediately without any delays, the traditional time-decaying response might be observed as far as the penetration level is less than 100%. Furthermore, the results of this investigation show that the breaking current converges to the same level of the initial symmetrical SC current (I_{k}'') with the increased penetration of NSGs until they coincide at

100% scenario. Note that these results and conclusions were derived from several time-domain simulations and steady-state fault calculations in DIgSILENT PowerFactory.

After that, the performance of steady-state fault calculation (SSFC) methods in power systems including high penetration of NSGs based on FRC technologies has been studied and evaluated. In particular, the modelling and calculating the fault currents on the basis of the updated versions of the IEC60909 as well as complete methods. The estimated fault currents from these SSFC methods are compared with the dynamic simulation results considering different fault locations (i.e. voltage dip levels) accounting for faults near and far from NSGs. The simulations are conducted using single machine-infinite Bus and the IEEE 9-Bus test systems considering several scenarios which cover large-scale of penetration levels of NSGs. It was shown that complete methods can provide the best estimation for breaking current (I_{b}). However, most SSFC methods showed poor performance in estimating of sub-transient (I_{k}'') and maximum peak (I_{p}) currents in power systems with high penetration of NSG utilising FRC. Further, it was observed that all SSFC methods have tangible error gaps for estimating fault currents compared to actual fault levels calculated using dynamic simulations in power systems with high penetration of NSG utilising FRC.

Consequently, the necessity was raised for augmenting the existing modelling methodologies used in the SSFC methods to better represent the dynamic behaviour of NSG utilising FRC for such an analysis. Therefore, two new fault level calculation methods have been proposed in this thesis to provide results that are more accurate in future scenarios with high penetrations of NSG-based RESs.

An enhancement on the steady-state fault calculations according to the IEC60909 method is proposed and evaluated (chapter 5). This proposed method has augmented the methodology

in the latest version of the IEC60909 standard by improving the reactive current injection modelling for NSG-based RES during the fault. The simulation results show that the proposed method can provide better estimates for the fault currents with smaller error margins compared to the IEC60909. In particular, the proposed method has shown a maximum absolute error of 4.75% and 12.5% using a modified IEEE 14-Bus system for the cases when (k=2) and (k=10) respectively. On the other hand, the IEC60909 standard illustrated a maximum absolute error of 23.31% and 20.9% for the same cases. Hence, it can be concluded that the error margin in steady-state fault calculation of power systems with high penetration of NSG-based RES can be reduced at least by 50% using the proposed method.

The other enhancement is represented by proposing a novel method for steady-state FLC including the impact of high penetration of NSGs-based RES, which also referred here as PE-based generation. The newly proposed method is formulated on the basis of the correlation between the fault level and the penetration of PE-based generation in the power system. This includes a generic modelling method which can assist in estimating/predicting of the system fault level in a wide range of future grid scenarios without a need for detailed system modelling or time-domain simulations. The proposed new FLC method has been tested using three representative test systems, i.e. a) 2-area test system b) IEEE 9-bus test system and c) IEEE 39-bus test system. The results obtained using the proposed FLC method has demonstrated adequate applicability, with small absolute errors, smaller than 5.1%, when compared to the full-scale dynamic simulation results on the basis of detailed network modelling. Furthermore, the results obtained have shown that the proposed FLC method has a superior accuracy when compared with the IEC60909-based fault calculations which may result in conservative/inaccurate outcomes in some cases. Furthermore, this proposed FLC

method estimated the accurate trend of variable fault level with the increased penetration of PE-based generation, as confirmed by dynamic simulations.

Although the simulation results showed that the transmission system fault level may decrease with the increased penetration of PE-based generation, these reductions may show different trends in different power systems, depending on the fault location and the synchronous generation (SG) displacement scenarios. For instance, it can be noted that those Buses which are closer to the displaced SGs, may experience lower fault levels, compared to the remote ones. On the other hand, an approximately homogeneous fault level reduction may be experienced in the network when the SGs are uniformly replaced by PE-based generation. This implies the impact of PE-based generation location on the fault level reduction, and our FLC method can assist researchers and system operators to analyse large numbers of FG scenarios with different possibilities for type, size and location of PE-based RES.

Finally, the impact of operating the system under low fault conditions and the negative implications on the system strength, which is characterised by the voltage stiffness, is studied and evaluated in scenarios of high penetration of NSGs (in chapter 7). The results have shown that the strength of the system is negatively affected by the low fault level. For instance, the voltage stiffness at the system Buses is strongly dependent on the fault level of those Buses as the higher fault level Buses have shown more stiffness and a less voltage change in response to switching events or to faults occurred at other Buses in the system.

This indicates a need to suggest some possible solutions for substituting the low fault level resulted from the increased penetration level of NSGs. Subsequently, three different solutions have been proposed to improve the fault level profile and to overcome the negative implications resulted from the fault level decline accompanied by the increased penetration

levels of NSGs. These three proposed solutions include enhancement of FRT capability of the NSGs by increasing the *k*-factor, enhancement of the transient overrating capability of NSGs and installation of synchronous condensers in low fault level systems (chapter 7). The results show the effectiveness of the suggested solutions in improving the fault level profile and mitigating the negative implications of the low fault level on the system due to the increased penetration of NSGs. For instance, an average fault level increment of 19% has been achieved by maximizing the *k*-factor (i.e. k=10) in compared to the original case (i.e. k=2). On the other hand, general fault level increments of (13.8% and 35.8%) have been registered for the cases (I_{Max}= 1.5 p.u. and I_{Max}=2 p.u.), as compared to the original system fault level respectively. These two suggested solutions have evenly improved the fault level at all Buses in the system. In other words, their impact can be observed at all system Buses either close or far Buses from the NSGs. Lastly, average increments of 7.4%, 13.8 % and 19% have been observed in the system fault level considering all Buses after installation of 100 MVAr, 200 MVAr and 300 MVAr respectively. Although this result demonstrated the efficiency of this solution represented by the installation of synchronous condensers, the results show that the synchronous condensers mainly affect the fault level at those Buses close to them, while the far Buses from the installed synchronous condensers are marginally affected.

8.2 Contributions and Key Findings

The conclusions and key findings drawn from the thesis are summarised as follows:

1. Presenting a comprehensive background and an up-to-date literature review about the theme of fault level in power systems and the related challenges in future power systems with high penetration of NSGs-based RESs.
2. Extending the existing knowledge of the NSG-based RESs through achieving a better understanding of the very different SC current response of NSGs.
3. Discovering that the fault current contribution of NSGs is generally concluded as a transient followed by a steady-state SC current. While the transient SC contribution is mainly determined by the pre-fault operation conditions, the location of the fault (i.e. voltage dip seen during) and the speed of reactive current injection, the steady-state contribution is only affected by the transient overrating capability of the converter as well as the proportional gain for the reactive current injection (i.e. *k*-factor).
4. Concluding that the SC current response is very sensitive to the generation mix (SGs and NSGs) resulted from the increased penetration of NSGs and displacing the traditional SGs in future scenarios. It can be concluded that not only the SC currents will decrease to lower levels with the increased penetration of NSGs, but also the SC current response may witness some significant changes compared to the one observed in conventional power systems on the basis of SGs. This includes, but not restricted to, a delayed maximum contribution (i.e. very low initial contribution), multiple peak values and different levels of current decaying after exceeding some critical penetration levels NSGs penetration in the grid, more specifically after exceeding (40% penetration of NSGs).

5. Concluding that the existing modelling methodologies used for representations of NSGs in steady-state fault calculations methods (e.g. IEC60909 standard) cannot accurately represent the dynamic behaviour of NSG utilising FRC technologies, especially in high penetrations of NSGs scenarios. This necessitates a continuous need to augment the existing modelling methodologies used in the SSFC methods to achieve a better consideration for the fault current contributions of the NSGs and to provide more accurate estimations of the fault currents in future systems with high penetration of NSGs.
6. Contributing to the enhanced accuracy of the IEC60909-based steady-state fault calculation method by proposing a modification for the way of calculating the fault contribution of NSGs to the grid faults considering the FRT control and the reactive current injection capability more precisely. The proposed method has proven its accuracy by reducing the error margin at least by 50% in steady-state fault calculation of power systems with high penetration of NSG-based RESs when compared to the results obtained from IEC60909-based calculation method before the proposed modification.
7. Proposing a novel MVA-based FLC method to quantify the fault level in future grid scenarios, including various penetration levels of NSGs, i.e. RESs. The newly proposed method is formulated on the basis of the correlation between the fault level and the penetration of NSGs in the power system. This includes a generic modelling method that can assist in estimating/predicting the system fault level in a wide range of future grid scenarios without a need for a detailed system modelling or time-domain simulations. The results obtained after applying the proposed FLC method to calculate the fault level using three representative test systems i.e. a) 2-area test system b) IEEE 9-bus test system and c) IEEE 39-bus test system, have demonstrated adequate applicability, with small absolute errors, smaller than 5.1%, when compared to the full-

scale dynamic simulation results on the basis of detailed network modelling. Furthermore, the results obtained have shown that the proposed FLC method has superior accuracy when compared with the IEC60909-based fault calculations, which may result in conservative/inaccurate outcomes in some cases.

8. Concluding that the transmission system fault level decreases with the increased penetration of NSGs generation. However, this reduction may show different trends in different power systems, depending on the fault location and the SG displacement scenarios. For instance, those Buses which are closer to the displaced SGs may experience lower fault levels, compared to the remote ones. On the other hand, an approximately homogeneous fault level reduction may be experienced in the network when the SGs are uniformly replaced by NSGs. This implies the impact of the location of the NSGs on the fault level reduction, which is already considered in the novel proposed FLC method in this thesis (chapter 6). Hence, this can assist researchers and system operators to analyse large numbers of FG scenarios with different possibilities for the type, size, and location of NSG-based RESs.
9. Showing that the operation of the power system under low fault level conditions resulted from the increased penetration level of NSGs, would negatively affect the strength of the system that can be characterised by the voltage stiffness after exposure to an event, e.g., switching of Capacitor banks or SC faults. In other words, the voltage stiffness at the system Buses is strongly dependent on the fault level of those Buses as the higher fault level Buses have shown more stiffness and a less voltage change in response to either switching events or SC faults occurred at other Buses in the system.
10. Concluding that there is a need to substitute the low fault level to improve the fault level profile and to overcome the negative implications resulted from the fault level decline accompanied by the increased penetration levels of NSGs.

11. Proposing three possible alternatives to substitute the low fault level in future systems including optimizing the of the FRT capability of the NSGs by maximizing the *k*-factor, enhancement of the capability of NSGs by maximizing the transient overrating and installation of synchronous condensers in low fault level systems (chapter 7). Taken together, the results of applying these suggested solutions show their effectiveness in improving the fault level profile and mitigating the negative implications of the low fault level on the system due to the increased penetration of NSGs.

8.3 Future Work

The research undertaken in the present thesis has effectively covered the majority of the objectives and successfully proposed several key contributions. Nevertheless, the presented work has opened new dimensions for more studies and future ideas on the theme of fault level in future power systems with high penetration of NSGs. Hence, several possible areas might be open for further development of this current research as follows:

- To extend the research to cover different types of asymmetrical faults, such single line-ground faults which might be higher than the three-phase faults under specific circumstances. Also, to develop the proposed FLC methods to consider majority of fault types in power systems, especially with high penetration of NSGs.
- To study the SC response of Type-3 wind turbines, i.e. double-fed induction generators, and their modelling and representation in steady-state fault calculations and compare it with the SC response of the FRC-based NSGs studied in the present thesis.
- To study the impact of considering the negative sequence components on the FRT control of the NSG on the SC response under different faulty conditions.

- To consider the harmonics and high-frequency components which might appear in NSGs faults current, and their modelling to allow investigating the impact of such components on the dynamic characteristics of the fault current response in power systems with high penetration of NSG-based RESs.

Furthermore, some directions of the future research might continue to consider different aspects related to fault level calculations and their applications in power systems such as:

- To study the performance of the different protective devices in power systems (e.g. overcurrent, distance and differential relays) under low fault level conditions with altered SC current response due to the high penetration of NSG-based RESs.
- To launch research on the limitation for maximum penetration levels of NSGs due to the reduced fault level accompanied by the more integration of such NSGs and the displacement of conventional SGs.
- To study the power quality issues and other challenges related to the low fault level in future scenarios with high penetration of NSGs.
- To develop computational methods and computer-aided programs on the basis of DPL (DIgSILENT Programming Language) script that perform the fault calculations on the basis of the proposed modification of the IEC60909 standards (presented in chapter 5) and the proposed novel FLC method (presented in chapter 6) to be applied to any future scenarios with high penetration of NSGs.
- Another challenging, but an attractive task of future work is to conduct laboratory-based testing using actual NSGs and monitoring the actual waveforms considering the different control strategies and all practical factors discussed in the thesis. This might be interestingly achieved by using a real-time digital simulator (RTDS).

References

[1] Migrate Project, "Massive Integration of Power Electronic Devices," 2016, URL: https://www.h2020-migrate.eu/

[2] National Grid, "Impact of declining short circuit levels," National Grid ESO, UK, 2018.

[3] National Grid, "Whole System Short Circuit Levels," National Grid ESO, UK, 2018.

[4] AEM Operator, "System Strength Requirements and Fault Level Shortfalls" Australian Energy Market Operator, Australia, 2018.

[5] B. Kroposki, B. Johnson, Y. Zhang, V. Gevorgian, P. Denholm, B. M. Hodge, and B. Hannegan, "Achieving a 100% Renewable Grid: Operating Electric Power Systems with Extremely High Levels of Variable Renewable Energy," *IEEE Power and Energy Magazine*, vol. 15, no. 2, pp. 61-73, 2017.

[6] IEC, "Short-circuit currents in three-phase a.c. systems," *Part 0: Calculation of currents*, 2001.

[7] IEEE, "Recommended Practice for Calculating AC Short-Circuit Currents in Industrial and Commercial Power Systems," *IEEE Std 551-2006 [The Violet Book]*, pp. 1-308, 2006.

[8] D. Turcotte, and F. Katiraei, "Fault contribution of grid-connected inverters." pp. 1-5.

[9] R. J. Nelson, and H. Ma, "Short-circuit contributions of full-converter wind turbines." pp. 1-4.

[10] E. Muljadi, N. Samaan, V. Gevorgian, L. Jun, and S. Pasupulati, "Short circuit current contribution for different wind turbine generator types." pp. 1-8.

[11] N. D. Tleis, *Power Systems Modelling and Fault Analysis: Theory and Practice*: Newnes, 2008.

[12] H. Urdal, R. Ierna, J. Zhu, C. Ivanov, A. Dahresobh, and D. Rostom, "System strength considerations in a converter dominated power system," *IET Renewable Power Generation*, vol. 9, no. 1, pp. 10-17, 2015.

[13] P. Venkatesh, B. Manikandan, S. C. Raja, and A. Srinivasan, *Electrical power systems: analysis, security and deregulation*: PHI Learning Pvt. Ltd., 2012.

[14] S. H. Horowitz, "Protective Relaying for Power Generation Systems [Book Review]," *IEEE Power and Energy Magazine*, vol. 4, no. 5, pp. 78-79, 2006.

[15] D. Das, *Electrical power systems*: New Age International, 2007.

[16] National Grid, "System operability framework," 2015.

[17] R. Li, C. Booth, A. Dyśko, A. Roscoe, H. Urdal, and J. Zhu, "Protection challenges in future converter dominated power systems: demonstration through simulation and hardware tests, " 2015.

[18] V. Telukunta, J. Pradhan, A. Agrawal, M. Singh, and S. G. Srivani, "Protection challenges under bulk penetration of renewable energy resources in power systems: A review," *CSEE journal of power and energy systems,* vol. 3, no. 4, pp. 365-379, 2017.

[19] NERC, "Integrating InverterBased Resources into Low Short Circuit Strength Systems," USA, 2017.

[20] A. G. Paspatis, G. C. Konstantopoulos, T. A. Papadopoulos, and V. C. Nikolaidis, "Dynamic grid voltage support from distributed energy resources during short-circuits." pp. 1-6.

[21] G. Lammert, J. C. Boemer, D. Premm, O. Glitza, L. D. P. Ospina, D. Fetzer, and M. Braun, "Impact of fault ride-through and dynamic reactive power support of photovoltaic systems on short-term voltage stability." pp. 1-6.

[22] A. Camacho, M. Castilla, J. Miret, A. Borrell, and L. G. d. Vicuña, "Active and Reactive Power Strategies With Peak Current Limitation for Distributed Generation Inverters During Unbalanced Grid Faults," *IEEE Transactions on Industrial Electronics,* vol. 62, pp. 1515-1525, 2015.

[23] G. Carpinelli, C. Di Perna, P. Caramia, P. Varilone, and P. Verde, "Methods for assessing the robustness of electrical power systems against voltage dips," *IEEE Transactions on Power Delivery,* vol. 24, no. 1, pp. 43-51, 2008.

[24] P. Caramia, E. Di Mambro, P. Varilone, and P. Verde, "Impact of distributed generation on the voltage sag performance of transmission systems," *Energies*, vol. 10, pp. 959, 2017.

[25] IEEE, "IEEE Guide for Planning DC Links Terminating at AC Locations Having Low Short-Circuit Capacities," *IEEE Std 1204-1997,* 1997, pp. 1-216.

[26] E. Rahimi, A. M. Gole, J. B. Davies, I. T. Fernando, and K. L. Kent, "Commutation Failure Analysis in Multi-Infeed HVDC Systems," *IEEE Transactions on Power Delivery,* vol. 26, pp. 378-384, 2011.

[27] M. H. Nawir, "Integration of wind farms into weak grids" PhD Dissertation, Cardiff University, UK, 2017.

[28] J. Z. Zhou, H. Ding, S. Fan, Y. Zhang, and A. M. Gole, "Impact of Short-Circuit Ratio and Phase-Locked-Loop Parameters on the Small-Signal Behavior of a VSC-HVDC Converter," *IEEE Transactions on Power Delivery,* vol. 29, pp. 2287-2296, 2014.

[29] H. Urdal, S. Martinez Villanueva, J. Kilter, J. Jahn, J. Sprooten, and A. Baranauskas, "Future system challenges in Europe. Contributions to solutions from connection network codes," in *CIGRÉ USNC International Colloquium Evolution of Power System Planning to Support Connection of Generation, Distributed Resources and Alternative Technologies, Philadelphia, United States of America*, 2016.

[30] K. Nagrath, *Power System Engineering*: Tata McGraw-Hill, 2008.

[31] O. Anaya-Lara, D. Campos-Gaona, E. Moreno-Goytia, and G. Adam, *Offshore wind energy generation: control, protection, and integration to electrical systems*: John Wiley & Sons, 2014.

[32] J. Das, *Power system analysis: short-circuit load flow and harmonics*: CRC press, 2016.

[33] T. A. Loehlein, "Calculating generator reactances," *white paper, power topic*, vol. 6008, 2006.

[34] I. Kasikci, *Short Circuits in Power Systems: A Practical Guide to IEC 60909-0*: John Wiley & Sons, 2018.

[35] IEC, "Short-circuit currents in three-phase a.c. systems," *Part 0: Calculation of currents*, 2016.

[36] H. Abu-Rub, M. Malinowski, and K. Al-Haddad, *Power electronics for renewable energy systems, transportation and industrial applications*: John Wiley & Sons, 2014.

[37] R. Nelson, *Full-Converter Wind Turbine Technology*, 2014.

[38] F. Blaabjerg, M. Liserre, and K. Ma, "Power Electronics Converters for Wind Turbine Systems," *IEEE Transactions on Industry Applications*, vol. 48, pp. 708-719, 2012.

[39] R. Kabiri, D. Holmes, and B. McGrath, "DigSILENT Modelling of Power Electronic Converters for Distributed Generation Networks," in *PowerFactory Users' Conference and Future Networks Technical Seminar*, 2013.

[40] S. Engelhardt, I. Erlich, C. Feltes, J. Kretschmann, and F. Shewarega,"Reactive power capability of wind turbines based on doubly fed induction generators," *IEEE Transactions on Energy Conversion*, vol. 26, no. 1, pp. 364-372, 2010.

[41] O. Anaya-Lara, N. Jenkins, J. B. Ekanayake, P. Cartwright, and M. Hughes, *Wind energy generation: modelling and control*: John Wiley & Sons, 2011.

[42] S. Muyeen, *Wind energy conversion systems: technology and trends*: Springer, 2012.

[43] W. Sun, R. E. Torres-Olguin, and O. Anaya-Lara, "Investigation on Fault-ride Through Methods for VSC-HVDC Connected Offshore Wind Farms," *Energy Procedia*, vol. 94, pp. 29-36, 2016.

[44] F. Hassanzadeh, H. Sangrody, A. Hajizadeh, and S. Akhlaghi, "Back-to-back converter control of grid-connected wind turbine to mitigate voltage drop caused by faults," in *2017 North American Power Symposium (NAPS)*, 2017, pp. 1-6.

[45] P. V. Patel, "Modeling and control of three-phase grid-connected PV inverters in the presence of grid faults," 2018.

[46] F. Blaabjerg, *Control of power electronic converters and systems*: Academic Press, 2018.

[47] A. Keyhani, and M. Albaijat, *Smart power grids 2011*: Springer Science & Business Media, 2012.

[48] C. Sourkounis and P. Tourou, "Grid code requirements for wind power integration in Europe," in *Conference Papers in Science*, 2013.

[49] M. Curzi, R. Sharma, and F. Martin, "In fault ride through reactive current rise time requirements of various European grid codes—analysis based on a full-converter wind turbine," *Wind Energy*, vol. 19, pp. 1121-1133, 2016.

[50] M. Tsili and S. Papathanassiou, "A review of grid code technical requirements for wind farms," *IET Renewable Power Generation*, vol. 3, pp. 308-332, 2009.

[51] M. Tarafdar Hagh and T. Khalili, "A review of fault ride through of PV and wind renewable energies in grid codes," *International Journal of Energy Research*, vol. 43, pp. 1342-1356, 2019.

[52] J. Morren, "Grid support by power electronic converters of Distributed Generation units," PhD thesis, TU Delft, 2006.

[53] M. Mohseni and S. M. Islam, "Review of international grid codes for wind power integration: Diversity, technology and a case for global standard," *Renewable and Sustainable Energy Reviews*, vol. 16, pp. 3876-3890, 2012.

[54] J. Muñoz-Cruzado-Alba, J. Villegas-Núñez, J. Vite-Frías, and J. Carrasco Solís, "A new fast peak current controller for transient voltage faults for power converters," *Energies*, vol. 9, p. 1, 2016.

[55] J. Fortmann, R. Pfeiffer, E. Haesen, F. v. Hulle, F. Martin, H. Urdal, and S. Wachtel, "Fault-ride-through requirements for wind power plants in the ENTSO-E network code on requirements for generators, " *IET Renewable Power Generation*, vol. 9, pp. 18-24, 2015.

[56] W. Chen, T. Zheng, and J. Han, "Fault Characteristic and Low Voltage Ride-Through Requirements Applicability Analysis for a Permanent Magnet Synchronous Generator-Based Wind Farm," *Energies*, vol. 12, pp. 3400, 2019.

[57] ENTSO-E, "ENTSO-E Network Code for Requirements for Grid Connection Applicable to all Generators," ed, 2013.

[58] C. T. Lee, C. W. Hsu, and P. T. Cheng, "A Low-Voltage Ride-Through Technique for Grid-Connected Converters of Distributed Energy Resources," *IEEE Transactions on Industry Applications,* vol. 47, pp. 1821-1832, 2011.

[59] ENTSO-E, "Fault current contribution from PPMS & HVDC," 2017.

[60] B. Weise, "Impact of K-factor and active current reduction during fault-ride-through of generating units connected via voltage-sourced converters on power system stability," *IET Renewable Power Generation,* vol. 9, pp. 25-36, 2015.

[61] B. Singh, and S. Singh, "Wind power interconnection into the power system: A review of grid code requirements," *The Electricity Journal,* vol. 22, pp. 54-63, 2009.

[62] E.ON Netz GmbH, "Grid code high and extra high voltage," Germany, 2006.

[63] I. J. Gabe, H. Pinheiro, and H. A. Gründling, "Wind turbines reactive current control during unbalanced voltage dips," *Modeling and Control Aspects of Wind Power Systems*, pp. 61, 2013.

[64] J. Jia, G. Yang, and A. H. Nielsen, "A review on grid-connected converter control for short-circuit power provision under grid unbalanced faults," *IEEE Transactions on Power Delivery,* vol. 33, no. 2, pp. 649-661, 2017.

[65] A. V. Stankovic, D. Schreiber, and X. Zheng, "Grid-Fault Ride-Through Control Method for a Wind Turbine Inverter," in *Smart Power Grids 2011*, ed: Springer, 2012, pp. 543-563.

[66] M. Ndreko, M. Popov, and M. A. van der Meijden, "Study on FRT compliance of VSC-HVDC connected offshore wind plants during AC faults including requirements for the negative sequence current control," *International Journal of Electrical Power & Energy Systems,* vol. 85, pp. 97-116, 2017.

[67] National Grid, "THE GRID CODE," UK, 2018.

[68] F. Iov, A. Hansen, P. Sorensen, and N. Cutululis, "Mapping of Grid Faults and Grid Codes,‖ Risø Nat. Lab., Roskilde," Denmark, Tech. Rep. Risoe, 2007.

[69] R. T. Energinet, "3.2. 5 Wind Turbines Connected to Grids With Voltages Above 100 kV," *Denmark, Dec,* vol. 3, 2010.

[70] J. Keller and B. Kroposki, "Understanding fault characteristics of inverter-based distributed energy resources," National Renewable Energy Lab.(NREL), Golden, CO (United States) 2010.

[71] N. Nimpitiwan, G. T. Heydt, R. Ayyanar, and S. Suryanarayanan, "Fault Current Contribution From Synchronous Machine and Inverter Based Distributed Generators," *IEEE Transactions on Power Delivery*, vol. 22, pp. 634-641, 2007.

[72] "Fault current contributions from wind plants," in *2015 68th Annual Conference for Protective Relay Engineers*, College Station, TX, 2015, pp. 137-227.

[73] R. A. Walling, E. Gursoy, and B. English, "Current contributions from Type 3 and Type 4 wind turbine generators during faults," in *2011 IEEE Power and Energy Society General Meeting*, 2011, pp. 1-6.

[74] C. A. Plet, M. Graovac, T. C. Green, and R. Iravani,"Fault response of grid-connected inverter dominated networks," in *IEEE PES General Meeting*, 2010, pp. 1-8.

[75] A. Darwish, A. Abdel-Khalik, A. Elserougi, S. Ahmed, and A. Massoud, "Fault current contribution scenario for grid-connected voltage source inverter-based distributed generation with an LCL filter," *Electric Power Systems Research*, vol. 104, pp. 93-103, 2013.

[76] R. A. Walling and M. L. Reichard, "Short circuit behavior of wind turbine generators," in *2009 62nd Annual Conference for Protective Relay Engineers*, 2009, pp. 492-502.

[77] R. J. Nelson, H. Ma, and N. M. Goldenbaum, "Fault ride-through capabilities of siemens full-converter wind turbines," in *2011 IEEE Power and Energy Society General Meeting*, 2011, pp. 1-5.

[78] T. Neumann, and I. Erlich, "Short circuit current contribution of a photovoltaic power plant," *IFAC Proceedings Volumes*, vol. 45, pp. 343-348, 2012.

[79] M. Valentini, V. Akhmatov, F. Iov, and J. Thisted, "Fault current contribution from VSC-based wind turbines to the grid," in *2nd International Symposium on Electrical and Electronics Engineering (ISEEE)*, 2008.

[80] J. Martínez, P. C. Kjær, P. Rodriguez, and R. Teodorescu, "Short circuit signatures from different wind turbine generator types," in *2011 IEEE/PES Power Systems Conference and Exposition*, 2011, pp. 1-7.

[81] F F. Katiraei, J. Holbach, T. Chang, W. Johnson, D. Wills, B. Young, *et al.*, "Investigation of solar PV inverters current contributions during faults on distribution and transmission systems interruption capacity," in *Western Protective Relay Conference*, 2012, pp. 70-78.

[82] SMA, "Short-Circuit Currents: Information on short-circuit currents of SMA PV inverters" URL: https://files.sma.de/dl/7418/Iscpv-TI-en-17.pdf.

[83] T. Wijnhoven, "Evaluation of fault current contribution strategies by converter based distributed generation," PhD thesis, KU Leuven, 2015.

[84] C. A. Plet, "Fault response of inverter-based distributed generation," Imperial College London, 2012.

[85] M. Chaudhary, S. M. Brahma, and S. J. Ranade, "Interpreting the short circuit behavior of Type 4 wind turbine generator," in *2014 IEEE PES T&D Conference and Exposition*, 2014, pp. 1-5.

[86] C. A. Plet, M. Brucoli, J. D. F. McDonald, and T. C. Green, "Fault models of inverter-interfaced distributed generators: Experimental verification and application to fault analysis," in *2011 IEEE Power and Energy Society General Meeting*, 2011, pp. 1-8.

[87] B. Karlson and J. Williams, "Wind power plant short-circuit modeling guide," Sandia National Laboratories, 2012.

[88] M. Fischer and M. Â, "Representation of variable speed full conversion Wind Energy Converters for steady state short-circuit calculations," in *PES T&D*, 2012, pp. 1-7.

[89] N. Samaan, R. Zavadil, J. C. Smith, and J. Conto, "Modeling of wind power plants for short circuit analysis in the transmission network," in *2008 IEEE/PES Transmission and Distribution Conference and Exposition*, 2008, pp. 1-7.

[90] L. Wang, H. Gao, and G. Zou, "Modeling methodology and fault simulation of distribution networks integrated with inverter-based DG," *Protection and Control of Modern Power Systems*, vol. 2, p. 31, 2017.

[91] E. Muljadi and V. Gevorgian, "Short-circuit modeling of a wind power plant," in *2011 IEEE Power and Energy Society General Meeting*, 2011, pp. 1-9.

[92] T. N. Boutsika and S. A. Papathanassiou, "Short-circuit calculations in networks with distributed generation," *Electric Power Systems Research*, vol. 78, pp. 1181-1191, 2008.

[93] G. Balzer, "Short-circuit calculation with fullsize converters according to iec 60909," in *21 st Conference of Electric Power Supply Industry, CEPSI*, 2016"

[94] L. Thurner and M. Braun, "Vectorized calculation of short circuit currents considering distributed generation-an open source implementation of iec 60909," in *2018 IEEE PES Innovative Smart Grid Technologies Conference Europe (ISGT-Europe)*, 2018, pp. 1-6.

[95] Y. Liu, R. Yu, L. Zhang, D. Jiang, N. Chen, and D. Zhao, "Research on Short-Circuit Currents Calculation Method Considering Dynamic Reactive Power Support of Renewable Energy Systems," in *2018 2nd IEEE Conference on Energy Internet and Energy System Integration (EI2)*, 2018, pp. 1-9.

[96] D. Van Tu, S. Chaitusaney, and A. Yokoyama, "Fault current calculation in distribution systems with inverter-based distributed generations," *IEEJ Transactions on Electrical and Electronic Engineering*, vol. 8, pp. 470-477, 2013.

[97] H. Margossian, J. Sachau, and G. Deconinck, "Short circuit calculation in networks with a high share of inverter based distributed generation," in *2014 IEEE 5th International Symposium on Power Electronics for Distributed Generation Systems (PEDG)*, 2014, pp. 1-5.

[98] N. Zhou, J. Wu, and Q. Wang, "Three-phase short-circuit current calculation of power systems with high penetration of VSC-based renewable energy," *Energies*, vol. 11, p. 537, 2018.

[99] H. Hooshyar, and M. E. Baran, "Fault analysis on distribution feeders with high penetration of PV systems," *IEEE Transactions on Power Systems*, vol. 28, pp. 2890-2896, 2012.

[100] S. Liu, T. Bi, and Y. Liu, "Theoretical Analysis on the Short-Circuit Current of Inverter-Interfaced Renewable Energy Generators with Fault-Ride-Through Capability," *Sustainability*, vol. 10, p. 44, 2018.

[101] A. Roy and B. K. Johnson, "Transmission side protection performance with Type-IV wind turbine system integration," in *North American Power Symposium (NAPS), 2014*, 2014, pp. 1-6.

[102] P. Anderson, A. Fouad, and H. Happ, "Power system control and stability," *IEEE Transactions on Systems, Man, and Cybernetics*, vol. 9, pp. 103-103, 1979.

[103] DIgSILENT PowerFactory, "17, 0 User manual," ed: Gommaringen, 2017.

[104] DIgSILENT GmbH, "Technical Reference Documentation: Static Generator," 2017.

[105] A. Kakilli, "System Analysis with the MVA Method for Symmetrical Three-Phase Faults," *Tem Journal*, vol. 2, pp. 51-56, 2013.

[106] T. H. Chen and W. T. Huang, "Evaluation of the variations of short-circuit capacities along a feeder due to distribution network upgrading," *IEEE Power Engineering Society General Meeting, 2005.*, San Francisco, CA, 2005, pp. 2536-2541.

[107] S. M. Halpin, R. A. Jones and L. Y. Taylor, "The MVA-Volt Index: A Screening Tool for Predicting Fault-Induced Low Voltage Problems on Bulk Transmission Systems," in *IEEE Transactions on Power Systems*, vol. 23, no. 3, pp. 1205-1210.

[108] P. Kundur, N. J. Balu, and M. G. Lauby, *Power system stability and control*: McGraw-hill New York, 1994.

[109] M. Pai, *Energy function analysis for power system stability*: Springer Science & Business Media, 2012.

[110] P. E. Marken, A. C. Depoian, J. Skliutas, and M. Verrier, "Modern synchronous condenser performance considerations," in *2011 IEEE Power and Energy Society General Meeting*, 2011, pp. 1-5.

[111] R. M. Mathur and R. K. Varma, *Thyristor-based FACTS controllers for electrical transmission systems*: John Wiley & Sons, 2002.

[112] S. Teleke, T. Abdulahovic, T. Thiringer, and J. Svensson, "Dynamic Performance Comparison of Synchronous Condenser and SVC," *IEEE Transactions on Power Delivery,* vol. 23, pp. 1606-1612, 2008.

[113] L. L. Grigsby, *Power systems*: CRC press, 2016.

[114] M. Nedd, Q. Hong, K. Bell, C. Booth, and P. Mohapatra, "Application of synchronous compensators in the gb transmission network to address protection challenges from increasing renewable generation," in *2017 CIGRE B5 Colloquium*, 2017.

[115] GE. Grid Solutions, "Synchronous Condenser Systems," 2017, URL: https://www.gegridsolutions.com/products/brochures/powerd_vtf/Synch_Cond_web.pdf.

[116] E. Marrazi, Y. Guangya, and P. Weinreich-Jensen, "Allocation of synchronous condensers for restoration of system short-circuit power," *Journal of Modern Power Systems and Clean Energy,* vol. 6, pp. 17-26, 2018.

[117] J. Jia, G. Yang, A. H. Nielsen, E. Muljadi, P. Weinreich-Jensen, and V. Gevorgian, "Synchronous Condenser Allocation for Improving System Short Circuit Ratio," in *2018 5th International Conference on Electric Power and Energy Conversion Systems (EPECS)*, 2018, pp. 1-5.

Appendices

Appendix A: Scenario and Case Studies-Chapters 3 &4

A.1 Single machine-infinite Bus test system

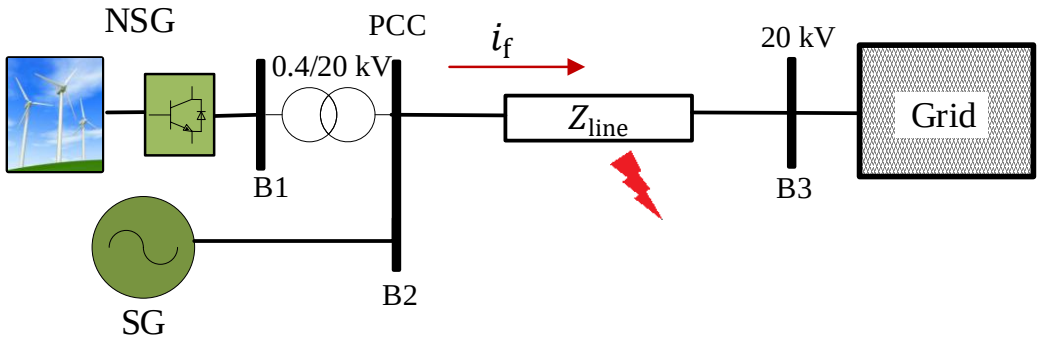

The adjusted single machine-infinite Bus test system

A.1.1 Network Data

Element	Data
External Grid	Short Circuit Power : 1000 MVA X/R ratio : 10
SG	Rating: 50 MVA & 20 kV & Power factor: 1 R_{stator}: 0.0504 p.u., $X_{leakage}$: 0.1 p.u. X_d: 1.5 p.u., X'_d: 0.256 p.u., X''_d: 0.168 p.u.
NSG (type-4 wind farm)	Rating: 50 MVA & Power factor: 1
Busbars	Voltages: B1=0.4 KV, B1=B2=20 KV
Transformer	Rating: 55 MVA & Voltage: 0.4/20 kV Vector configuration: Dyn5 Reactance: 0.060 p.u. Resistance: 0.001 p.u.
Line	Voltages: 20 KV & Length: 30 km Resistance: 0.2567 Ω/km Reactance: 0.1193 Ω/km Susceptance: 80.83 μS/km

A.1.2. Penetration Levels Scenario

Scenario	SG (MW)	NSG (MW)	SG+NSG (MW)	Penetration level %
1	50	0	50	0
2	40	10	50	20
3	30	20	50	40
4	20	30	50	60
5	10	40	50	80
6	0	50	50	100

$$Penetration\ level(\%) = \frac{NSG}{NSG + SG} \times 100\% \quad (3.6)$$

A.2 IEEE 9-Bus test system

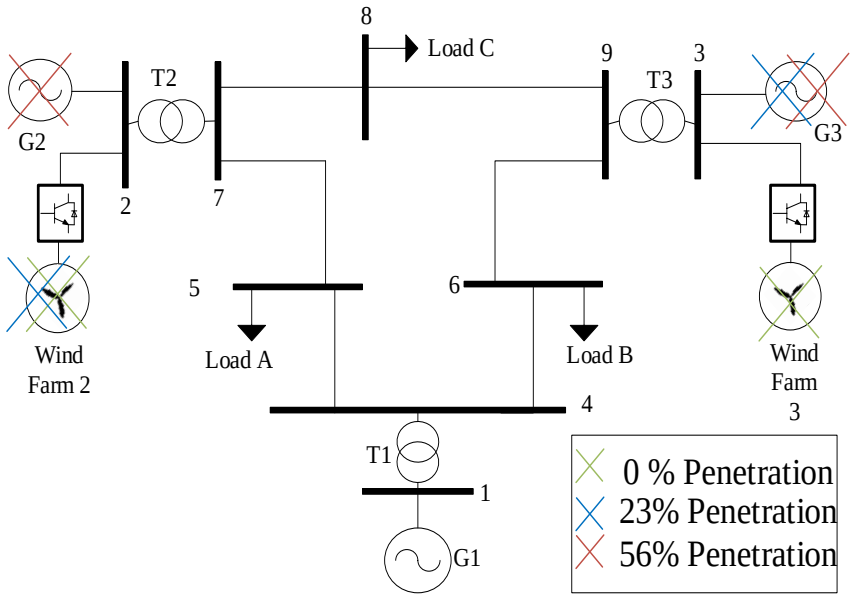

The adjusted IEEE 9-Bus test system

A.2.1 Generators and Loads Data

Quantity	G1	G2	G3
Nominal Power (MVA)	247.5	192.0	128.0
Nominal voltage (Kv)	16.5	18.0	13.8
Nominal power factor	1.00	0.85	0.85
X_d (p.u)	0.3614	1.7199	1.6800
X_q (p.u)	0.2328	1.6598	1.6100
X'_d (p.u)	0.1505	0.2300	0.2321
X'_q (p.u)	-	0.3780	0.3200
X''_d (p.u)	0.1	0.2	0.2
X''_q (p.u)	0.1	0.2	0.2
$X_{leakage}$ (p.u)	0.0832	0.1000	0.0950
Inertia Constant H (s)	9.5515	3.9216	2.7665

Load	P (MW)	Q (MVAr)
Load A	125	50
Load B	90	30
Load C	100	35

A.2.2 Scenario

Scenario	G1 (MVA)		G2 (MVA)		G3 (MVA)		Penetration Level (total)
	SG	NSG	SG	NSG	SG	NSG	%
1	247.5	0	192.0	0	128.0	0	0
2	247.5	0	192.0	0	0	128.0	23
3	247.5	0	0	192.0	0	128.0	56

A.2.3 Control parameters of NSGs (type-4 wind farms)

Scenario	k-factor			Overrating capability factor (α)			Time of reactive current injection (ms)		
	NSG1	NSG2	NSG3	NSG1	NSG2	NSG3	NSG1	NSG2	NSG3
1	-	2	2	1.1	1.1	1.1	-	0	0
2	-	2	2	1.1	1.1	1.1	-	20	20
3	-	2	2	1.1	1.1	1.1	-	50	50

Appendix B: Scenario and Case Studies-Chapter 5

B.1 IEEE 14-Bus Test System

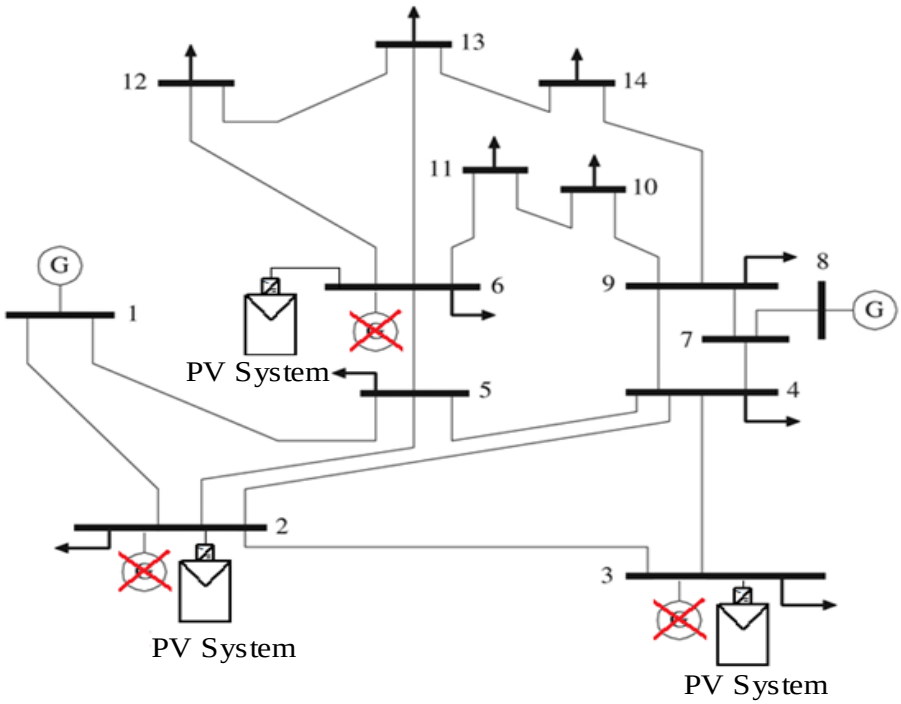

B.1.1 Generators and Loads Data

Loads	P in MW	Q in Mvar
Load 2	21.7	12.7
Load 3	94.2	19.0
Load 4	47.8	-3.9
Load 5	7.6	1.6
Load 6	11.2	7.5
Load 9	29.5	16.6
Load 10	9.0	5.8
Load 11	3.5	1.8
Load 12	6.1	1.6
Load 13	13.5	5.8
Load 14	14.9	5.0

Quantity	G1 (Slack)	G2	G3	G6	G8
Nominal Power (MVA)	400	100	100	100	100
Nominal voltage (kV)	132	132	132	33	11
Nominal power factor	0.8	0.8	1	1	1
X_d (p.u)	2	2	2	2	2
X_q (p.u)	2	2	2	2	2
X'_d (p.u)	0.3	0.3	0.3	0.3	0.3
X'_q (p.u)	0.3	0.3	0.3	0.3	0.3
X''_d (p.u)	0.2	0.2	0.2	0.2	0.2
X''_q (p.u)	0.2	0.2	0.2	0.2	0.2
$X_{leakage}$ (p.u)	0.1	0.1	0.1	0.1	0.1
Inertia Constant H (s)	10	10	10	10	10

B.1.2 Scenario

Studied Scenario	G1 (MVA)		G2 (MVA)		G3 (MVA)		G6 (MVA)		G8 (MVA)		Penetration Level (total)
	SG	NSG	SG	NSG	SG	NSG	SG	NSG	SG	NSG	%
	400	0	0	100	0	100	0	100	100	0	37.5

B.1.3 Control Parameters of NSGs (PV Systems)

Case Study	*k*-factor			Overrating capability factor (α) in p.u.			Time of reactive current injection (ms)		
	NSG2	NSG3	NSG6	NSG1	NSG2	NSG3	NSG1	NSG2	NSG3
Case 1	2	2	2	1.3	1.3	1.3	10	10	10
Case 2	10	10	10	1.3	1.3	1.3	10	10	10

Appendix C: Scenario and Case Studies-Chapter 6

C.1 Two-Area Test System

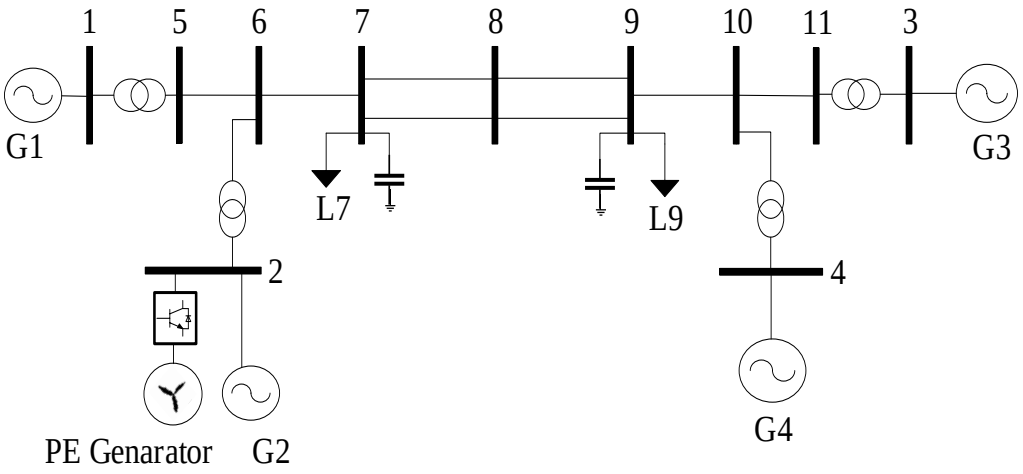

The adjusted two-area test system with a PE-based generation on Bus 2.

C.1.1 Generators and Loads Data

Quantity	G1	G2	G3	G4
Nominal (MVA)	900	900	900	900
voltage (Kv)	20	20	20	20
Nominal power factor	1	1	1	1
X_d (p.u)	1.8	1.8	1.8	1.8
X_q (p.u)	1.7	1.7	1.7	1.7
X'_d (p.u)	0.3	0.3	0.3	0.3
X'_q (p.u)	1.7	1.7	1.7	1.7
X''_d (p.u)	0.25	0.25	0.25	0.25
X''_q (p.u)	0.25	0.25	0.25	0.25
$X_{leakage}$ (p.u)	0.2	0.2	0.2	0.2
Inertia Constant H (s)	6.5	6.5	6.175	6.175

Loads	P in MW	Q in Mvar
Load 7	967	100
Load 9	1767	100

C.1.2 Scenario

i. Scenario 1 (Non-Uniform Penetration of NSG* at G2)

Penetration Level at G2 (%)	G1 (MVA)		G2 (MVA)		G3 (MVA)		G4 (MVA)	
	SG	NSG	SG	NSG	SG	NSG	SG	NSG
0	900	0	900	0	900	0	900	0
10	900	0	810	90	900	0	900	0
20	900	0	720	180	900	0	900	0
30	900	0	630	270	900	0	900	0
40	900	0	540	360	900	0	900	0
50	900	0	450	450	900	0	900	0
60	900	0	360	540	900	0	900	0
70	900	0	270	630	900	0	900	0
80	900	0	180	720	900	0	900	0
90	900	0	90	810	900	0	900	0
100	900	0	0	900	900	0	900	0

*NSG here is represented by type-4 wind farm

ii. Scenario 2 (Uniform Penetration of NSG at all Generators)*

Penetration Level at G2 (%)	G1 (MVA)		G2 (MVA)		G3 (MVA)		G4 (MVA)	
	SG	NSG	SG	NSG	SG	NSG	SG	NSG
0	900	0	900	0	900	0	900	0
10	810	90	810	90	810	90	810	90
20	720	180	720	180	720	180	720	180
30	630	270	630	270	630	270	630	270
40	540	360	540	360	540	360	540	360
50	450	450	450	450	450	450	450	450
60	360	540	360	540	360	540	360	540
70	270	630	270	630	270	630	270	630
80	180	720	180	720	180	720	180	720
90	90	810	90	810	90	810	90	810
100	0	900	0	900	0	900	0	900

*NSG here is represented by type-4 wind farm

C.2 IEEE 9-Bus test system

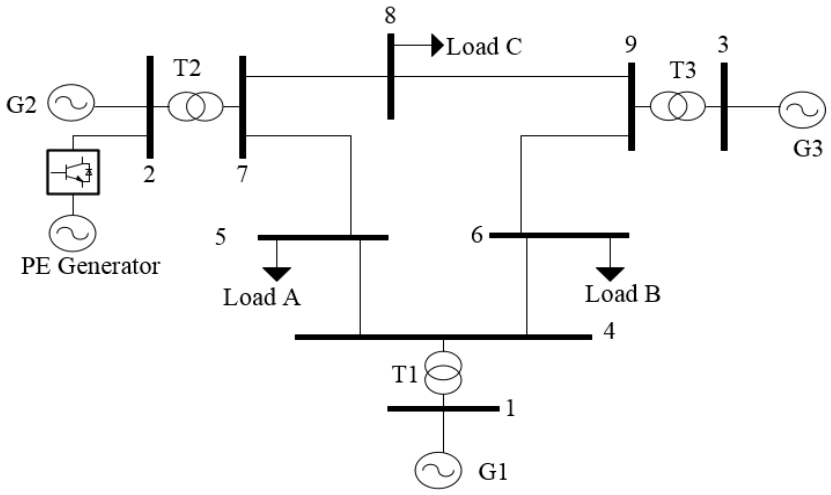

The adjusted IEEE 9-Bus test system

C.2.1 Generators and Loads Data

Quantity	G1	G2	G3
Nominal (MVA)	247.5	192.0	128.0
voltage (Kv)	16.5	18.0	13.8
Nominal power factor	1.00	0.85	0.85
X_d (p.u)	0.3614	1.7199	1.6800
X_q (p.u)	0.2328	1.6598	1.6100
X'_d (p.u)	0.1505	0.2300	0.2321
X'_q (p.u)	-	0.3780	0.3200
X''_d (p.u)	0.1	0.2	0.2
X''_q (p.u)	0.1	0.2	0.2
$X_{leakage}$ (p.u)	0.0832	0.1000	0.0950
H (s)	9.5515	3.9216	2.7665

Load	P (MW)	Q (MVAr)
Load A	125	50
Load B	90	30
Load C	100	35

C.2.2 Scenario

i. Scenario 1 (Non-Uniform Penetration of NSG* at G2)

Penetration Level at G2 (%)	G1 (MVA)		G2 (MVA)		G3 (MVA)	
	SG	NSG	SG	NSG	SG	NSG
0	247.5	0	192.0	0	128.0	0
10	247.5	0	172.8	19.2	128.0	0
20	247.5	0	153.6	38.4	128.0	0
30	247.5	0	134.4	57.6	128.0	0
40	247.5	0	115.2	76.8	128.0	0
50	247.5	0	96.0	96.0	128.0	0
60	247.5	0	76.8	115.2	128.0	0
70	247.5	0	57.6	134.4	128.0	0
80	247.5	0	38.4	153.6	128.0	0
90	247.5	0	19.2	172.8	128.0	0
100	247.5	0	0	192.0	128.0	0

*NSG here is represented by type-4 wind farm

ii. Scenario 2 (Uniform penetration of NSG* at all Generators)

Total Penetration Level (%)	G1 (MVA)		G2 (MVA)		G3 (MVA)	
	SG	NSG	SG	NSG	SG	NSG
0	247.5	0	192.0	0	128	0
10	222.75	24.75	172.8	19.2	115.2	12.8
20	198	49.5	153.6	38.4	102.4	25.6
30	173.25	74.25	134.4	57.6	89.6	38.4
40	148.5	99	115.2	76.8	76.8	51.2
50	123.75	123.75	96.0	96.0	64	64
60	99	148.5	76.8	115.2	51.2	76.8
70	74.25	173.25	57.6	134.4	38.4	89.6
80	49.5	198	38.4	153.6	25.6	102.4
90	24.75	222.75	19.2	172.8	12.8	115.2
100	0	247.5	0	192.0	0	128

*NSG here is represented by type-4 wind farm

C.3 39-Bus test system

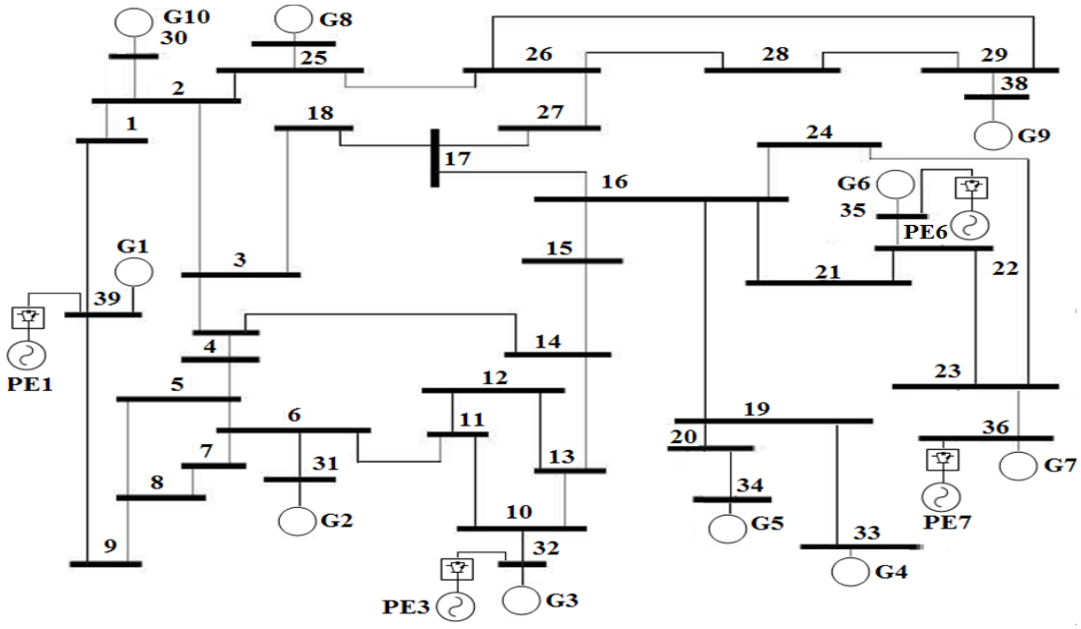

The adjusted IEEE 39-Bus system with PE-based generators

C.3.1 Generators and Loads Data

Quantity	G1	G2	G3	G4	G5	G6	G7	G8	G9	G10
Nominal (MVA)	10000	700	800	800	600	800	700	700	1000	1000
voltage (Kv)	345	16.5	16.5	16.5	16.5	16.5	16.5	16.5	16.5	16.5
power factor	0.85	0.85	0.85	0.85	0.85	0.85	0.85	0.85	0.85	0.85
x_d (p.u)	2	2.065	1.996	2.096	2.01	2.032	2.065	2.03	2.106	1
x_q (p.u)	1.9	1.974	1.896	2.064	1.86	1.928	2.044	1.96	2.05	0.69
X'_d (p.u)	0.6	0.4879	0.4248	0.3488	0.396	0.4	0.343	0.399	0.57	0.31
Xq' (p.u)	0.8	1.19	0.7008	1.328	0.498	0.6512	1.302	0.6377	0.587	0.5
$X_{d''}$ (p.u)	0.3	0.245	0.2432	0.236	0.162	0.1792	0.2254	0.196	0.298	0.125
Xq" (p.u)	0.3	0.245	0.2432	0.236	0.162	0.1792	0.2254	0.196	0.298	0.125
x_l (p.u)	0.3	0.245	0.2432	0.236	0.162	0.1792	0.2254	0.196	0.298	0.125
H (s)	5	4.329	4.475	3.575	4.333	4.35	3.771	3.471	3.45	4.2

Loads	P in MW	Q in Mvar
Load 03	322.0	2.4
Load 04	500.0	184.0
Load 07	233.8	84.0
Load 08	522.0	176.0
Load 12	7.5	88.0
Load 15	320.0	153.0
Load 16	329.0	32.3
Load 18	158.0	30.0
Load 20	628.0	103.0
Load 21	274.0	115.0
Load 23	247.5	84.6
Load 24	308.6	-92.2
Load 25	224.0	47.2
Load 26	139.0	17.0
Load 27	281.0	75.5
Load 28	206.0	27.6
Load 29	283.5	26.9
Load 31	9.2	4.9
Load 39	1104.0	250.0

C.3.2 Scenario

i. Scenario 1

Generator	*P*i	MVA	
G1	0.5	SG	5000
		NSG	5000
G2	0	SG	700
		NSG	0
G3	1	SG	0
		NSG	800
G4	0	SG	800
		NSG	0
G5	0	SG	600
		NSG	0
G6	0.5	SG	400
		NSG	400
G7	0	SG	700
		NSG	0
G8	0	SG	700
		NSG	0
G9	0	SG	1000
		NSG	0
G10	0	SG	1000
		NSG	0

$$Local\ Penetration\ level\ (P\mathrm{i}) = \frac{NSG_i}{NSG_i + SG_i}$$

$$Total\ Penetration\ level\ (P_{\mathrm{T}}) = \frac{NSG_{\mathrm{T}}}{NSG_{\mathrm{T}} + SG_{\mathrm{T}}} = \frac{6200}{6200 + 10900} = 0.36$$

ii. Scenario 2

Generator	*P*i	MVA	
G1	0.7	SG	3000
		NSG	7000
G2	0	SG	700
		NSG	0
G3	1	SG	0
		NSG	800
G4	1	SG	0
		NSG	800
G5	0	SG	600
		NSG	0
G6	1	SG	0
		NSG	800
G7	1	SG	0
		NSG	700
G8	0	SG	700
		NSG	0
G9	0	SG	1000
		NSG	0
G10	0	SG	1000
		NSG	0

$$Total\ Penetration\ level\ (P_{\mathrm{T}}) = \frac{10100}{10100 + 7000} = 0.59$$

C.4 Control Parameters of NSGs (Type-4 Wind Farms) in Ch.7 scenario

k-factor	Overrating capability factor (α) in p.u.	Time of reactive current injection (ms)
2	1.1	0.0

Appendix D: Scenario and Case Studies-Chapter 7

D.1 39-Bus test system

D.1.1 Generators and Loads Data

Data of all generators and loads are the same with those described in Appendix C.

D.1.2 Scenario

i. Scenario 1: All generators in both areas are SGs

Generator	*P*i	MVA	
G1	0	SG	10000
		NSG	0
G2	0	SG	700
		NSG	0
G3	0	SG	800
		NSG	0
G4	0	SG	800
		NSG	0
G5	0	SG	600
		NSG	0
G6	0	SG	800
		NSG	0
G7	0	SG	700
		NSG	0
G8	0	SG	700
		NSG	0
G9	0	SG	1000
		NSG	0
G10	0	SG	1000
		NSG	0

$$Total\ Penetration\ level\ (P_{\mathrm{T}}) = \frac{0}{17100} = 0.0$$

ii. Scenario 2: Area-2 generators are replaced by NSGs (i.e. type-4 wind farms)

Generator	*P*i	MVA	
G1	0	SG	10000
		NSG	0
G2	0	SG	700
		NSG	0
G3	0	SG	800
		NSG	0
G4	1	SG	0
		NSG	800
G5	1	SG	0
		NSG	600
G6	1	SG	0
		NSG	800
G7	1	SG	0
		NSG	700
G8	0	SG	700
		NSG	0
G9	1	SG	0
		NSG	1000
G10	0	SG	1000
		NSG	0

$$Total\ Penetration\ level\ (P_{\mathrm{T}}) = \frac{3900}{3900 + 13200} = 0.$$